NEW TECHNIQUES FOR PROTEOMICS STUDY: INSTRUMENTATION, SEPARATION, AND APPLICATION

By

SI WU

A dissertation submitted in partial fulfillment of the requirements for the degree of

DOCTOR OF PHILOSOPHY

WASHINGTON STATE UNIVERSITY
Department of Chemistry

December 2006

To the Faculty of Washington State University:

The members of the committee appointed to examine the dissertation of SI WU find it satisfactory and recommend that it be accepted.

_____
Chair

_____

_____

_____

ACKNOWLEDGEMENTS

My first, and most earnest, acknowledgment must go to my advisor and chair of my Thesis Committee James E. Bruce. Jim has been instrumental in ensuring my academic, professional, financial and moral well being ever since I joined his lab. In every sense, none of this work would have been possible without him. Many thanks also go to my committee members Dr. Michael D. Griswold, Dr. James O. Schenk, and Dr. William F. Siems, for their valuable time and suggestions, which significantly improved the quality of this dissertation.

Far too many people to mention individually have assisted me in so many ways during my work at WSU. In particular, I would like to thank Xiaoting Tang, whose help and support assisted me to start my research work in Jim's lab. I also want to thank Saiful Chowdhury, Nate Kaiser, Kai Zhang, Wei Yi, Natalia Zakharova, Mick Sakamoto, Deepen Kothari, Casey Schultz, Gunnar Skulason, Ethan Smith, and Shawn Riechers. As co-workers, they provide me a great laboratory environment during my research and dissertation preparations.

I would like to thank Dr. Ying Li, Dr. Shisheng Li, Rong Nie, and the entire Dr. Griswold's lab that have been so much helpful for the BACE expression profiling project. I am extremely grateful for the generosity of David Prior (PNNL) who provided the prototype flared inlet tubes, Gordon Anderson (PNNL) who provided the software ICR-2LS, and Dr. Li Zhou and Dr. Milton L. Lee (Brigham Young University) who provided the original design and a prototype air amplifier. Without these inputs, this dissertation would not have been possible.

My final, and most heartfelt, acknowledgment is to my husband Da Meng. His support, encouragement, and companionship have turned my journey through graduate school into a pleasure.

NEW TECHNIQUES FOR PROTEOMICS STUDY: INSTRUMENTATION, SEPARATION, AND APPLICATION

Abstract

By Si Wu, Ph.D.
Washington State University
December 2006

Chair: James E. Bruce

Proteomics, which is the study of all the proteins expressed by a genome, requires highly efficient analytical tools such as mass spectrometric techniques and advanced analytical protein separation methods. The common challenges of modern proteomics include efficient proteome separation techniques to reduce sample complexity, good quantitation strategies for comparative proteomics, new ionization sources for sampling sample at different environments, high sensitivity and resolving power of the MS instruments, and well-understanding of MS data.

My research work is focused on developing new strategies for several of the challenges mentioned above. First, to reduce the proteome complexity, we have developed a hybrid HPLC-Gel-MS method and applied it to the protein expression profiling. The application of step-gradient fractionation in a strong anion exchange column provided excellent reproducibility. Quantitative comparisons of protein abundance were done by side-by-side vertical comparison of band intensity in one gel. This separation strategy has been applied to the BACE and BACE2 over-expressed systems.

Second, to increase the mass measurement accuracy and protein identification confidence in FTICR-MS, we have developed a new calibration method, Calibration Optimization on

Fragment Ions (COFI), for fragmentation data to correct the effects of space charge in FTICR-MS. There is a post-data processing strategy, and no need to include an internal calibrant or to apply ion population control. COFI has been successfully applied to different types of LC-FTICR fragmentation data, including LC-MS/MS data and multiplexed LC-CID data.

A number of newly developed atmospheric pressure ionization methods, such as ESI, ESSI, DESI, AP-MALDI, and ELDI, have been set up. Different types of atmospheric pressure interfaces have been investigated. By using the flared inlet tube, improved ion transmission and sensitivity were demonstrated. Increased spray tip positional tolerance was also observed with the implementation of the flared inlet tube. We have developed a hybrid atmospheric pressure interface which couples an air amplifier with a flared inlet tube. A two nano-electrosprayer device has also been coupled with the hybrid interface, which can easily be used to introduce the internal calibrant. Finally, we reported our study of coupling on-target enzymatic digestion with ELDI-FTICR-MS.

TABLE OF CONTENTS

Page

ACKNOWLEDGEMENTS iii

ABSTRACT iv

TABLE OF CONTENTS vi

LIST OF TABLES ix

LIST OF FIGURES x

DEDICATION xvi

CHAPTER ONE: INTRODUCTION

1. PROTEOMICS AND MASS SPECTROMETRY 1
2. PROTEIN SEPARATION METHODS IN PROTEOMICS STUDY 4
3. ADVANCED MASS SPECTROMETRY METHODS IN PROTEOMICS STUDY 7
4. PROTEIN IDENTIFICATION METHODS IN PROTEOMICS STUDY 13
5. BACE AND ALZHEIMER'S DISEASE 16
6. OBJECTIVES OF THE RESEARCH 18
7. ATTRIBUTIONS 19
8. REFERENCES 20

CHAPTER TWO: INCREASED PROTEIN IDENTIFICATION CAPABILITIES THROUGH NOVEL TANDEM MS CALIBRATION STRATEGIES

1. TITLE PAGE 36
2. ABSTRACT 37
3. INTRODUCTION 38
4. EXPERIMENTAL PROCEDURES 42

5. RESULTS AND DISCUSSION 49

6. CONCLUSIONS 56

7. ACKNOWLEDGEMENTS 57

8. REFERENCES 58

CHAPTER THREE: A HYBRID LC-GEL-MS METHOD FOR PROTEOMICS RESEARCH AND ITS APPLICATION TO PROTEASE FUNCTIONAL PATHWAY MAPPING

1. TITLE PAGE 79

2. ABSTRACT 80

3. INTRODUCTION 81

4. EXPERIMENTAL 84

5. RESULTS AND DISCUSSION 91

6. CONCLUSIONS 99

7. ACKNOWLEDGEMENTS 101

8. REFERENCES 102

CHAPTER FOUR: INCORPORATION OF A FLARED INLET CAPILLARY TUBE ON A FOURIER TRANSFORM ION CYCLOTRON RESONANCE MASS SPECTROMETER

1. TITLE PAGE 116

2. ABSTRACT 117

3. INTRODUCTION 118

4. EXPERIMENTAL 122

5. RESULTS AND DISCUSSION 126

6. CONCLUSIONS 133

7. ACKNOWLEDGEMENTS 135

8. REFERENCES 136

CHAPTER FIVE: INTERGRATION OF A NEW INTERFACE WITH ATMOSPHERIC PRESSURE IONIZATION METHODS

1. TITLE PAGE 147

2. ABSTRACT 148

3. INTRODUCTION 149

4. EXPERIMENTAL 154

5. RESULTS AND DISCUSSION 157

6. CONCLUSIONS 164

7. ACKNOWLEDGEMENTS 165

8. REFERENCES 166

CHAPTER SIX: COUPLING ON-TARGET DIGESTION WITH AN ELECTROSPRAY-ASSISTD LASER DESORPTION IONIZATION FTICR MASS SPECTROMETER

1. TITLE PAGE 176

2. ABSTRACT 177

3. INTRODUCTION 178

4. EXPERIMENTAL 182

5. RESULTS AND DISCUSSION 185

6. CONCLUSIONS 190

7. ACKNOWLEDGEMENTS 192

8. REFERENCES 193

CHAPTER SEVEN: CONCLUSIONS

1. CONCLUSIONS 203

LIST OF TABLES

CHAPTER TWO:

Table 1: Fragment ion pairs in the MS/MS spectrum of substance P and their calculated frequency shifts. Pair numbering in this table corresponds to numbering used in Figure 3…....61

Table 2: Mass measurement errors for substance P fragment ions with/without COFI.....62

Table 3: Mass measurement errors for the identified fragments of three peptides from a single CID spectrum.....63

Table 4: MASCOT search results of a LC-FTICR-MS/MS separation.....64

CHAPTER THREE:

Table 1: Reproducibility of the retention time based on the major peaks in Figure 5A.....105

Table 2: Part of identified proteins and their physiological function.....106

CHAPTER FIVE:

Table 1: Measured mass errors for the BSA in-solution digested peptides using external and internal calibration.....168

CHAPTER SIX:

Table 1: Summary of identified peptides originating from the on-target tryptic digestion of BSA.....197

LIST OF FIGURES

CHAPTER ONE:

Figure 1: Schematic representation of an ESI source…….31

Figure 2: Diagram of the principle of MALDI 32

Figure 3: (A) Excitation and detection in FTICR cell. (B) Schematic presenting of data processing in FTICR mass spectra…….....33

Figure 4: Schematic representation of a DESI source 34

Figure 5: Schematic representation of an ELDI source.....35

CHAPETR TWO:

Figure 1: Mass errors of the fragment ions in the MS/MS spectrum of substance P before COFI. The graph shows a systematic linear increase in error with increasing *m/z*. The average mass measurement error of these fragment ions is 45.122 ppm……..…….....…….65

Figure 2: The relationship between the average absolute mass measurement error of the identified fragment ions of substance P and frequency shift is shown in this plot. The calculated frequency shift to obtain the minimum mass error is 5.5 Hz…….66

Figure 3: Application of COFI to the candidate pairs in the MS/MS spectra of substance P. Nine candidate pairs were chosen by COFI, as numbering in Table 2. For each pair, the absolute value of the difference between the exact amino acid mass (M_{aa}) and the measured amino acid mass (ΔM) ($\left|M_{aa} - \Delta M\right|$) is plotted as a function of frequency shift. *Delta Diff. refers to the difference $\left|M_{aa} - \Delta M\right|$. The optimal frequency shift calculated by COFI was 5.3 Hz….....67

Figure 4: Mass errors of the fragment ions in the MS/MS spectrum of substance P after frequency shift correction with COFI. The average error after calibration is 1.943 ppm.....68

Figure 5: Multiplexed CID spectrum of a three peptide mixture with labeled fragment ions attributed to each individual peptide. The three peptides are bradykinin (B), angiotensin I (A), and substance P (S). Only a-type, b-type, and y-type ions are selected here…….....69

Figure 6: Number of the identified fragments for tryptic digested peptides of BSA during a multiplexed LC-CID-FTICR-MS separation.....70

CHAPTER THREE:

Figure 1: Western blot analysis of BACE overexpression and BACE2 overexpression in HEK 293 cells versus controls of vector-transfected HEK 293 cells and untransfected HEK 293 cells…….....107

Figure 2: LC/MS/MS analysis of enzyme assay reaction mixture. (A) Extracted ion chromatogram (EIC) of full length peptide ($(M+2H)^{2+}$ at 590.2) and N-terminal product ($(M+H)^{+}$ at *m/z* 561.2) for vector control and BACE, respectively; (B) MS/MS mass spectrum of full length peptide; (C) MS/MS spectrum of N-terminal product.....108

Figure 3: Schematic diagram illustrating combined liquid chromatography gel electrophoresis separation of proteins.....109

Figure 4: SAX HPLC on protein separation and gel separation of fractions. (A) UV chromatogram. The step-gradient elution profile is shown here. F1 to F11 represented the fractions collected at 3 minute intervals corresponding to different elution condition, and CS represented unfractionated cell lysate; (B) 8-16% SDS-PAGE gel (Bio-Rad) image of individual fractions.....110

Figure 5: Multiple analyses of HEK 293 cell lysates with SAX HPLC and gel separation of fractions. (A) UV chromatograms; marked peaks are used to evaluate the reproducibility of retention time (in Table 1). (B) 4-12% SDS-PAGE gel (Invitrogen) image of individual fractions from triplicate analyses; (C) Quantitative data (average and standard deviation) of sets of gel bands marked in (B).....111

Figure 6: BSA spiking in control HEK 293 cell lysates. (A) UV chromatograms; (B) 4-12% SDS-PAGE gel (Invitrogen) image of individual fraction; (C) Intensity ratio after normalization by Western blot of internal control beta-actin on the same gel. "BSA1" refers to cell lysate spiked 10 μg BSA and "BSA2" refers to cell lysate spiked 20 μg BSA.....112

Figure 7: Mass spectra from in-gel tryptic digestion of band circled in Figure 6B "BSA2" sample. (A) MALDI-TOF based peptide mass fingerprint; the identified peptides are labeled by using their $(M+H)^+$ and sequence range. (B) ESI-FTICR-MS/MS spectrum of the 2+ charge state ions of the peptide denoted with an asterisk in Figure 7A. The observed y-series ions confirm the sequence of this BSA tryptic fragment.....113

Figure 8: Ovalbumin spiking in control HEK 293 cell lysates. (A) 4-12% SDS-PAGE gel (Invitrogen) image; (B) Intensity ratio after subtracting control as the background. Quantitative data are shown here with average values and standard deviations.....114

Figure 9: Comparison of BACE and BACE2 overexpressing cells with pcDNA3-transfected control cells. (A) UV chromatograms; (B) 8-16% SDS-PAGE gel (Bio-Rad) image of individual fractions (B = BACE, B2 = BACE2, C = control). The bands marked with numbers are the identified proteins shown in Table 2.....115

CHAPTER FOUR:

Figure 1: Schematic diagram of the implementation of the flared inlet tube. Distance Z is the distance between the spray tip and the inlet interface. Distance X is the distance that the spray tip is away from the inlet tube center. When the spray tip is aligned with the center of the inlet tube, distance X is 0.....140

Figure 2. Total ion intensity of substance P as a function of spray potential. 10 μM substance P solution was prepared in 50:50 MeOH:H_2O with 0.1% acetic acid. Infusion was performed using a syringe pump with a flow rate of 250 nl/min.....141

Figure 3: Total ion intensity of substance P as a function of the distance between spray tip and inlet interface (distance Z). Ion intensities were normalized individually using the most intense peak with or without flared inlet tube. 10 μM substance P solution was prepared in 50:50 MeOH:H_2O with 0.1% acetic acid. Infusion was performed using a syringe pump with a flow rate of 250 nl/min.....142

Figure 4: Normalized total ion intensity of substance P as a function of the distance that the spray tip was away from the inlet tube center (distance X). Ion intensities were normalized individually using the most intense peak with or without flared inlet tube. A 10 μM substance P solution was infused at a flow rate of 250 nl/min. (A) The distance between spray tip and inlet interface (distance Z) is 1mm. (B) The distance between spray tip and inlet interface (distance Z) is 10 mm.....143

Figure 5: DESI of angiotensin II on the PTFE surface. (A) DESI spectra with the highest ion intensity among 300 spectra with the flared inlet tube or with the non-flared control inlet tube. The average surface concentration of angiotensin II was 500 fmol/ mm^2. Each spectrum was accumulated 0.5 seconds and a total of 300 spectra were collected for one spot. (B) Plot of mass spectral total ion intensity versus the amount of angiotensin II spotted on the same sample holder

with disposable surface. The average of 10 highest intensities achieved from each spot was compared. Triplicate experiments were performed for each sample concentration. Inset illustrates the data in the low concentration region.....144

Figure 6: Average ion current profiling on the skimmer1 using AP-MALDI ion source. Each plot is an average of 16 laser shots on the same sample spot. The error bars represent the standard deviation of the peak measured ion current from three different sample spots 146

CHAPTER FIVE:

Figure 1: Schematic of the new interface which couples an air amplifier with a flared inlet tube. (A) Implement of the new interface with the FTICR-MS instrument; (B) Incorporation the AP-MALDI source with the new interface.....169

Figure 2: Current profile using different interface setups. (A) with flared inlet tube and no air amplifier; (B) with flared inlet tube and air amplifier (20 psi); (C) with standard inlet tube and no air amplifier; (D) with flared inlet tube and air amplifier (0 psi).....170

Figure 3: Ion intensity profile using a dual nanoelectrospray ionization device. (A) with the standard inlet tube interface; (B) with the hybrid air amplifier-flared inlet tube interface. Line with triangles indicates the ion intensity profile of angiotensin II, and line with squares indicates the ion intensity profile of substance P.....171

Figure 4: Corresponding mass spectra from the point a, b, c in Figure 3, which indicates that the adjustment of relative positions of spray tips allows the adjustment of the observed signal intensities of the two analytes.....172

Figure 5: Mass spectrum obtained using the dual nanoelectrospray device: substance P (10 μM) in one spray tip and BSA digest (10 μM) in another spray tip. The distance X in Figure 3 was

tuned until the intensity of substance P was close to the average intensity of the BSA digested peptides peaks. Peak marked with * indicates the noise peak. Part of identified BSA digested peptide peaks are marked with Δ, and the whole peak list is shown in Table 1…….....173

Figure 6: Average ion current (AP-MALDI) on skimmer1 with the air amplifier and the calculated average peak areas. (A) Coupling the air amplifier with different types of inlet tubes; (B) Comparing the interface with and without the air amplifier.....174

Figure 7: Two second ion current scan on skimmer1 using AP-MALDI ion source. A laser repetition frequency of 20 Hz was used. (A) with standard inlet tube; (B) with flared inlet tube.....175

CHAPTER SIX:

Figure 1: Mass spectra obtained from substance P deposited on the surface of aluminum using the ELDI set-up. The following operating conditions of ELDI are compared: (A) no laser pulse applied; (B) ELDI with the standard inlet tube; and (C) ELDI with the flared inlet tube.....198

Figure 2: Plot of mass spectral total ion intensity using ELDI versus the amount of substance P spotted on the sample target.....199

Figure 3: ELDI mass spectrum of substance P deposited on the surface of nitrocellulose membrane.....200

Figure 4: ELDI mass spectra of BSA in-solution digestion deposited on the surface of aluminum. (A) with the standard inlet tube; and (B) with the flared inlet tube.....201

Figure 5: (A) ELDI mass spectrum of tryptic peptides produced by on-target digestion of BSA; (B) MASCOT search results using different mass tolerances.....202

DEDICATION

To my father Youshi Wu and my mother Meixian Fang

To my sister Nan Fang

To my husband Da Meng

And

To my unborn daughter

CHAPTER ONE

Introduction

1. Proteomics and mass spectrometry

Different properties have been used to characterize bio-molecules (such as proteins and oligonucleotides). Among them, molecular weight is one of the most important and straightforward properties. A few traditional techniques could be used to determine the molecular weight of bio-molecules, including electrophoretic, chromatographic, and ultracentrifugation methods. However, the results from these methods were not very precise because they depended also on characteristics other than the molecular weight. At that time, the mass spectrometric ionization techniques such as electron ionization (EI) [1] and chemical ionization (CI) [2] required gas phase analyte molecules to be present, and thus were only suitable for volatile compounds or for samples subjected to derivatization to make them volatile. This limited considerably the application of mass spectrometry on large non-volatile biological molecules such as proteins and peptides. At the beginning of the 1990s, two new Nobel-winning ionization methods — electrospray ionization (ESI) [3] and matrix-assisted laser desorption /ionization (MALDI) [4] — were developed, which allowed a breakthrough for mass spectrometry in the field of bio-analysis.

As introduced by Fenn *et al.* [3], the electrospray ionization method is to apply a strong electric field to the solution passing through a capillary tip with a relatively slow flow rate, and an electrospray can be produced under atmospheric pressure (Figure 1). The electric field is obtained by applying a potential difference of 2-6 kV between the tip and counter electrode which are separated by several millimeters to several centimeters. The plume of droplets is

generated by electrically charging the liquid to a very high voltage, which induce a large charge accumulation at the liquid surface located at the end of the capillary tip. When the surface tension of the charged liquid drop at the tip is broken, the shape of the liquid drop changes to a "Taylor cone" and the electrospray appears. ESI has some important characteristics: it is able to produce multiply charged ions from large molecules; the electrospray current is limited by the electrochemical process that occurs at the probe tip; and it is sensitive to concentration rather than to the total amount of sample [5]. Since ESI allows very high sensitivity to be reached and is easy to couple with high performance liquid chromatography (HPLC), micro-HPLC, or capillary electrophoresis (CE), it has become the most used ionization method for high throughput proteomics study [6, 7].

MALDI is achieved in two steps (Figure 2). In the first step, the analytes are mixed in a saturated matrix solution which has a strong absorption at the applied laser wavelength. When the mixture is dried on the sample target, the matrix will form co-crystal with the analyte compounds, and the resulting analyte-doped matrix crystals can be ablated by intense pulses of laser for a short duration. The laser irradiation helps heat the crystals rapidly by the accumulation of a large amount of energy in the condensed phase through excitation of the matrix molecules. The rapid heating causes the sublimation of the matrix crystals and the formation of the expanding matrix plume. The analytes are entrained in the gas phase matrix plume. Little internal energy is then transferred to the analyte molecules, and they may be cooled during the expansion process. However, the origin of the ions produced in MALDI is still not fully understood. Typically MALDI spectra include mainly the mono-charged molecular species. MALDI-TOF-based peptide mass fingerprinting has become an important protein identification method [8-10].

With the revolution of genomics study and the development of the modern ionization sources (MALDI and ESI), mass spectrometry-based proteomics study was accelerated. Proteomics is a term in the study of all the proteins expressed by a genome; proteomics involves the identification of proteins in the body and the determination of their role in physiological and patho-physiological functions [6, 11-13]. The proteome contains information critical to the comprehensive study of biological organisms which is now known as part of the "systems biology" [14]. Proteomics research technologies are rapidly changing our understanding of complex and dynamic biological systems through different types of applications [6, 15]: 1) *Proteome mining* identifies as many proteins as possible in a sample. 2) *Protein expression profiling* identifies proteins which are differentially expressed in one system compared to another system. These proteins can be important to a particular state of the organism or cell, or as a function of physical stimulus. 3) *Protein network mapping* determines how proteins interact with each other in living systems, such as protein-protein interaction. 4) *Mapping of protein modifications* identifies how and where proteins are modified.

The necessity of characterizing the proteome requires highly efficient analytical tools that are high resolution, high sensitivity, high throughput, and robust. Modern mass spectrometric techniques and advanced analytical protein separation methods are important tools in proteomics which can provide investigators with sensitive, specific means of identifying and characterizing proteins. Mass spectrometry instrumentation has undergone tremendous change over the past decade, culminating in the development of highly sensitive, robust instruments that can reliably analyze biomolecules, particularly proteins and peptides. Protein separations serve two purposes in proteomics. First, they simplify complex protein mixtures by resolving them into small groups of proteins. Second, because they also permit apparent differences in protein

levels to be compared among different samples, protein separations can target protein abundance changes in comparative proteomics. Therefore, mass spectrometry–based proteomic research commonly consists of three stages [6]: 1) Protein samples (such as cell lysate) are isolated from their biological source. To decrease the sample complexity, protein samples are separated into different fractions using HPLC or other techniques. The final protein sample is then digested and the resulting peptide sample is further fractionated. 2) The peptide mixture is subjected to qualitative and quantitative mass-spectrometric analysis. Sometimes, the peptide mixture is further simplified to allow identification of the greatest number of components. 3) The data sets generated from the mass spectrometers are analyzed by suitable software tools to generate the possible amino acid sequences in a sample. Peptide mass fingerprinting and MS/MS spectra through database searching can be used for further protein identifications. Overall, it is the integration of protein separation and mass spectrometry technologies that provides the current technology of proteomics. We will consider each of these analytical tools in proteomics study next.

2. Protein separation methods in proteomics study

Mass spectrometry methodologies combined with other protein separation methods are the routine technologies for proteomics study. Traditionally, proteomic analyses of complex protein samples involve the resolving of proteins using two-dimensional gel electrophoresis followed by tryptic in-gel digestion. The peptides formed from tryptic digestion are then analyzed and identified either by peptide mass fingerprinting or by LC/MS/MS method. HPLC-based separation method has also been applied either to the protein complex or to the peptide complex.

2.1 Gel electrophoresis

In two-dimensional gel electrophoresis, proteins are first separated across a gel strip according to their isoelectric point (isoelectric focusing), and then separated in a perpendicular direction on the SDS-PAGE gel based on their molecular weight. Two-dimensional gel electrophoresis provides a useful analytical tool for the generation of global protein expression profiles of complex protein samples. Once the proteins are resolved in gels, protein can be visualized using various staining techniques such as Coomassie blue staining, silver staining, and SYPRO ruby staining. Two-dimensional gel electrophoresis is one of the most powerful protein separation methods, as if can resolve thousands of proteins in a single gel. However, the limited sample loading amount, reproducibility, and quantification on the first dimension of 2D gel have restricted the application of this approach to membrane protein complex, large dynamic range sample system, or comparative proteomics study. Compared to 2D gel electrophoresis technology, 1D SDS-PAGE for protein separation can minimize some of these disadvantages; it has a relatively larger sample loading amount, and multiple sample comparisons can be done in one gel by loading samples lane-by-lane. The major limitation for 1D SDS-PAGE is limited resolving capacity, which increases the complexity in a single gel band.

2.2 MudPIT

Recently, a new shotgun chromatography, Multi-Dimensional Protein Identification Technology (MudPIT), coupled with MS/MS for protein identification was developed by the Yates group [15-17]. This method can overcome some limitations of gel-based approaches and has been one of the most powerful and most popular methods for proteomics study. In this approach,

protein complexes are first digested into a more complicated peptide mixture system, and are then analyzed directly by LC-MS/MS. To decrease the complexity of the peptide mixture system, MudPIT utilizes a two-dimensional HPLC (strong cation exchange and reverse phase) for the separation of the peptide complex. Further protein identification by MS/MS data uses pattern-matching algorithms such as SEQUEST [18]. This method is robust and applicable to various systems. However, most of the complicated sample systems produce a large number of peptides after digestion, which limits the identifications of low abundance proteins using the MudPIT approach.

2.3 Other protein separation methods

Multi-dimensional liquid chromatography separation methods have also been applied to the protein complex such as cell lysates. Comprehensive 2D LC systems have been devised for the study of native and non-native proteins expressed by *E. coli*. [19, 20] The first dimension is a cation exchange column, and the second dimension is performed by RPLC. RPLC can be directly interfaced to MS for intact protein measurements. Also, the fractions from RPLC can be collected for proteolytic digestion. Recently, 2D NP-RP-HPLC has been implemented in studies for human erythroleukemia (HEL) cells [21, 22]. More than 100 proteins in the mass range up to 30 kD were identified. Overall, the advantages of performing multi-dimensional LC for protein separation are that it is relatively fast, easy to automate of sample and fraction handling, and able to interface with MS. However, compared to 2D PAGE, it has less separation capacity and does not allow the simultaneous visualization and quantification of proteins, which limits its application to protein expression profiling. To overcome this problem and provide reproducible quantitative information, we described a 2D method for protein mixture separation using a

combination of high performance liquid chromatography (HPLC) and 1D SDS-PAGE. This alternative method should be more robust, with its larger sample loading amount and higher reproducibility. We also applied this hybrid LC-Gel method for protease functionality profiling.

3. Advanced mass spectrometry methods in proteomics study

3.1 FTICR and other mass analyzers

The development of mass analyzers has been accelerated with the increasing requirements of proteomics study. Different types of mass analyzers have been developed for two different types of information: accurate molecular weight measurements and sequence information from fragmentation.

One of the commonly used mass analyzers for relatively high mass accuracy is the time-of-flight analyzer (TOF). In TOF analyzers, the mass-to-charge ratio of an analyte ion is determined by its flight time through a vacuum tube of specified length. The performance of TOF analyzers has greatly improved, particularly in terms of resolution and mass accuracy. A resolving power exceeding 12,000 has become routine on many TOF instruments, and with a proper mass calibration protocol, mass accuracies in the low parts per million (ppm) range are achievable. TOF mass analyzers can be coupled with both ESI and MALDI. Now a TOF mass analyzer can be used in conjugation with another mass analyzer, such as Q-TOF and TOF-TOF. These multistage mass analyzers can provide both accurate mass information and fragment information. For MS/MS study, however, the ion trap (IT) has unmatched sensitivity and fast acquisition time. After ion injection, however, the ions of different masses are stored together in the trap. Mass analysis can be done by ion ejection at the stability limit or by resonant ejection. MS/MS can be done by selecting one mass-to-charge ratio ion species and then fragmenting

them through the collisions with He gas. However, IT analyzers have limited resolution, low ion-trapping capacity, and low mass measurement accuracy (MMA) due to the space-charging effects. The development of linear ion trap (LIT) analyzers with higher ion-trapping capacities has expanded the dynamic range and the overall sensitivity of this technique, and LITs have been replacing classical quadrupole trapping devices. Typically, LIT instruments have an optional slow-scanning function to increase resolution. They also have multiple-stage, sequential MS/MS capabilities, in which fragment ions are iteratively isolated and further fragmented, a strategy that has proven to be very useful for the analysis of posttranslational modifications.

Fourier transform ion cyclotron resonance (FTICR) mass spectrometry provides the highest resolving power and mass measurement accuracy, which makes it a powerful technology for addressing important challenges currently faced in proteomics study. In the FTICR technique, all of the ions present in the cyclotron cell are simultaneously excited by a rapid scan of a large frequency range within a time span, which induces a trajectory that comes close to the wall perpendicular to the orbit and also put ions in phase. This allows one to transform the complex wave detected as a time-dependent function into a frequency-dependent intensity function through a Fourier transform (Figure 3). The relationship between the intensity and m/z can further be achieved using different calibration equations. Since frequency can be measured more accurately than most of the other characteristics, Fourier transform ion cyclotron resonance (FTICR) mass spectrometry has the potential for ultra-high mass measurement accuracy. Other than the accurate mass information, FTICR can also offer advantages when MS/MS approaches are applied. MS/MS can be applied either external to the ICR cell or in the ICR cell. Unlike QIT or TOF instruments, FTICR has the unique ability to simultaneously isolate various ions of

different *m/z* values by using SWIFT or correlated harmonic excitation field techniques. Different fragmentation methods can be used in the ICR cell, such as IRMPD, SORI, and ECD.

High mass measurement accuracy from FTICR-MS can increase the confidence of the protein identification. It is possible to use a single tryptic peptide mass to identify a protein if peptides can be measured at a high enough MMA. However, space charge effects in the ICR cell can reduce MMA in FTICR spectra [23-25]. These space charge effects arise from the Columbic interaction of the trapped ions in the ICR cell. They are an unavoidable consequence of ion trapping. The frequency shift induced by these space charge effects depends on changes in the total ion population in the ICR cell during experimental conditions, as compared to the total ion population present during calibration.

A number of calibration methods have been developed to correct space charge effects to obtain more accurate mass measurements. Easterling et al. [25] proposed an external calibration method using the total ion population in the ICR cell. However, this calibration method works best when the total ion population used in the calibration procedure and that of the analyte ions are carefully matched. Internal calibration using lock mass has also been introduced. An internal calibrant is added to the analyte to correct space charge-induced frequency shifts. Since the calibrant and analyte in the spectrum experience the same total ion intensity, a very similar space charge-induced frequency-shift results for both species [26]. This frequency shift is determined by matching the measured mass to the expected mass of the internal calibrant. High MMA can be achieved after the internal calibration. For LC-FTICR-MS, an internal calibrant could be applied to the whole LC run with a simultaneous dual-ESI setup, one from the LC column and one from a syringe containing the calibrant[27, 28]. However, internal calibration can be problematic since the introduction of the internal calibrant may cause ion signal suppression

in the spectra and lose the useful information of the low abundant sample. Without using an internal calibrant, Deconvolution of Columbic Affected Linearity (DeCAL) has been presented to correct space charge-induced cyclotron frequency shifts by mapping the multiple charge states of one species [29]. This is done without knowledge about exact molecular weight, ion abundances, or the identity of the species. However, for MS/MS spectra of peptides, multiple charge states are not always observable, and DeCAL may not be applicable. In our study, we have developed a novel internal calibrant-free calibration method that corrects for space charge-induced frequency shifts in FTICR fragment spectra called Calibration Optimization on Fragment Ions (COFI). This new strategy utilizes the information from fixed mass differences between two neighboring peptide fragment ions (such as y_1 and y_2) to correct the frequency shift after data collection.

3.2 Newly developed ambient ion sources

In 2004, the Cooks group introduced a new type of ambient ionization method, which is called desorption electrospray ionization (DESI) [30-32]. DESI applies to both large and small molecules. In Figure 4, the charged microdroplets used as projectiles in DESI pick up proteins and other large biomolecules from the surface, ionize them, and transport them to the mass spectrometer. This process gives the mass spectra of proteins and peptides in the solid phase, which typically closely resemble the ESI spectra of protein solutions. In addition, gas-phase solvent ions in the spray protonate or otherwise react with analyte molecules on the surface, generating ions from compounds that have low desorption energies, including volatile and semivolatile compounds (e.g., aromatic hydrocarbons and pesticides), low-polarity molecules of smaller size (e.g., terpenes and lipids), low–molecular weight polar compounds (e.g., amino acids

and drug molecules), and certain inorganic ions (e.g., perchlorate). In MS, free gas-phase analyte ions are characterized by their *m*/*z* ratio and sometimes, in more detail, by the recording of their dissociation products (MS/MS spectra) and their ion-molecule reactivity. Similar to other atmospheric ionization methods, DESI causes minimum fragmentation; that is, it is a soft ionization technique that produces low-energy, intact molecular ions. This feature is associated with fast collisional cooling of nascent ions at atmospheric pressure and ambient temperature.

Another important ambient desorption ionization method is atmospheric pressure matrix-assisted laser desorption/ionization (AP-MALDI) [33, 34]. An AP-MALDI source includes a metal sample target on which high voltage can be applied to help charged ions transfer to the mass spectrometer, a focused laser beam which provides enough energy for the desorption and ionization of analyte ions, and a nebulizing gas which can assist ion transmission from the atmospheric pressure to the high vacuum. AP-MALDI has many features in common with conventional vacuum MALDI, such as the nature of the matrix, the proportions of the matrix and analyte, sample preparation, and laser beam energy on the sample target. Both techniques are based on the process of pulsed laser beam desorption of a solid-state matrix sample mixture. For conventional MALDI, after laser desorption the target material density drops rapidly from the high value of solid phase to a low value corresponding to the high vacuum of the mass analyzer. Also, the metastable decay of ions due to the low pressure is sometimes problematic in conventional MALDI. For AP-MALDI, ions produced are less energetic than those produced by vacuum MALDI, and are thus subject to significantly less metastable decay.

A new desorption/ionization method, electrospray-assisted laser desorption ionization (ELDI) [35, 36], has been introduced by the Shiea's group, which combines some of the features of ESI with those of MALDI. This technique provides the advantage of allowing the direct,

sensitive, and rapid characterization of major proteins in biological samples such as dried biological fluids, bacterial cultures, and tissues. As shown in Figure 5, analytes are desorbed from a solid metallic or insulating sample target using a pulsed nitrogen laser. Gaseous neutral protein molecules desorbed through laser desorption are then post-ionized by their fusion with charged solvent droplets, and the subsequent ESI processes from the newly formed droplet. Since ELDI has independent control of the ionization and desorption processes, it can potentially extend the analytical capabilities of ambient ion sources.

3.3 Atmospheric pressure interface for improved ion transmission efficiency

A common challenge for the atmospheric ion source is related to the transfer of ions produced at atmospheric pressure to the mass analyzer which is normally operated under the vacuum. For all atmospheric pressure ion sources, the ions generated at atmospheric pressure are transferred to the mass analyzer in the lower pressure region through conductance limits such as a metal capillary or an orifice [37, 38]. Since ions must enter the MS through a limited cross section, the ion cloud expansion and dispersion can significantly decrease the ion transmission to the lower pressure region, and thus decrease the sensitivity of the analysis. It has also been reported that the ion transmission efficiency between the ESI emitter and the inlet of the mass spectrometer is only 0.01-0.1% [39-41]. For AP-MALDI, even with precise aperture alignment and source positioning, sampling efficiency is generally lower than the sampling efficiency in ESI [42].

Several approaches have been developed to improve ion transmission efficiencies between the ion source and the mass spectrometer. Smith et al. have developed an electrodynamic ion funnel interface that can be situated immediately after the atmospheric pressure interface of the MS for electrospray ionization mass spectrometry [37, 43-45]. The ion

funnel consists of a series of ring electrodes of progressively smaller internal diameters to which rf and dc electric potentials are co-applied. The use of the ion funnel can significantly improve the ion transmission to the analyzer region. However, the ion funnel has not achieved widespread implementation in the atmospheric pressure region where most ion losses may occur between the electrospray tip and ion sampling interface. A new dynamic focusing technique called pulsed dynamic focusing (PDF) has been developed and applied to the AP-MALDI ion source to improve ion transmission into a mass spectrometer [42, 46]. Henion et al. [47] reported an "ion spray" device in which a high-velocity sheath flow nebulizing gas was directed past the electrospray aperture tip. By optimizing the flow rate for desolvating the ions generated from the electrospray, an increase of about 30% in ion signal intensity was obtained as compared to that obtained with a lower flow rate. Covey et al. [48] developed an ESI source in which a heated gas flow was directed at an angle toward the flow axis of a nebulizer-assisted electrospray source and intersected the droplet flow in a region upstream of the orifice of the MS. This intersecting flow device can provide an increase in sensitivity of more than a factor of 10, and can significantly lower the background in the resulting mass spectra. Recent studies by Lee *et al.* [49] and Muddiman *et al.* [41] have shown large increases in ion abundance resultant from the implementation of a commercial air amplifier or a modified Venturi device in the high pressure region. They reported an 18-fold increase in ion abundance and a 34-fold reduction in the detection limit. These advancements were achieved without any aperture or capillary entrance modifications.

4. Protein identification methods in proteomics study

Known for protein identification in MudPIT, SEQUEST has been widely applied in interpreting MS/MS data based on fragment pattern matching algorithms, which provides a statistical basis for protein identification based on database search [15, 18, 50, 51]. However, it has been pointed out that a large fraction of the tentative peptide identification still falls in a gray area, wherein the peptide assignment is uncertain [52]. Additionally, sometimes the highest scoring peptide is not the real peptide. To overcome this limitation, several different groups have recommended combining the elution time from LC with MS/MS information [53, 54]. A LC normalized elution time (NET) predication method based on peptide sequence can provide accuracy within 5% of the actual elution time. This NET information can eliminate part of the errant matches from MS/MS data and also improve identification of peptides having poor fragmentation efficiencies.

Smith's group [55] proposed the concept of accurate mass tags (AMTs) and demonstrated that they can be used for proteome-wide protein identification. The most unique advantage of FTICR as a mass analyzer is that the ion mass-to-charge ratio is experimentally manifested as a frequency which can be measured more accurately than any other experimental parameters. High MMA achieved by FTICR is as low as a ppm level [56]. For some small proteomes such as *Saccharomyces*, up to 85% of the peptides predicted can function as AMTs at sub-ppm MMA levels attainable using FTICR. Smith's group also coupled high performance, high pressure chromatography with FTICR-MS to provide more sensitive and comprehensive proteome analyses based on accurate mass and elution time tags. The AMT tag database was developed using both ion trap MS/MS data and accurate mass measurement from FTICR-MS.

Robinson and Goodlett [57] pointed out that shotgun chromatography such as MudPIT (using serial data-dependent ion selection for collision induced dissociation (CID) during LC

introduction of a sample) had notable limitations with regard to both total proteome coverage and the reproducibility of detecting the same proteins in replicate analyses when used to analyze very complex mixtures. Technical breakthroughs are required for shotgun proteomic methods to minimize these limitations. These breakthroughs include increasing peak capacity of separation methods prior to the MS/MS analysis and increasing the duty cycle at which the mass spectrometer can select a single ion and move to the next available ion [58]. Rather than solving these problems, the Goodlett group proposed an alternate shotgun proteomic study method --- shotgun CID [59]. They used alternate high or low nozzle-skimmer voltage (Vns) potentials to generate two sets of parallel data: low Vns resulted in no detectable fragmentation, allowing parent ions to be measured, and high Vns caused sufficient fragmentation in the source region. Tandem mass spectra were also interpreted by SEQUEST. This method can maximize duty cycle and dynamic range by avoiding ion selection. However, more complicated fragment spectra will be produced without single ion selection. It increases the difficulties in data processing by SEQUEST, which is based on single selected ion fragmentation. Furthermore, relatively low MMA of the ion trap and TOF limit the application of this approach.

Another peptide identification method is accurate mass multiplexed tandem mass spectrometry. Peptide complex mass spectra were achieved using FTICR-MS and multiplexed tandem mass spectrometry using IRMPD [60]. With the help of the high mass accuracy from FTICR-MS, three fragment ions for one parent ion mass in this research result in 99% identification. Still, this approach uses multiple parent ion selection before fragmentation and it decreases the duty cycle due to ion selection.

Common scoring algorithms compare theoretical spectrum with collected data, scored based on their similarity, and choose the highest score for identification. In 1994, Yates first

developed a cross-correlation algorithm by which they calculated the correlated relationship between theoretical spectrum and experimental spectrum [61]. This was adopted by SEQUEST. Different protein identification software based on tandem mass spectrum have been developed such as Mascot [62], MOWSE [63], MS-Tag [64], SONOR [65], ProbID [66], and Protocall [67]. However, there are significant false positive identifications occurring in these methods [68]. Dancik [69] introduced a statistical model for the probability of formation of different type ions. This statistic model has been introduced into a newly developed tandem mass scoring algorithm named PepSearch [70]. Compared to SEQUEST, this algorithm can provide more accurate peptide identification.

5. BACE and Alzheimer's disease

Alzheimer's disease (AD) is the most common reason for dementia in old people. The prevalence of AD has been shown to increase exponentially with age [71]. There are two hallmarks of AD: senile plaques and neurofibrillary tangles (NFTs). Some other significant lesions found in AD compared to normal aging include neuronal loss, synaptic alternations, and lewy bodies [72]. Changes in the expression of proteins related to apoptotic pathways or plasticity have also been reported [71, 73-75]. However, the exact mechanism of neuron cell loss in AD is still unknown.

Braak et al. [73] proposed a model for the procession of neurofibrillary changes in AD: NFTs develop first in the entorhinal region during the preclinical stage, and then they form in the hippocampus of the patients with mild symptoms. Neocortical accumulation of NFTs formed during the later stages of AD was proposed to induce neuron cell loss. However, there are plaque-only AD cases in which NFTs are absent or very limited but a high number of senile plaques and clinically dementia are present.

Senile plaques are composed of the 4-kD Aβ peptides which are formed by the proteolytical processes of amyloid precursor protein (APP), a large transmembrane protein. Genetic and pathological evidence strongly supports the amyloid cascade hypothesis of AD, which states that Aβ42, a proteolytic derivative of APP, has an early and vital role in all cases of AD. Aβ42 forms aggregates that are thought to initiate the pathogenic cascade, leading ultimately to neuronal loss and dementia [76]. Crition [77] has proposed the amyloid cascade hypothesis, which points out that overproduction or enhanced aggregation of Aβ42 initiate the pathogenic cascade in an AD brain. Since the first proteolytical cleavage of APP to form Aβ42 occurs at β-cleavage site, β-secretase has an important role in the amyloid pathway and it has become the molecule target in many research studies [78].

BACE (β-site APP-cleaving enzyme) is an aspartyl protease recently identified by several groups[79-81], which displays all the properties expected from a real β-secretase. BACE is an acidic protease mainly localized in the Golgi apparatus and in endosomal compartments that exhibits a lumenal active site, fitting well with the luminal cleavage of βAPP occurring in these acidic compartments where Aβ has been detected [79]. Tissue culture and animal experiments indicate that BACE expressed in all tissues, but the levels are higher in the brain. Also, increased BACE activity in sporadic AD has been reported [82-84]. Since the initial behavior of the BACE knockout mice showed no obvious deficits in basal neurological and physiological functions, BACE inhibition seems to be therapeutically useful [85]. However, some abnormal behaviors such as a timid and less exploratory behavior were reported in BACE knockout mice [86]. To determine whether BACE is a good therapeutic target of AD, complete functionality of BACE and BACE interaction partner mapping should be critical.

BACE2 is a homologue protein of BACE and has 64% sequence similarity with BACE. BACE2 has the highly conserved active site with BACE [87]. It can also cut APP protein at the beta cutting site. The physiological role of BACE2 and its substrates are unknown. However, BACE2 could be important in Down syndrome pathology because the enzyme is encoded by chromosome 21 and elevated BACE2 expression is observed in trisomic brains [88]. In our study, we used both BACE overexpressed HEK293 cells and BACE2 overexpressed HEK293 cells as our model systems for the protease functionality mapping.

6. Objective of the research

Our research work addresses to several of the challenges of proteomics study. First, to reduce the proteome complexity, we have developed a hybrid HPLC-Gel-MS method and applied it to the protein expression profiling. The application of step-gradient fractionation in a strong anion exchange column provided excellent reproducibility. Protein abundance level changes were visualized with side-by-side vertical comparison in one gel. We have applied this separation strategy to the BACE and BACE2 overexpressed systems. Second, to increase the MMA and protein identification confidence in FTICR-MS, we have developed a new calibration method, COFI, for fragmentation data to correct the effects of space charge in FTICR-MS. There is no need to include an internal calibrant or to apply ion population control. COFI has been successfully applied to LC-FTICR fragmentation data. We also incorporated different atmospheric pressure ionization methods and atmospheric pressure interfaces with FTICR-MS to investigate the ionization and the ion transmission efficiencies. We set up different atmospheric pressure ionization sources such as ESI, ESSI, DESI, AP-MALDI, and ELDI. Different types of

atmospheric pressure interfaces such as a Venturi air amplifier and flared inlet tube have also been investigated.

Attributions: The text of the dissertation is in the format required for submission to the journals. Chapter two was published in *the Journal of Proteome Research*. Da Meng and I did the computer programming work. Kai Zhang provided part of the LC data. Other lab work and data analysis were performed and written by me. Chapter three was published in the *Journal of Chromatography B*. Xiaoting Tang and I did the cell overexpression and Figure 1 together. Xiaoting Tang also contributed to Figure 2. Other experiments and data analysis were done by me. Chapter four was published in the *Journal of American Society of Mass Spectrometry*. Chapter five is formatted for submission to *Journal of mass spectrometry* as a research article for publication. Chapter six is also formatted for submission as a research article for publication. All the experiments in these chapters were conducted and written by me. David C. Prior provided the initial prototype flared inlet tubes. Dr. Li Zhou and Dr. Milton L. Lee provided the original design and a prototype air amplifier. Gordon A. Anderson provided the ICR-2LS software for data procession. Therefore, their name appeared in some of the aforementioned research articles. Consultation with Dr. William F. Siems, Nathan K. Kaiser, Kai Zhang, and Gunnar Skulason has greatly enriched my work. Therefore, their names also appeared as co-authors for the respective research articles. In all these research articles, scholastic guidance and funding were provided by my advisor, Dr. James E. Bruce.

REFERNCES

1. Bleakney, W. (1929). New method of positive ray analysis and its application to the measurement of ionization potentials in mercury vapor. *Phys. Rev.* **34,** 157-160.

2. Harrison, A. G. (1983). *Chemical ionization mass spectrometry*. CRC Press, Boca Raton, FL.

3. Fenn, J. B., Mann, M., Meng, C. K., Wong, S. F. & Whitehouse, C. M. (1989). Electrospray ionization for mass spectrometry of large biomolecules. *Science* **246,** 64-71.

4. Karas, M., Bachmann, D., Bahr, U. and Hillenkamp, F. (1987). Matrix-assisted ultraviolet laser desorption of non-volatile compounds. *Int. J. Mass Spectrom. Ion Process.* **78**.

5. Mora, J. F., Van Berkel, G. J., Enke, C. G., Cole, R. B., Martinez-Sanchez, M. & Fenn, J. B. (2000). Electrochemical processes in electrospray ionization mass spectrometry. *J Mass Spectrom* **35,** 939-952.

6. Domon, B. & Aebersold, R. (2006). Mass spectrometry and protein analysis. *Science* **312,** 212-217.

7. Griffin, T. J., Han, D. K., Gygi, S. P., Rist, B., Lee, H., Aebersold, R., *et al.* (2001). Toward a high-throughput approach to quantitative proteomic analysis: expression-dependent protein identification by mass spectrometry. *J Am Soc Mass Spectrom* **12,** 1238-1246.

8. Jungblut, P. & Thiede, B. (1997). Protein identification from 2-DE gels by MALDI mass spectrometry. *Mass Spectrom Rev* **16,** 145-162.

9. Thiede, B., Hohenwarter, W., Krah, A., Mattow, J., Schmid, M., Schmidt, F., *et al.* (2005). Peptide mass fingerprinting. *Methods* **35,** 237-247.

10. Webster, J. & Oxley, D. (2005). Peptide mass fingerprinting: protein identification using MALDI-TOF mass spectrometry. *Methods Mol Biol* **310,** 227-240.

11. Aebersold, R. & Mann, M. (2003). Mass spectrometry-based proteomics. *Nature* **422,** 198-207.

12. Wu, C. C. & Yates, J. R., 3rd (2003). The application of mass spectrometry to membrane proteomics. *Nat Biotechnol* **21,** 262-267.

13. McDonald, W. H. & Yates, J. R., 3rd (2003). Shotgun proteomics: integrating technologies to answer biological questions. *Curr Opin Mol Ther* **5,** 302-309.

14. Ideker, T., Galitski, T. & Hood, L. (2001). A new approach to decoding life: systems biology. *Annu Rev Genomics Hum Genet* **2,** 343-372.

15. Washburn, M. P., Wolters, D. & Yates, J. R., 3rd (2001). Large-scale analysis of the yeast proteome by multidimensional protein identification technology. *Nat Biotechnol* **19,** 242-247.

16. Washburn, M. P., Ulaszek, R., Deciu, C., Schieltz, D. M. & Yates, J. R., 3rd (2002). Analysis of quantitative proteomic data generated via multidimensional protein identification technology. *Anal Chem* **74,** 1650-1657.

17. Wolters, D. A., Washburn, M. P. & Yates, J. R., 3rd (2001). An automated multidimensional protein identification technology for shotgun proteomics. *Anal Chem* **73,** 5683-5690.

18. Eng, J. K., McCormack, A. L. & Yates, J. R., 3rd, (1994). An approach to correlate tandem mass spectral data of peptides with amino acid sequences in a protein database. *J. Am. Soc. Mass. Spectrom.* **5,** 976-989.

19. Opiteck, G. J., Lewis, K. C., Jorgenson, J. W. & Anderegg, R. J. (1997). Comprehensive on-line LC/LC/MS of proteins. *Anal Chem* **69,** 1518-1524.

20. Opiteck, G. J., Ramirez, S. M., Jorgenson, J. W. & Moseley, M. A., 3rd (1998). Comprehensive two-dimensional high-performance liquid chromatography for the isolation of overexpressed proteins and proteome mapping. *Anal Biochem* **258,** 349-361.

21. Wall, D. B., Kachman, M. T., Gong, S., Hinderer, R., Parus, S., Misek, D. E.*, et al.* (2000). Isoelectric focusing nonporous RP HPLC: a two-dimensional liquid-phase separation method for mapping of cellular proteins with identification using MALDI-TOF mass spectrometry. *Anal Chem* **72,** 1099-1111.

22. Chen, Y., Wall, D. & Lubman, D. M. (1998). Rapid identification and screening of proteins from whole cell lysates of human erythroleukemia cells in the liquid phase, using non-porous reversed phase high-performance liquid chromatography separations of proteins followed by matrix-assisted [correction of multi-assisted] laser desorption/ionization mass spectrometry analysis and sequence database searching. *Rapid Commun Mass Spectrom* **12,** 1994-2003.

23. Ledford, E. B., Jr., Rempel, D. L. & Gross, M. L. (1984). Space charge effects in Fourier transform mass spectrometry. I. Electrons. *International Journal of Mass Spectrometry and Ion Processes* **55,** 143-154.

24. Ledford, E. B., Jr., Rempel, D. L. & Gross, M. L. (1984). Space charge effects in Fourier transform mass spectrometry. Mass calibration. *Anal Chem* **56,** 2744-2748.

25. Easterling, M. L., Mize, T. H. & Amster, I. J. (1999). Routine part-per-million mass accuracy for high-mass ions: space-charge effects in MALDI FT-ICR. *Analytical Chemistry* **71,** 624-632.

26. Taylor, P. K. & Amster, I. J. (2003). Space charge effects on mass accuracy for multiply charged ions in ESI-FTICR. *International Journal of Mass Spectrometry* **222,** 351-361.

27. Flora, J. W., Hannis, J. C. & Muddiman, D. C. (2001). High-mass accuracy of product ions produced by SORI-CID using a dual electrospray ionization source coupled with FTICR mass spectrometry. *Anal Chem* **73,** 1247-1251.

28. Lee, S. W., Berger, S. J., Martinovic, S., Pasa-Tolic, L., Anderson, G. A., Shen, Y.*, et al.* (2002). Direct mass spectrometric analysis of intact proteins of the yeast large ribosomal subunit using capillary LC/FTICR. *Proc Natl Acad Sci U S A* **99,** 5942-5947.

29. Bruce, J. E., Anderson, G. A., Brands, M. D., Pasa-Tolic, L. & Smith, R. D. (2000). Obtaining more accurate Fourier transform ion cyclotron resonance mass measurements without internal standards using multiply charged ions. *Journal of the American Society for Mass Spectrometry* **11,** 416-421.

30. Takats, Z., Wiseman, J. M., Gologan, B. & Cooks, R. G. (2004). Mass spectrometry sampling under ambient conditions with desorption electrospray ionization. *Science* **306,** 471-473.

31. Takats, Z., Wiseman, J. M., Gologan, B. & Cooks, R. G. (2004). Electrosonic spray ionization. A gentle technique for generating folded proteins and protein complexes in the gas phase and for studying ion-molecule reactions at atmospheric pressure. *Anal Chem* **76,** 4050-4058.

32. Takats, Z., Cotte-Rodriguez, I., Talaty, N., Chen, H. & Cooks, R. G. (2005). Direct, trace level detection of explosives on ambient surfaces by desorption electrospray ionization mass spectrometry. *Chem Commun (Camb)* 1950-1952.

33. Laiko, V. V., Baldwin, M. A. & Burlingame, A. L. (2000). Atmospheric pressure matrix-assisted laser desorption/ionization mass spectrometry. *Anal Chem* **72,** 652-657.

34. Laiko, V. V., Moyer, S. C. & Cotter, R. J. (2000). Atmospheric pressure MALDI/ion trap mass spectrometry. *Anal Chem* **72,** 5239-5243.

35. Shiea, J., Huang, M. Z., Hsu, H. J., Lee, C. Y., Yuan, C. H., Beech, I., *et al.* (2005). Electrospray-assisted laser desorption/ionization mass spectrometry for direct ambient analysis of solids. *Rapid Commun Mass Spectrom* **19,** 3701-3704.

36. Huang, M. Z., Hsu, H. J., Lee, J. Y., Jeng, J. & Shiea, J. (2006). Direct protein detection from biological media through electrospray-assisted laser desorption ionization/mass spectrometry. *J Proteome Res* **5,** 1107-1116.

37. Shaffer, S. A., Prior, D. C., Anderson, G. A., Udseth, H. R. & Smith, R. D. (1998). An ion funnel interface for improved ion focusing and sensitivity using electrospray ionization mass spectrometry. *Anal Chem* **70,** 4111-4119.

38. Burlingame, A. L., Boyd, R. K. & Gaskell, S. J. (1998). Mass spectrometry. *Anal Chem* **70,** 647R-716R.

39. Cech, N. B. & Enke, C. G. (2001). Practical implications of some recent studies in electrospray ionization fundamentals. *Mass Spectrom Rev* **20,** 362-387.

40. Mann, M. (1990). *In*: *Ion formation from Organic Solids V*. (Hedin, A., Sundqvist, B., Benninghoven, A., Ed), pp. 139-144. John Willey and Sons, New York.

41. Hawkridge, A. M., Zhou, L., Lee, M. L. & Muddiman, D. C. (2004). Analytical performance of a venturi device integrated into an electrospray ionization fourier transform ion cyclotron resonance mass spectrometer for analysis of nucleic acids. *Anal Chem* **76,** 4118-4122.

42. Kellersberger, K. A., Tan, P. V., Laiko, V. V., Doroshenko, V. M. & Fabris, D. (2004). Atmospheric pressure MALDI-fourier transform mass spectrometry. *Anal Chem* **76,** 3930-3934.

43. Shaffer, S. A., Tolmachev, A., Prior, D. C., Anderson, G. A., Udseth, H. R. & Smith, R. D. (1999). Characterization of an improved electrodynamic ion funnel interface for electrospray ionization mass spectrometry. *Anal Chem* **71,** 2957-2964.

44. Belov, M. E., Gorshkov, M. V., Udseth, H. R., Anderson, G. A., Tolmachev, A. V., Prior, D. C., *et al.* (2000). Initial implementation of an electrodynamic ion funnel with Fourier transform ion cyclotron resonance mass spectrometry. *J Am Soc Mass Spectrom* **11,** 19-23.

45. Belov, M. E., Gorshkov, M. V., Udseth, H. R., Anderson, G. A. & Smith, R. D. (2000). Zeptomole-sensitivity electrospray ionization--Fourier transform ion cyclotron resonance mass spectrometry of proteins. *Anal Chem* **72,** 2271-2279.

46. Tan, P. V., Laiko, V. V. & Doroshenko, V. M. (2004). Atmospheric pressure MALDI with pulsed dynamic focusing for high-efficiency transmission of ions into a mass spectrometer. *Anal Chem* **76,** 2462-2469.

47. Henion, J. D., Covey, T. R. & Bruins, A. P. (1989). US patent 4,861,988.), US patent 4,861,988.

48. Covey, T. R. (1995).), U.S. Patent 5,412,208.

49. Zhou, L., Yue, B., Dearden, D. V., Lee, E. D., Rockwood, A. L. & Lee, M. L. (2003). Incorporation of a venturi device in electrospray ionization. *Anal Chem* **75,** 5978-5983.

50. Link, A. J., Eng, J., Schieltz, D. M., Carmack, E., Mize, G. J., Morris, D. R., *et al.* (1999). Direct analysis of protein complexes using mass spectrometry. *Nat Biotechnol* **17,** 676-682.

51. MacCoss, M. J., Wu, C. C. & Yates, J. R., 3rd (2002). Probability-based validation of protein identifications using a modified SEQUEST algorithm. *Anal Chem* **74,** 5593-5599.

52. Strittmatter, E. F., Kangas, L. J., Petritis, K., Mottaz, H. M., Anderson, G. A., Shen, Y., *et al.* (2004). Application of peptide LC retention time information in a discriminant function for peptide identification by tandem mass spectrometry. *J Proteome Res* **3,** 760-769.

53. Palmblad, M., Ramstrom, M., Markides, K. E., Hakansson, P. & Bergquist, J. (2002). Prediction of chromatographic retention and protein identification in liquid chromatography/mass spectrometry. *Anal Chem* **74,** 5826-5830.

54. Petritis, K., Kangas, L. J., Ferguson, P. L., Anderson, G. A., Pasa-Tolic, L., Lipton, M. S., *et al.* (2003). Use of artificial neural networks for the accurate prediction of peptide liquid chromatography elution times in proteome analyses. *Anal Chem* **75,** 1039-1048.

55. Smith, R. D., Anderson, G. A., Lipton, M. S., Pasa-Tolic, L., Shen, Y., Conrads, T. P., *et al.* (2002). An accurate mass tag strategy for quantitative and high-throughput proteome measurements. *Proteomics* **2,** 513-523.

56. Belov, M. E., Zhang, R., Strittmatter, E. F., Prior, D. C., Tang, K. & Smith, R. D. (2003). Automated gain control and internal calibration with external ion accumulation capillary liquid chromatography-electrospray ionization Fourier transform ion cyclotron resonance. *Anal Chem* **75,** 4195-4205.

57. Spahr, C. S., Davis, M. T., McGinley, M. D., Robinson, J. H., Bures, E. J., Beierle, J., *et al.* (2001). Towards defining the urinary proteome using liquid chromatography-tandem mass spectrometry. I. Profiling an unfractionated tryptic digest. *Proteomics* **1,** 93-107.

58. Goodlett, D. R. & Yi, E. C. (2002). Proteomics without polyacrylamide: qualitative and quantitative uses of tandem mass spectrometry in proteome analysis. *Funct Integr Genomics* **2,** 138-153.

59. Purvine, S., Eppel, J. T., Yi, E. C. & Goodlett, D. R. (2003). Shotgun collision-induced dissociation of peptides using a time of flight mass analyzer. *Proteomics* **3,** 847-850.

60. Masselon, C., Anderson, G. A., Harkewicz, R., Bruce, J. E., Pasa-Tolic, L. & Smith, R. D. (2000). Accurate mass multiplexed tandem mass spectrometry for high-throughput polypeptide identification from mixtures. *Anal Chem* **72,** 1918-1924.

61. Yates, J. R., 3rd, Eng, J. K. & McCormack, A. L. (1995). Mining genomes: correlating tandem mass spectra of modified and unmodified peptides to sequences in nucleotide databases. *Anal Chem* **67,** 3202-3210.

62. Perkins, D. N., Pappin, D. J., Creasy, D. M. & Cottrell, J. S. (1999). Probability-based protein identification by searching sequence databases using mass spectrometry data. *Electrophoresis* **20,** 3551-3567.

63. Pappin, D. J., Hojrup, P. & Bleasby, A. J. (1993). Rapid identification of proteins by peptide-mass fingerprinting. *Curr Biol* **3,** 327-332.

64. Clauser, K. R., Baker, P. & Burlingame, A. L. (1999). Role of accurate mass measurement (+/- 10 ppm) in protein identification strategies employing MS or MS/MS and database searching. *Anal Chem* **71,** 2871-2882.

65. Field, H. I., Fenyo, D. & Beavis, R. C. (2002). RADARS, a bioinformatics solution that automates proteome mass spectral analysis, optimises protein identification, and archives data in a relational database. *Proteomics* **2,** 36-47.

66. Zhang, N., Aebersold, R. & Schwikowski, B. (2002). ProbID: a probabilistic algorithm to identify peptides through sequence database searching using tandem mass spectral data. *Proteomics* **2,** 1406-1412.

67. Wool, A. & Smilansky, Z. (2002). Precalibration of matrix-assisted laser desorption/ionization-time of flight spectra for peptide mass fingerprinting. *Proteomics* **2,** 1365-1373.

68. Keller, A., Purvine, S., Nesvizhskii, A. I., Stolyar, S., Goodlett, D. R. & Kolker, E. (2002). Experimental protein mixture for validating tandem mass spectral analysis. *Omics* **6,** 207-212.

69. Dancik, V., Addona, T. A., Clauser, K. R., Vath, J. E. & Pevzner, P. A. (1999). De novo peptide sequencing via tandem mass spectrometry. *J Comput Biol* **6,** 327-342.

70. Sheng, Q. H., Tang, H. X., Xie, T., Wang, L. S. & Ding, D. F. (2003). [A novel approach for peptide identification by tandem mass spectrometry]. *Sheng Wu Hua Xue Yu Sheng Wu Wu Li Xue Bao (Shanghai)* **35,** 734-740.

71. Jorm, A. F. & Jolley, D. (1998). The incidence of dementia: a meta-analysis. *Neurology* **51,** 728-733.

72. Esiri, M. M. (1996). The basis for behavioural disturbances in dementia. *J Neurol Neurosurg Psychiatry* **61,** 127-130.

73. Braak, H. & Braak, E. (1995). Staging of Alzheimer's disease-related neurofibrillary changes. *Neurobiol Aging* **16,** 271-278; discussion 278-284.

74. Crawford, F. A., Jr., Anderson, R. P., Clark, R. E., Grover, F. L., Kouchoukos, N. T., Waldhausen, J. A., *et al.* (1996). Volume requirements for cardiac surgery credentialing: a critical examination. The Ad Hoc Committee on Cardiac Surgery Credentialing of The Society of Thoracic Surgeons. *Ann Thorac Surg* **61,** 12-16.

75. Mikkonen, M., Soininen, H., Alafuzof, I. & Miettinen, R. (2001). Hippocampal plasticity in Alzheimer's disease. *Rev Neurosci* **12,** 311-325.

76. Hardy, J. (2002). Testing times for the "amyloid cascade hypothesis". *Neurobiol Aging* **23,** 1073-1074; author reply 1101-1075.

77. Citron, M. (2004). Strategies for disease modification in Alzheimer's disease. *Nat Rev Neurosci* **5,** 677-685.

78. John, V., Beck, J. P., Bienkowski, M. J., Sinha, S. & Heinrikson, R. L. (2003). Human beta-secretase (BACE) and BACE inhibitors. *J Med Chem* **46,** 4625-4630.

79. Vassar, R. (2001). The beta-secretase, BACE: a prime drug target for Alzheimer's disease. *J Mol Neurosci* **17,** 157-170.

80. Vassar, R., Bennett, B. D., Babu-Khan, S., Kahn, S., Mendiaz, E. A., Denis, P., *et al.* (1999). Beta-secretase cleavage of Alzheimer's amyloid precursor protein by the transmembrane aspartic protease BACE. *Science* **286,** 735-741.

81. Yan, R., Bienkowski, M. J., Shuck, M. E., Miao, H., Tory, M. C., Pauley, A. M., *et al.* (1999). Membrane-anchored aspartyl protease with Alzheimer's disease beta-secretase activity. *Nature* **402,** 533-537.

82. Fukumoto, H., Cheung, B. S., Hyman, B. T. & Irizarry, M. C. (2002). Beta-secretase protein and activity are increased in the neocortex in Alzheimer disease. *Arch Neurol* **59,** 1381-1389.

83. Holsinger, R. M., McLean, C. A., Beyreuther, K., Masters, C. L. & Evin, G. (2002). Increased expression of the amyloid precursor beta-secretase in Alzheimer's disease. *Ann Neurol* **51,** 783-786.

84. Li, R., Lindholm, K., Yang, L. B., Yue, X., Citron, M., Yan, R., *et al.* (2004). Amyloid beta peptide load is correlated with increased beta-secretase activity in sporadic Alzheimer's disease patients. *Proc Natl Acad Sci U S A* **101,** 3632-3637.

85. Roberds, S. L., Anderson, J., Basi, G., Bienkowski, M. J., Branstetter, D. G., Chen, K. S., *et al.* (2001). BACE knockout mice are healthy despite lacking the primary beta-secretase activity in brain: implications for Alzheimer's disease therapeutics. *Hum Mol Genet* **10,** 1317-1324.

86. Harrison, S. M., Harper, A. J., Hawkins, J., Duddy, G., Grau, E., Pugh, P. L., *et al.* (2003). BACE1 (beta-secretase) transgenic and knockout mice: identification of neurochemical deficits and behavioral changes. *Mol Cell Neurosci* **24,** 646-655.

87. Farzan, M., Schnitzler, C. E., Vasilieva, N., Leung, D. & Choe, H. (2000). BACE2, a beta -secretase homolog, cleaves at the beta site and within the amyloid-beta region of the amyloid-beta precursor protein. *Proc Natl Acad Sci U S A* **97,** 9712-9717.

88. Motonaga, K., Itoh, M., Becker, L. E., Goto, Y. & Takashima, S. (2002). Elevated expression of beta-site amyloid precursor protein cleaving enzyme 2 in brains of patients with Down syndrome. *Neurosci Lett* **326,** 64-66.

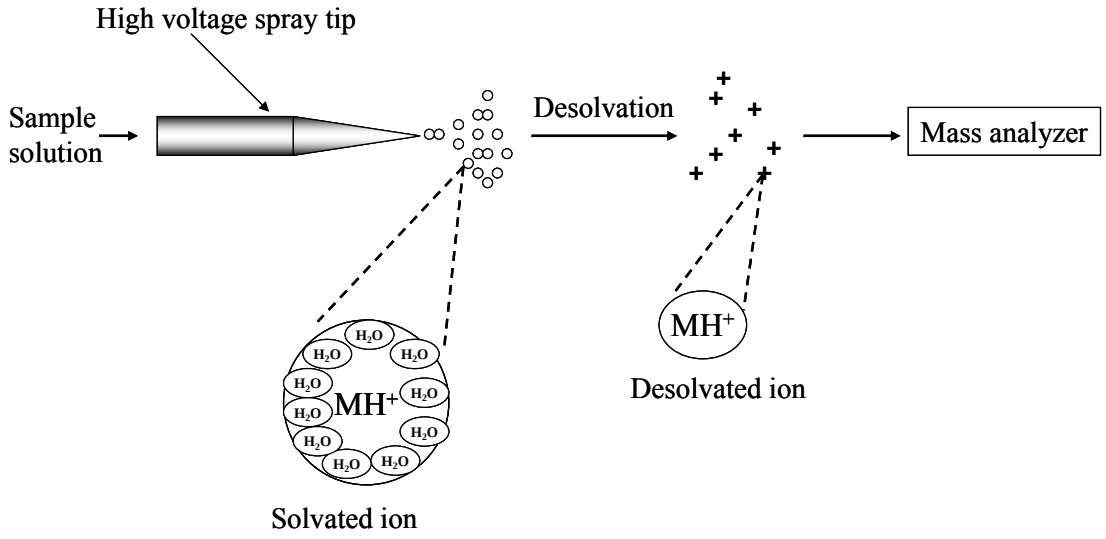

Figure 1. Schematic representation of an ESI source

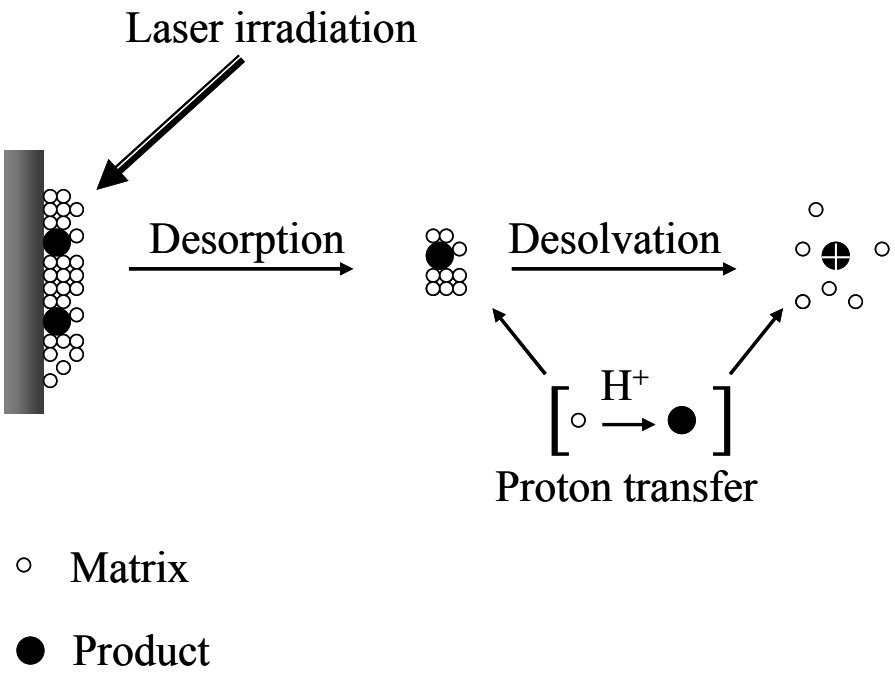

Figure 2. Diagram of the principle of MALDI.

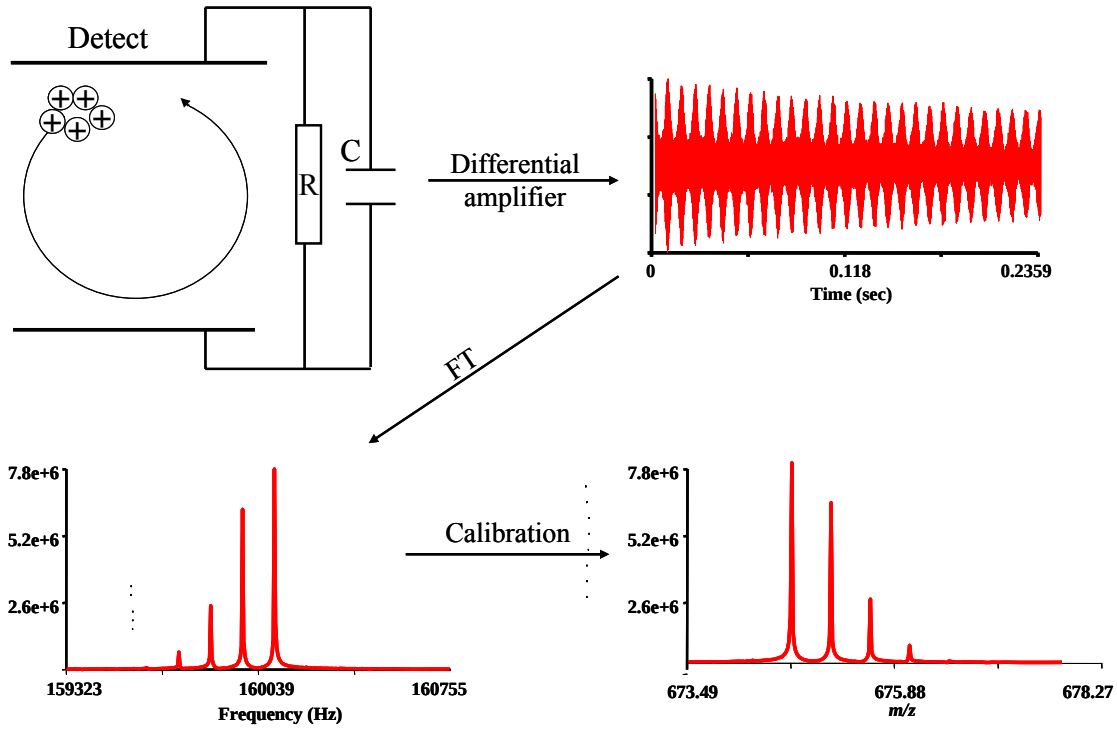

Figure 3. Schematic presenting of data processing in FTICR mass spectra.

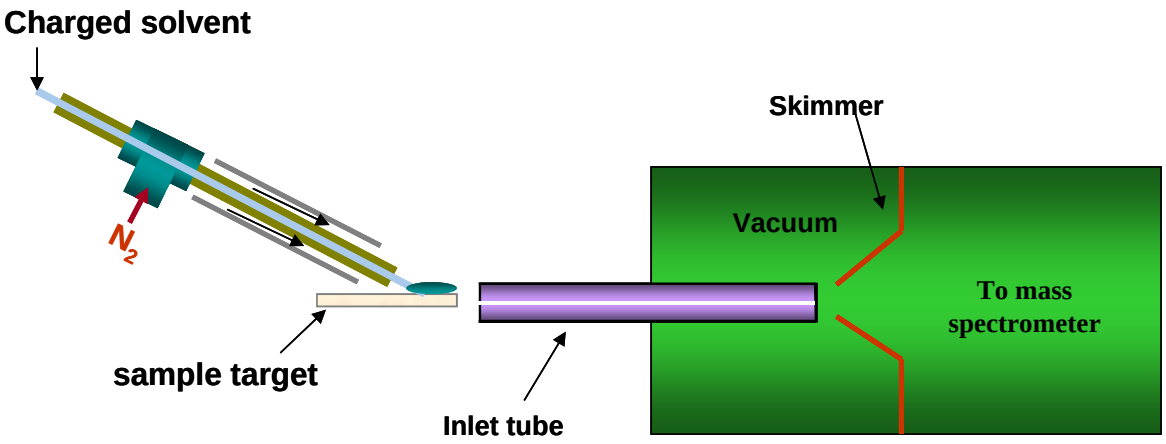

Figure 4. Schematic representation of a DESI source.

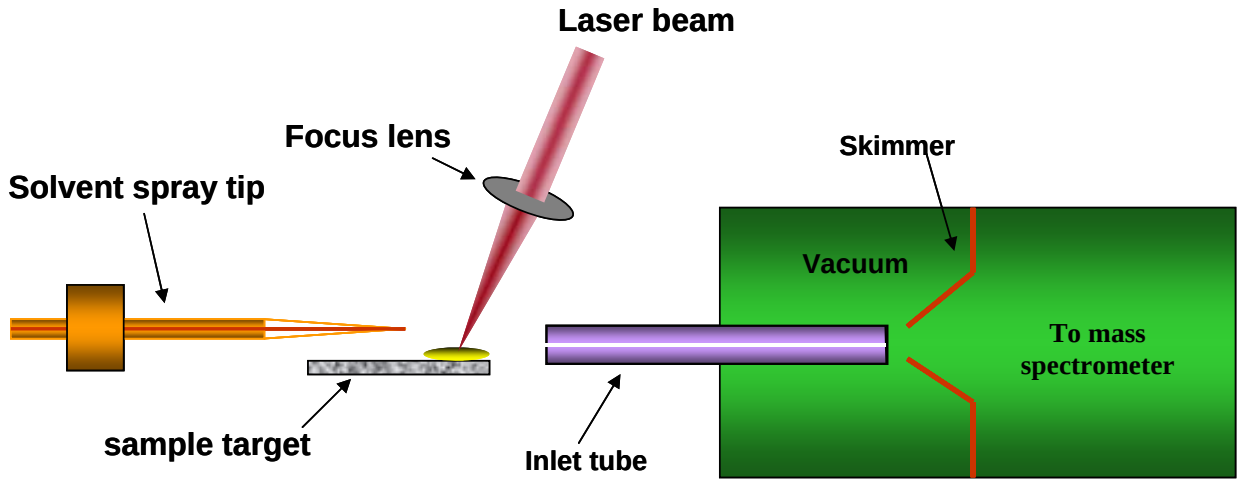

Figure 5. Schematic representation of an ELDI source.

CHAPTER TWO

Increased Protein Identification Capabilities through Novel Tandem MS Calibration Strategies

Si Wu[1], Nathan K. Kaiser[1], Da Meng[2], Gordon A. Anderson[3],

Kai Zhang[1], and James E. Bruce[1*]

[1] Department of Chemistry, Washington State University, Pullman, WA 99164

[2] Department of EECS, Washington State University, Pullman, WA 99164

[3] Environmental Molecular Research Laboratory, Pacific Northwest National Laboratory, Richland, WA 99352

*Corresponding author: James E. Bruce
Washington State University
Department of Chemistry
P.O. Box 644630
Pullman, WA, 99164-4630
Fax: (509) 335-8867
Email: james_bruce@wsu.edu

Published at *Journal of Proteome Research 2005*;4:1434-41.

ABSTRACT

High mass measurement accuracy is critical for confident protein identification and characterization in proteomics research. Fourier transform ion cyclotron resonance (FTICR) mass spectrometry is a unique technique which can provide unparalleled mass accuracy and resolving power. However, the mass measurement accuracy of FTICR-MS can be affected by space charge effects. Here we present a novel internal calibrant-free calibration method that corrects for space charge-induced frequency shifts in FTICR fragment spectra called Calibration Optimization on Fragment Ions (COFI). This new strategy utilizes the information from fixed mass differences between two neighboring peptide fragment ions (such as y_1 and y_2) to correct the frequency shift after data collection. COFI has been successfully applied to LC-FTICR fragmentation data. Mascot MS/MS ion search data demonstrate that most of the fragments from BSA tryptic digested peptides can be identified using a much lower mass tolerance window after applying COFI to LC-FTICR-MS/MS of BSA tryptic digest. Furthermore, COFI has been used for multiplexed LC-CID-FTICR-MS which is an attractive technique because of its increased duty cycle and dynamic range. After the application of COFI to a multiplexed LC-CID-FTICR-MS of BSA tryptic digest, we achieved an average measured mass accuracy of 2.49 ppm for all the identified BSA fragments.

INTRODUCTION

Mass spectrometry (MS) has been widely applied to many areas of biological research. One of those areas is the study of the proteome in which MS is used for protein identification, protein modification characterization, protein interaction mapping, and biomarker identification [1-5]. In proteomics research, one of the major challenges has been to develop high-throughput approaches for systematic and comprehensive protein analysis from biological samples [6]. Mass measurement accuracy is a critical feature of high-throughput proteomics. It is well-known that the number of protein or peptide candidates drops rapidly with increasing mass measurement accuracy (MMA) [5, 7, 8]. Smith and co-workers did a detailed exploration of the importance of MMA for the identification of tryptic digest products from yeast and *C. elegans* and proposed that a single peptide mass could serve as an accurate mass tag (AMT) to identify a protein if measured at sufficiently high MMA [5, 9].

Fourier transform ion cyclotron resonance (FTICR) mass spectrometry has the potential for ultra-high mass measurement accuracy, large dynamic range, and high sensitivity, which can provide the highest quality data for biological analyses [5, 9-11]. Accurate mass information from FTICR-MS provides more confidence in characterization of bio-molecules. However, space charge effects in the ICR cell can reduce MMA. These space charge effects arise from the Columbic interaction of the trapped ions in the ICR cell [12-14]. The frequency shift induced by these space charge effects depends on changes in the total ion population in the ICR cell during experimental conditions, as compared to the total ion population present during calibration [14]. Even after very careful external calibration, spaced charge-induced frequency shifts can result in

mass measurement errors of more than 100 ppm when the total ion populations vary between the calibration and analyte spectra [14-16].

A number of calibration methods have been developed to correct space charge effects to obtain more accurate mass measurements. External calibration works best when the total ion population used in the calibration procedure and that of the analyte ions are carefully matched [14]. An internal calibrant can be added to the analyte to correct space charge-induced frequency shifts. Since calibrant and analyte in the spectrum experience the same total ion intensity, a very similar space charge-induced frequency shift results for both species [17]. This frequency shift is determined by matching the measured mass to the expected mass of calibrant by shifting the calibration equation and then this revised calibration equation is applied to all ions present in the ICR cell to obtain improved mass measurement accuracy. In effect, this results in a constant frequency offset that is either added or subtracted from the entire set of measured frequencies and high mass measurement accuracy can be achieved after the internal calibration. For LC-FTICR-MS, Lee et al. [18, 19] applied an internal calibrant to the whole LC run with a simultaneous dual-ESI setup, one from the LC column and one from a syringe containing the calibrant. This internal calibrant is used as a "lock mass" during data processing. Another method has been developed which does not require the use of an internal calibrant. Deconvolution of Columbic Affected Linearity (DeCAL) has been presented to correct space charge-induced cyclotron frequency shifts by mapping multiple charge states of one species [16]. This was done without knowledge about exact molecular weight, ion abundances, or the identity of the species.

High mass measurement accuracy can also be very critical for efficient usage of fragmentation spectra. The number of fragment ion masses required for positive identification of a peptide is decreased as the mass accuracy increases [20]. Therefore, high mass measurement

accuracy in fragmentation spectra will benefit protein identification in a complex peptide mixture sample. For FTICR-MS/MS experiments, an internal calibrant can also be incorporated. A stable peptide was introduced as the internal calibrant for FTICR-MS/MS on an oligonucleotide using Infrared Multiphoton Photodissociation (IRMPD) [21]. In product spectra, the oligonucleotide was dissociated to form fragment ions while the stable peptide remained intact. However, in some cases the spiked internal standard can limit the dynamic range of biological sample analysis. Another internal calibrant method using a dual electrospray source was presented by Muddiman et al. [18] Singly charged low molecular weight oligomer PEG ions were chosen as the internal calibrants and were introduced by hexapole accumulation and gated trapping after parent ion dissociation. Simultaneous detection of the product ions and PEG ions results in accurate mass detection of fragment ions. However, hexapole accumulation time needs to be controlled to establish sufficient internal standard intensity for mass calibration. DeCAL has been applied on protein electron capture dissociation (ECD) spectra and improvement in mass measurement accuracy has been demonstrated [22]. However, at least two charge states of the same molecular species are required for this calibration strategy, which may not be always present in peptide fragment ion spectra.

To achieve high mass measurement accuracy in LC-FTICR-MS/MS, automated gain control can be used to control the number of ions entering the ICR cell [23-25]. Mass accuracy of 2 ppm with external calibration has been reported. However, this method limits the need to correct for space charge effects by controlling the total ion population that enters the ICR cell. However, control of the ion population by limiting the number of ions allowed in the ICR cell can be problematic since low abundant peptides may not produce enough fragment ion information to be detected. This method can reduce the dynamic range of the instrument. Also, an additional

apparatus is needed for automated gain control, which can increase the complexity of the experiment.

In this paper, we describe a novel post-acquisition data processing method to improve mass measurement accuracy in fragmentation spectra. For protein or peptide fragmentation, a series of fragments are typically observed and the mass difference of two neighboring fragments (such as y_1 and y_2) is one amino acid residue mass. Space charge-induced frequency shifts can be compensated by linearly shifting the cyclotron frequency to match the mass difference of two neighboring fragments to the exact mass of the amino acid residue. The optimum correction for the effect of space charge on cyclotron frequency is produced when the minimum mismatch error is obtained between corresponding monoisotopic peaks from selected neighboring fragment pairs. A new linearity-*k*-test method is also demonstrated in this paper to verify the calculated frequency shift based on the observed linearity trend of the mass measurement errors vs. ***m/z*** values. Our calibration program called Calibration Optimization on Fragment Ions, or COFI, optimizes frequency shift and then uses this frequency shift as the basis to recalculate all masses in the spectrum. Improved mass accuracy has been demonstrated in this paper by correcting for the frequency shift calculated by COFI. As was the case with DeCAL, this method does not require the addition of internal standards because the exact mass of the peptide fragment pairs need not be known. However, an advantage of present approach is that multiple charge states are not needed in COFI which makes it extremely useful for fragmentation experiments using any ionization sources such as ESI or MALDI. Also, COFI is performed by post-acquisition data processing, which is particularly attractive for coupling with LC on-line separations where large scan-to-scan variations in ion population typically occur in the absence of trapped ion population control strategies.

EXPERIMENTAL PROCEDURES

Chemicals

All the standard proteins and peptides were purchased from Sigma (St. Louis, MO) and used without further purification. Sequencing grade modified trypsin was purchased from Promega (Madison, WI). Water used in these experiments was purified (18 MΩ*cm) using a Nanopure ultra-purified water system (Barnstead International, Boston, MA).

Instrumentation

Bruker-Daltonics Apex-Q FTICR mass spectrometer with a 7.0 T superconducting magnet was used for all the MS experiments. All nano-ESI spray tips were made by etching from a 20-μm-i.d., 360-μm-o.d. fused-silica capillary with 49% HF. The voltage on the capillary inlet tube was set at -2 kV. For direct infusing experiments, solutions of the peptides were prepared in 49:49 MeOH:H_2O with 2% acetic acid. Infusion was performed using a syringe pump at a flow rate of 250 nl/min. The ions were sent to the first hexapole through a glass capillary. The ions then passed through a quadrupole which can be used to select the specific ***m/z*** species of interest to be fragmented. A second hexapole was used for either accumulating ions or fragmenting ions using different collision cell trap energy. After passing the second hexapole, the ions were then sent toward the ICR cell using a series of electrostatic focusing elements. The ions were trapped in the ICR cell using a low energy sidekick potential [26] to keep the ions close to the central Z axis of the ICR cell. All Data sets acquired were 128k points and the achieved mass resolution was approximately 20,000. The mass spectral data were acquired using Xmass 7.0.6 as the data acquisition software program. The external calibration was done

with a mixture solution of standard peptides. The calibration function that was used to convert ion cyclotron frequency to *m/z* values is represented by Equation 1, where *A* and *B* are calibration constants, and *f* is the measured cyclotron frequency.

$$m/z = \frac{A}{(f - B)} \qquad (1)$$

LC-FTICR-MS/MS and multiplexed LC-FTICR-MS

Nano-HPLC separation was performed with an LC packings Ultimate Nano-HPLC system equipped with a Famos micro autosampler and a Swichos micro column switching module (Dionex, Sunnyvale, CA, USA). Reverse phase solvents were (A) 0.1 % TFA in 2% acetonitrile and (B) 0.1% TFA in 95% acetonitrile. Samples were first injected by the autosampler and loaded onto a micro trap column (C18 PepMap, 300 μm × 1mm, 5μm, LC packings) at a flow rate of 50 μl/min with solvent A. 10 μl BSA digestion solution (1 μM) was injected onto the RPLC column. The loaded sample was continuously washed with solvent A for 3 minutes to remove salts. Peptides were then eluted at a flow rate of 300 nL/min to an analytical column (C18 PepMap, 75μm × 150mm, 3μm, 100 Å, LC packings) and separated using the following gradient: 0% B for 0-5 min, 0-15% B for 5-15 min, 15-25% B for 15-60 min, 25-40% B for 60-80 min, 95% B for 80-90 min, and 0% B for 91-120 min. The eluant from the analytical column was sprayed on-line with the mass spectrometer.

For the LC-FTICR-MS/MS experiment, the initial MS scan utilized an ***m/z*** range of 300-2500 followed by a tandem MS scan. Dynamic exclusion was activated to discriminate against previously selected ions. Collision cell energies were selected according to the default energy file in XMASS 7.0.6. For the multiplexed LC coupled collision-induced dissociation experiment (LC-CID-FTICR-MS), no isolation of the previously selected ions was done. After MS scan, all

the ions were sent to the hexapole. Collision cell energies were also selected according to the default energy file (peptides.cef) in XMASS 7.0.6. This file contains the slope and intercept values for calculation the optimal MS/MS collision energy for a specific charge state. For 1+ ions, the slope is 0.027 and the intercept is 17.044. For 2+ ions, slope is 0.0386 and the intercept is -3.5576. For 3+ or charge state larger than 3 ions, the slope is 0.0291 and the intercept is -1.0453.

Data analysis

All FTICR-MS data were analyzed using ICR-2LS software package [27]. Time-domain signals were apodized (Welch) and zero-filled (2) before Fourier transformation to the mass spectra. COFI was applied for the data calibration. All the programs in COFI were coded in MATLAB 6.5, and computations and simulations were performed on a HP Pavilion computer. Mass Spectrometry protein sequence DataBase (MSDB) was applied for all the study of the algorithm performance.

Methodology

Fragmentation of a peptide or a protein in MS experiments can provide sequence information by forming peptide fragments that differ by one amino acid residue [9, 28, 29]. For convenience we adopted the concept of type-1 edge to describe a pair of neighboring fragment ions described by Yan et al.[30] The mass difference between the masses of a type-1 edge such as y_n and y_{n+1} should be the exact mass of the lost amino acid residue. However, space charge effects arise if the total charge in the ICR cell during the experiment is different than the total charge in the ICR cell during calibration. The resultant cyclotron frequency shift of all ions in

the ICR cell should be the same to a first-order approximation. Due to this constant frequency shift across the entire spectrum, the higher ***m/z*** species will experience a larger relative mass measurement error. Since ***m/z*** values are shifted to different degrees in the mass spectrum resultant from the inverse relationship between ***m/z*** and measured frequency *f*, the mass difference between the calculated masses of a type-1 edge which has the identical charge state is not the exact mass of the lost amino acid residue. Since FTICR allows direct measurement of charge state, verification the mass differences between identically-charged fragment ions can be examined. By correcting the frequency shift, the measured mass difference of a type-1 edge should match the exact mass of the lost amino acid residue.

For a singly positively charged species resulting from protonation or other cation attachment, the relationship between the mass of a given fragment ion and the ion cyclotron frequency is represented by Equation 2. M in the equation is the molecular weight, s is a proportionality constant which relates ***m/z*** to the magnetic field B and the cyclotron frequency f, and M_c is the mass of the charge carrier.

$$M = (\frac{sB}{f}) - M_c \tag{2}$$

For a type-1 edge, the mass difference (ΔM) between two singly charged fragment ions (M_1 and M_2) is shown in Equation 3 (where M_2 is larger than M_1):

$$\Delta M = M_2 - M_1 = \frac{sB}{f_2} - \frac{sB}{f_1} \tag{3}$$

When the space charge-induced frequency shift (Δf) is corrected, M_1 approaches $M_{1,theoretical}$, M_2 approaches $M_{2,theoretical}$, and ΔM approaches the exact mass (M_{aa}) of the amino acid residue between the fragment pair since

$$M_{aa} = M_{1.theoretical} - M_{2,theoretical} \tag{4}$$

This resultant delta frequency should be the same as the frequency shift due to the space charge effects. The optimal frequency offset can be determined by matching ΔM to M_{aa}.

Linearity-*k*-test

Figure 1 illustrates the mass measurement errors of the fragment ions of substance P before frequency correction. The observed mass errors of the fragment ions in the spectrum give a visual indication of the systematic error that occurs. As the ***m/z*** values increase, the errors also increase in a linear fashion. This relationship can be described using a linear equation as below, in which *k* is used as the proportionality constant.

$$\frac{(m/z)_{measured} - (m/z)_{theoretical}}{(m/z)_{theoretical}} = k \times (m/z)_{theoretical} \tag{5}$$

So,

$$(m/z)_{measured} - (m/z)_{theoretical} = k \times (m/z)^2_{theoretical} \tag{6}$$

For a true type-1 edge, the difference ($M_{aa} - \Delta M$) between the exact amino acid mass (M_{aa}) and the measured amino acid mass (ΔM) can be described using the following equation:

$$\begin{aligned} \Delta M - M_{aa} &= [(m/z)_{1,measured} - (m/z)_{2,measured}] - [(m/z)_{1,theoretical} - (m/z)_{2,theoretical}] \\ &= k \times [(m/z)^2_{1,theoretical} - (m/z)^2_{2,theoretical}] \end{aligned} \tag{7}$$

For any type-1 edge,

$$k = (\Delta M - M_{aa}) \Big/ [(m/z)^2_{1,theoratical} - (m/z)^2_{2,theoratical}] \tag{8}$$

When $(\Delta M - M_{aa}) = 0, k \equiv 0$. Since $[(m/z)^2_{1,theoretical} - (m/z)^2_{2,theoretical}]$ is independent of frequency, all the type-1 edges in the same spectrum should have the same *k* value, and this *k* value is only affected by the resultant frequency shift.

After correcting the frequency shift using type-1 edge information, all the ***m/z*** values are recalculated. The resultant ***m/z*** values of true fragment ions should be close to their theoretical ***m/z*** values. If we then use the recalculated ***m/z*** values to substitute $(m/z)_{theoretical}$ in Equation 8 and use ΔM before correcting the frequency shift, the resultant *k* values of the type-1 edges should approximate the true value of *k* before the frequency shift. For each predicted type-1 edge in a single spectrum, a *k* value can be calculated. The *k* values of the type-1 edges are clustered around the same value, while the *k* values of misassigned fragment pairs, should be distributed randomly. These misassigned pairs can be eliminated by applying statistical tests on the calculated *k* values of all the selected type-1 edges. Here we call it linearity-*k* test. The linearity-*k* test is also used to verify the calculated frequency shift. We implemented this linearity-*k* test in our program COFI.

Program

To apply COFI to unknown fragmentation data, the Horn mass transformation program [31] in ICR-2LS is used to generate mass information saved in the data structures to be corrected by COFI. The original data structures in COFI include charge state, ***m/z***, intensity, fit, average MW, monoisotopic MW, and most abundant MW. The calibration function that was used to convert ion cyclotron frequency to ***m/z*** values is represented by Equation 2. The candidate pairs are selected by matching the mass differences to the exact amino acid residue masses within the chosen mass tolerance range. Each pair is then used to calculate the frequency shift for the

minimum $\left|M_{aa} - \Delta M\right|$ (as described above). A Q test was implemented in the algorithm to discard questionable data with 95% confidence level, as described elsewhere[32]. After the Q-test was performed, a frequency shift is determined by calculating a weighted average of the frequency shifts measured for each candidate pair. The resultant frequency shift applies to all ***m/z*** species in the spectrum. A linearity-*k* test is then applied for all the ***m/z*** values in the spectrum to verify all the candidate pairs. After the linearity-*k*-test, a new frequency shift is then recalculated. The resulting "optimal" frequency shift is then used as the basis to recalculate all masses that are reported.

RESULTS AND DISCUSSION

Tandem mass spectrum of substance P

A plot of resultant errors in ppm of the identified fragment ions vs. *m/z* of the MS/MS spectrum of substance P is shown in Figure 1. We plotted the absolute average mass error of all the identified substance P fragment ions shown in Figure 1 with the frequency offset (Figure 2). The frequency offset corresponding to the smallest average mass error is 5.5 Hz (plotted and calculated by a Matlab 6.5 coded program). COFI was applied to the same set of fragmentation data to allow determination of frequency shift. The candidate pairs were chosen by using the mass tolerance of 0.03 Da. Only singly charged fragment pairs were used here. After Q-test, nine candidate pairs were chosen by COFI, as shown in both Figure 3 and Table 1. In Figure 3, the absolute value of the difference between the exact amino acid mass (M_{aa}) and the measured amino acid mass (ΔM) is plotted as a function of the frequency offset. All the calculated frequency offset values are listed in Table 1. From both Figure 3 and Table 1, we found that the frequency offsets obtained from these pairs were not only close to each other but also very close to the frequency offset when the average mass error reached a minimum value in Figure 2.

After COFI, the resultant "optimal" frequency shift was 5.3 Hz and agreed well with the calculated frequency offset from the minimum average mass error (in Figure 2). We applied this frequency offset to the entire spectrum, and recalculated all the masses. The resultant mass errors of the fragment ions before and after the frequency shift are listed in Table 2. After COFI, the absolute mass errors ranged from 0 ppm to 4 ppm. The average mass error after frequency correction was 1.93 ppm. The mass measurement errors of the fragment ions of substance P after frequency correction were then plotted with their *m/z* values (Figure 4). As compared to

Figure 1, this plot shows a substantial improvement in error and the feasibility of correction of systematic errors resultant from a constant frequency offset.

Multiplexed CID spectrum

Multiplexed fragmentation is an extremely attractive technique to couple with LC on-line separation because of its increased duty cycle and dynamic range [33-38]. Instead of isolating and fragmenting one specific *m/z* species at a time, multiplexed fragmentation fragments multiple peptides simultaneously. This is done by either selecting several of the most abundant peptides [37, 38], or by fragmenting every *m/z* species present during a LC run [33]. COFI is most advantageous for the analysis of multiplexed fragmentation spectra. When all the *m/z* species present are fragmented, most of the abundant peptides have a chance to generate intense fragment species, while less abundance peptides are less likely to produce intense fragment species. After COFI, the "optimal" frequency shift is applied to all the ***m/z*** species in the spectrum. Importantly, COFI corrects fragment masses not only from the most abundance peptides but also from low abundance peptides so that all ions are measured with high mass accuracy after frequency shift correction.

Figure 5 is the fragmentation (CID) spectrum of a peptide mixture without isolating any parent ions. The three standard peptides in the mixture include bradykinin, angiotensin I, and substance P. The concentration of each peptide was 10 μM. The instrument was calibrated using 10 μM angiotensin I several days before the experiment. Since the total concentration of this sample was 3 times larger than the concentration of the calibration solution, ion population of the CID spectrum of the peptide mixture was different from the ion population used for the external calibration. This difference can lead to relatively large mass errors. Before COFI, the

average mass measurement error of all the matched fragment ions is about 45.66 ppm as shown in Table 3. COFI was then applied to the correct space charge-induced frequency shift in this spectrum. After COFI application, more than 20 fold improvement on mass measurement accuracy was achieved (Table 3). This suggested that COFI can be used to correct space charge-induced frequency shifts within a complex spectrum and this capability should be useful with on-line chromatographic separation experiments.

LC-FTICR-MS/MS

COFI has been applied to an LC-FTICR-MS/MS separation of BSA tryptic digest solution without using any known BSA fragment information. After the corresponding "optimal" frequency shift for each scan was generated, COFI was applied to correct the frequency shifts and regenerated accurate mass data for each scan. The average CPU running time for each LC scan was approximately 0.01 s on a HP pavilion laptop with Pentium M (1.6 GHz). The data before and after COFI were used in the database search to determine the mass accuracy affects on the ability to identify the protein based on the fragment masses. The precursor mass list was produced from Xmass 7.0.6 as dd_results file. Since we didn't calibrate precursor masses in dd_results file, we could expect relatively large mass error for parent ions. We chose 1 Da as the parent mass tolerance and varied fragment ion mass tolerance to search MASCOT [29]. Other search parameters were: database (MSDB), taxonomy (all), enzyme (trypsin), missing cleavage (2), and modification (carbamidomethylation for cysteine and oxidation for methionine). All the MASCOT results are listed in Table 4. Before COFI application, if we used fragment mass tolerance less than 0.05 Da to search the database, none of the MS/MS spectra were identified as BSA. After increasing fragment mass tolerance to 0.1 Da,

33 MS/MS spectra were identified as BSA, and BSA was the highest ranked significant protein hit. With 0.2 Da fragment mass tolerance, more MS/MS spectra were identified as BSA. No significant changes were found on either Mascot score or identified number of MS/MS spectra when we further increased fragment mass tolerance (data not shown here). With the use of COFI, BSA was detected with confidence within the fragment mass tolerance of 0.01 Da, with the highest rank of significant hits. Unfortunately, Mascot MS/MS ion search results are based on how many of the most intense peaks are identified in the queried spectrum, and a tighter fragment mass tolerance window normally does not increase the Mascot score. This is true in spite of the greater confidence that should come from spectrum identification with tighter precursor and fragment mass constraints. However, tighter tolerance does increased the speed of search and the Mascot score indicates how many fragments and MS/MS spectra are identified. As in Table 4, 59 MS/MS spectra can be matched to BSA tryptic peptides at the mass tolerance of 0.2 Da (23 unique peptide sequences), and 44 MS/MS spectra can be identified at the mass tolerance of 0.01 Da. We manually checked the unmatched MS/MS spectra, and found that type-1 edges were either not observed (8 spectra) or the intensities were too low to be chosen for COFI correction (2 spectra). For the other 5 MS/MS spectra, COFI can not assign the correct frequency shift since insufficient type-1 edges are available for statistical tests. Overall, COFI was successfully applied to LC/MS/MS spectra, resulting in significantly improved data quality. With the application of COFI, the fragment mass tolerance range can be decreased or tightened. In theory, more confident protein identification can be achieved with implementation of advanced scoring algorithms that can efficiently utilize high fragment mass accuracy.

Multiplexed LC-CID-FTICR-MS

COFI is extremely attractive for LC-coupled multiplexed experiments. As mentioned above, when more than one peptide in the same spectrum is dissociated, most of abundant peptides are likely to give intense fragment ions. The type-1 edges used for COFI calibration are more likely from the most abundant peptides. However after COFI, all the *m/z* species in the spectrum are corrected, not only fragments from the most abundant peptides. The increased mass measurement accuracy can increase the possibility of identification using a smaller number of fragments. We also used BSA tryptic digest to demonstrate the application of COFI to the multiplexed LC-CID-FTICR-MS separation. Since no commercial protein identification software is available for multiplexed LC-CID-FTICR data, we used our own program coded using Matlab 6.5 to demonstrate the utility of COFI on protein identification. For a MS scan, potential parent species are chosen based on the selected intensity cut-off. Each parent ion is used to search the database for parent peptide candidates, and the multiplexed CID data are used to match fragments of candidates. The other database search parameters include: enzyme (trypsin), missing cleavage (1), and fragment ion types (b ions and y ions). Results are reported based on the matched fragment number and the average absolute mass measurement accuracy. Since only external calibration was applied on LC-FTICR-MS data, we chose 0.3 Da as the mass tolerance of parent peptide to get maximum number of parent peptide candidates. All the search work was done using only the BSA sequence, and identified fragments for each scan were used as the reference data to demonstrate the improvement in peptide identification using this approach. COFI was applied to the entire LC-CID-FTICR-MS run data without using any known BSA fragment information. After generating the corresponding "optimal" frequency shift for each scan, COFI was applied to correct these corresponding frequency shifts and produce accurate mass data.

The average absolute mass measurement errors for each scan are listed in Supplementary Table 1 and Supplementary Table 2. The calculated frequency shifts after COFI are also shown in Supplementary Table 2. Figure 6 illustrates the number of the identified fragments before and after COFI of using different fragment mass tolerance range. Without COFI, when we used the mass tolerance of 0.02 Da to search for fragments from BSA tryptic digested peptides, only 12 fragments were matched for BSA tryptic digested peptides. After increasing mass tolerance to 0.2 Da, lots of fragments can be found. The total number of the identified fragments was 1010 from a total of 129 CID spectra. However, the average mass measurement error of these fragments was as large as 85.03 ppm in the absence of any frequency shift correction. The application of COFI to these data significantly reduced mass measurement errors. After COFI application, a mass tolerance of 0.1 Da was applied to search for fragments of BSA tryptic peptides from these data, and the average mass measurement error decreased to 6.43 ppm. The total number of identified fragments increased to 1106 from the same 129 CID spectra mentioned above. When we decreased the mass tolerance further to 0.01 Da, the total number of identified fragments was 1029, and the average mass measurement error was 2.49 ppm. Only 11 of 129 CID spectra can not be accurately corrected with COFI to result in fragment mass tolerance values within the 0.01 Da window. These spectra are indicated in **bold** in Supplementary Table 2. 92 % of the CID spectra were well-calibrated by using COFI. For the 11 CID spectra which failed to be corrected by COFI, the type-1 edges in these spectra were either not observed or the intensities were too low to be chosen for COFI correction. Overall, COFI application resulted in low ppm fragment mass measurement errors and many more fragments from BSA tryptic digested peptides were identified at lower mass tolerance windows. These results indicated that the application of COFI significantly reduced the average mass

measurement errors, which can increase our confidence for protein and peptide identification during multiplexed LC-CID-FTICR-MS analyses.

CONCLUSIONS

A new calibration method for fragmentation data has been developed to correct the effects of space charge in FTICR-MS. COFI provides a useful way to obtain high mass accuracy on FTICR data with the information that is inherent in the spectra. There is no need to include an internal calibrant or to apply ion population control. COFI has been successfully applied to LC-FTICR-MS/MS fragmentation data. With COFI, we were able to unambiguously identify proteins with the mass tolerance set to much tighter constraints. COFI can also be applied to multiplexed LC-CID-FTICR-MS. Low ppm mass measurement errors are achieved with the application of COFI to multiplexed LC-CID-FTICR-MS of BSA tryptic digested peptides. With COFI, many more fragments from BSA tryptic digested peptides are identified when searching with a tighter mass tolerance. The combination of COFI and multiplexed LC-CID-FTICR-MS can be extremely attractive for high throughput proteome research with implementation of advanced database searching software that effectively utilizes accurate peptide fragment masses.

ACKNOWLEDGEMENTS

This work was supported by grants from the M.J. Murdock Charitable Trust; the Directorate of Biological Sciences, National Science Foundation, Grant No. DBI-0352451; and the Office of Science (BER), U.S. Department of Energy, Grant No. DE-FG02-04ER63924. We are also grateful to PNNL for providing the software ICR-2LS used for data analysis.

REFERENCES

(1) Shevchenko, A.; Jensen, O. N.; Podtelejnikov, A. V.; Sagliocco, F.; Wilm, M.; Vorm, O.; Mortensen, P.; Boucherie, H.; Mann, M. *Proc Natl Acad Sci U S A* 1996, *93*, 14440-14445.

(2) Wolters, D. A.; Washburn, M. P.; Yates, J. R., 3rd *Anal Chem* 2001, *73*, 5683-5690.

(3) Aebersold, R.; Goodlett, D. R. *Chem Rev* 2001, *101*, 269-295.

(4) Kelleher, N. L. *Anal Chem* 2004, *76*, 197A-203A.

(5) Conrads, T. P.; Anderson, G. A.; Veenstra, T. D.; Pasa-Tolic, L.; Smith, R. D. *Anal Chem* 2000, *72*, 3349-3354.

(6) Yates, J. R., 3rd *Trends Genet* 2000, *16*, 5-8.

(7) Clauser, K. R.; Baker, P.; Burlingame, A. L. *Anal Chem* 1999, *71*, 2871-2882.

(8) He, F.; Emmett, M. R.; Hakansson, K.; Hendrickson, C. L.; Marshall, A. G. *J Proteome Res* 2004, *3*, 61-67.

(9) Goodlett, D. R.; Bruce, J. E.; Anderson, G. A.; Rist, B.; Pasa-Tolic, L.; Fiehn, O.; Smith, R. D.; Aebersold, R. *Analytical Chemistry* 2000, *72*, 1112-1118.

(10) Marshall, A. G.; Hendrickson, C. L.; Jackson, G. S. *Mass Spectrometry Reviews* 1998, *17*, 1-35.

(11) Bogdanov, B.; Smith, R. D. *Mass Spectrom Rev* 2005, *24*, 168-200.

(12) Ledford, E. B., Jr.; Rempel, D. L.; Gross, M. L. *Anal Chem* 1984, *56*, 2744-2748.

(13) Ledford, E. B., Jr.; Rempel, D. L.; Gross, M. L. *International Journal of Mass Spectrometry and Ion Processes* 1984, *55*, 143-154.

(14) Easterling, M. L.; Mize, T. H.; Amster, I. J. *Analytical Chemistry* 1999, *71*, 624-632.

(15) Bogdanov, B.; Smith, R. D. *Mass Spectrom Rev* 2004, *24*, 168-200.

(16) Bruce, J. E.; Anderson, G. A.; Brands, M. D.; Pasa-Tolic, L.; Smith, R. D. *Journal of the American Society for Mass Spectrometry* 2000, *11*, 416-421.

(17) Taylor, P. K.; Amster, I. J. *International Journal of Mass Spectrometry* 2003, *222*, 351-361.

(18) Flora, J. W.; Hannis, J. C.; Muddiman, D. C. *Anal Chem* 2001, *73*, 1247-1251.

(19) Lee, S. W.; Berger, S. J.; Martinovic, S.; Pasa-Tolic, L.; Anderson, G. A.; Shen, Y.; Zhao, R.; Smith, R. D. *Proc Natl Acad Sci U S A* 2002, *99*, 5942-5947.

(20) Meng, F.; Cargile, B. J.; Miller, L. M.; Forbes, A. J.; Johnson, J. R.; Kelleher, N. L. *Nat Biotechnol* 2001, *19*, 952-957.

(21) Liu, C.; Tolic, L. P.; Hofstadler, S. A.; Harms, A. C.; Smith, R. D.; Kang, C.; Sinha, N. *Anal Biochem* 1998, *262*, 67-76.

(22) Kaiser, N. K.; Anderson, G. A.; Bruce, J. E. *J Am Soc Mass Spectrom* 2005, *16*, 463-470.

(23) Belov, M. E.; Zhang, R.; Strittmatter, E. F.; Prior, D. C.; Tang, K.; Smith, R. D. *Analytical Chemistry* 2003, *75*, 4195-4205.

(24) Syka, J. E.; Marto, J. A.; Bai, D. L.; Horning, S.; Senko, M. W.; Schwartz, J. C.; Ueberheide, B.; Garcia, B.; Busby, S.; Muratore, T.; Shabanowitz, J.; Hunt, D. F. *J Proteome Res* 2004, *3*, 621-626.

(25) Senko, M.; Zabrouskov, V.; Lange, O.; Wieghaus, A.; Griep-Raming, J.; S., H. *52nd ASMS Conference on Mass Spectrometry and Allied Topics, Nashville, TN* 2004.

(26) Polfer, N. C.; Haselmann, K. F.; Zubarev, R. A.; Langridge-Smith, P. R. *Rapid Commun Mass Spectrom* 2002, *16*, 936-943.

(27) Anderson, G. A.; Bruce , J. E.; Smith , R. D., ICR-2LS, Version 2.18 ed.; Pacific Northwest National Laboratory: Richmond, WA, 1996 released.

(28) Mann, M.; Wilm, M. *Anal Chem* 1994, *66*, 4390-4399.

(29) Perkins, D. N.; Pappin, D. J.; Creasy, D. M.; Cottrell, J. S. *Electrophoresis* 1999, *20*, 3551-3567.

(30) Yan, B.; Pan, C.; Olman, V. N.; Hettich, R. L.; Xu, Y. *Bioinformatics* 2004.

(31) Horn, D. M.; Zubarev, R. A.; McLafferty, F. W. *J Am Soc Mass Spectrom* 2000, *11*, 320-332.

(32) Rorabacher, D. B. *Anal Chem* 1991, *63*, 139-146.

(33) Purvine, S.; Eppel, J. T.; Yi, E. C.; Goodlett, D. R. *Proteomics* 2003, *3*, 847-850.

(34) Masselon, C.; Pasa-Tolic, L.; Lee, S. W.; Li, L.; Anderson, G. A.; Harkewicz, R.; Smith, R. D. *Proteomics* 2003, *3*, 1279-1286.

Table 1. Fragment ion pairs in the MS/MS spectrum of substance P and their calculated frequency shifts. Pair numbering in this table corresponds to numbering used in Figure 3.

pair number	***m/z*** before calibration		calculated frequency shift (*Hz*)
	ion 1	ion2	
1	578.3804	706.4512	5.3
2	606.3790	734.4480	4.7
3	706.4512	853.5285	5.4
4	734.4480	881.5294	4.9
5	853.5285	1000.6087	4.9
6	881.5294	1028.6113	5.8
7	966.5109	1094.6186	4.8
8	1000.6087	1057.5822	4.2
9	1028.6113	1085.6352	6.2

Table 2. Mass measurement errors for substance P fragment ions with/without COFI

theoretical ***m/z***	fragment type	error (ppm)	
		before COFI	after COFI
579.3731	a5	26.17	-3.318
607.368	b5	31.025	0.111
707.4317	a6	38.639	2.632
735.4266	b6	39.807	2.375
854.5001	a7	42.46	-1.032
882.495	b7	47.854	2.937
967.4711	y8	49.2	0
1001.5685	a8	47.993	-2.985
1029.5634	b8	54.179	1.776
1058.59	a9	57.656	3.775
1086.5849	b9	53.569	-1.736
1095.5661	y9	55.04	-0.639
average absolute error(ppm)		**45.299**	**1.943**

Table 3. Mass measurement errors for the identified fragments of three peptides from a single CID spectrum

theoretical	error (ppm)		assignment	
m/z	before COFI	after COFI	peptide	fragment
269.1614	14.49	3.34	Angiotensin I	y2
371.2043	24.18	-0.55	Angiotensin I	b3
392.7089	26.10	-0.10	Angiotensin I	b6
416.2298	28.11	-0.48	Angiotensin I	y3
506.2727	34.78	1.05	Angiotensin I	a4
513.2825	33.70	0.58	Angiotensin I	y4
534.2676	37.26	1.67	Angiotensin I	b4
569.3015	37.22	-0.74	Angiotensin I	a9
583.299	38.64	-0.26	Angiotensin I	b9
619.3568	42.18	0.92	Angiotensin I	a5
647.3517	46.38	3.25	Angiotensin I	b5
756.4157	51.60	1.20	Angiotensin I	a6
763.4255	47.55	3.27	Angiotensin I	y6
784.4106	52.74	0.48	Angiotensin I	b6
1025.5573	65.23	3.12	Angiotensin I	y8
1028.5318	67.78	-0.75	Angiotensin I	b8
370.1982	25.31	0.61	Bradykinin	b7
419.2407	28.15	-0.24	Bradykinin	y3
506.2727	34.76	-0.99	Bradykinin	y4
527.3094	35.05	-0.09	Bradykinin	a5
530.788	34.57	-0.86	Bradykinin	$[M+2H]^{2+}$
555.3043	37.84	0.84	Bradykinin	b5
614.3415	42.49	1.56	Bradykinin	a6
642.3364	40.38	-2.42	Bradykinin	b6
653.3411	43.01	0.46	Bradykinin	y5
710.3626	51.10	-3.80	Bradykinin	y6
739.3891	53.22	3.96	Bradykinin	b7
807.4153	50.53	3.22	Bradykinin	y7
858.4626	58.08	0.88	Bradykinin	a8
886.4575	61.17	2.11	Bradykinin	b8
904.4681	55.06	5.20	Bradykinin	y8
1060.5687	71.88	1.14	Bradykinin	$[M+H]^{+}$
586.3406	40.35	1.24	Substance P	a10
674.8634	45.78	0.74	Substance P	$[M+2H]^{2+}$
882.495	57.23	-1.57	Substance P	b7
967.4711	62.33	2.07	Substance P	y8
1095.5661	68.46	4.56	Substance P	y9
1348.7194	90.45	0.52	Substance P	$[M+H]^{+}$
average absolute error(ppm)	**45.66**	**1.60**		

Table 4. MASCOT search results of a LC-FTICR-MS/MS separation

Fragment mass tolerance(Da)	without COFI		with COFI	
	identified MS/MS number	Mascot score	identified MS/MS number	Mascot score
0.2	59	773	59	885
0.1	33	234	54	870
0.05	--------	--------	50	830
0.02	--------	--------	46	825
0.01	--------	--------	44	785

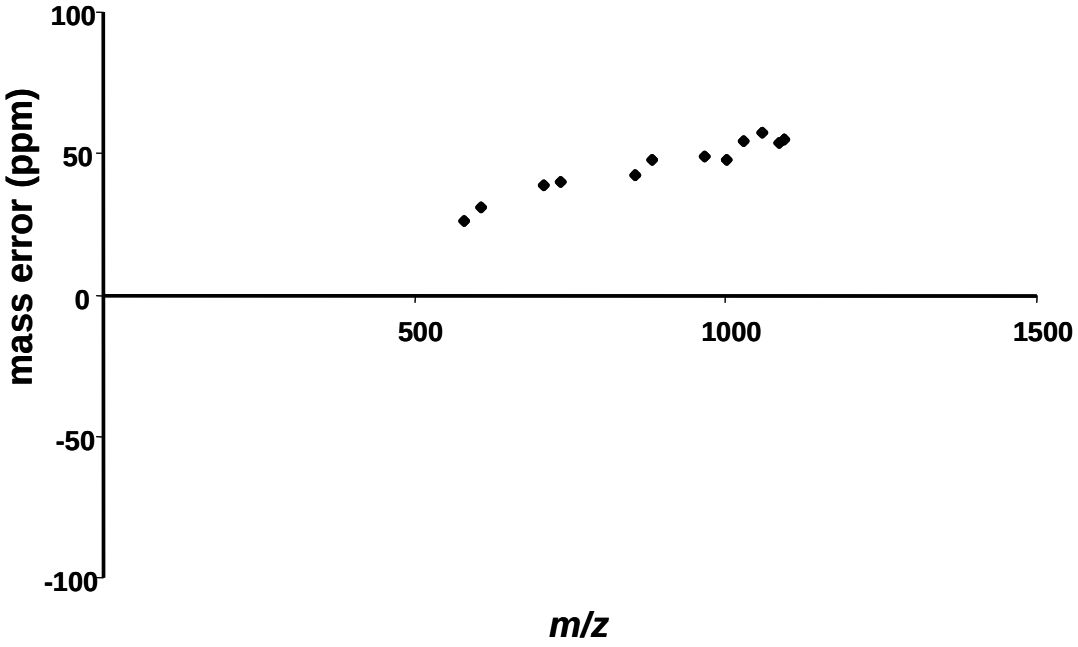

Figure 1. Mass errors of the fragment ions in the MS/MS spectrum of substance P before COFI. The graph shows a systematic linear increase in error with increasing *m/z*. The average mass measurement error of these fragment ions is 45.122 ppm

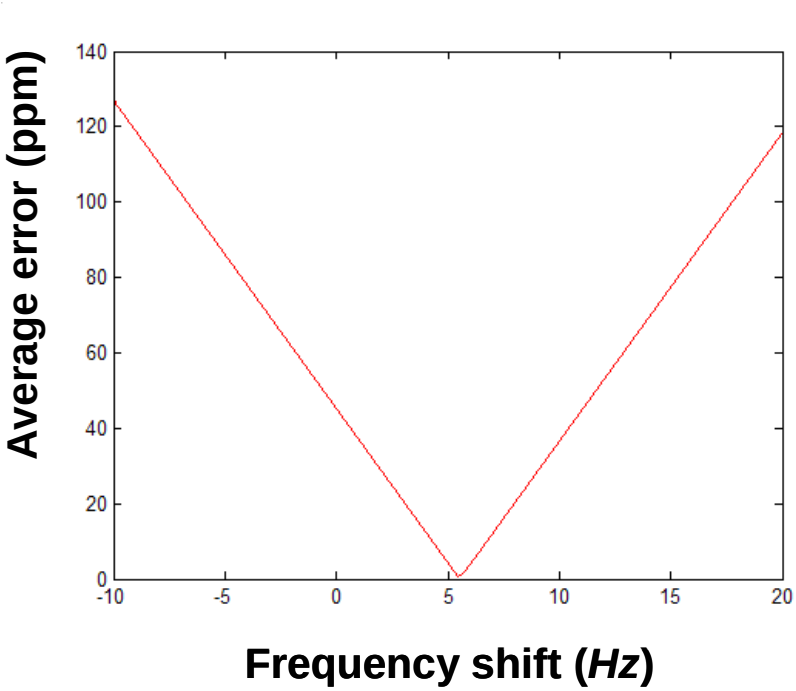

Figure 2. The relationship between the average absolute mass measurement error of the identified fragment ions of substance P and frequency shift is shown in this plot. The calculated frequency shift to obtain the minimum mass error is 5.5 Hz.

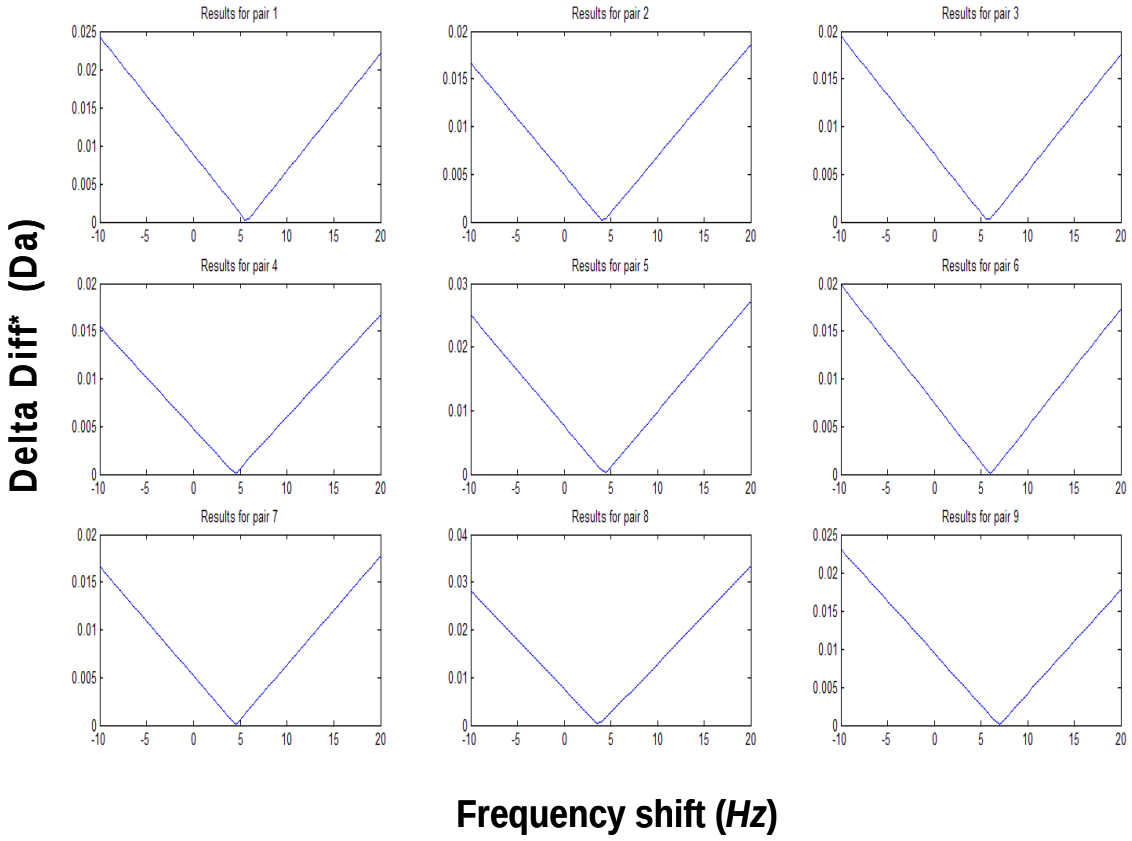

Figure 3. Application of COFI to the candidate pairs in the MS/MS spectra of substance P. Nine candidate pairs were chosen by COFI, as numbering in Table 2. For each pair, the absolute value of the difference between the exact amino acid mass (M_{aa}) and the measured amino acid mass (ΔM) ($\left|M_{aa} - \Delta M\right|$) is plotted as a function of frequency shift. *Delta Diff. refers to the difference $\left|M_{aa} - \Delta M\right|$. The optimal frequency shift calculated by COFI was 5.3 Hz.

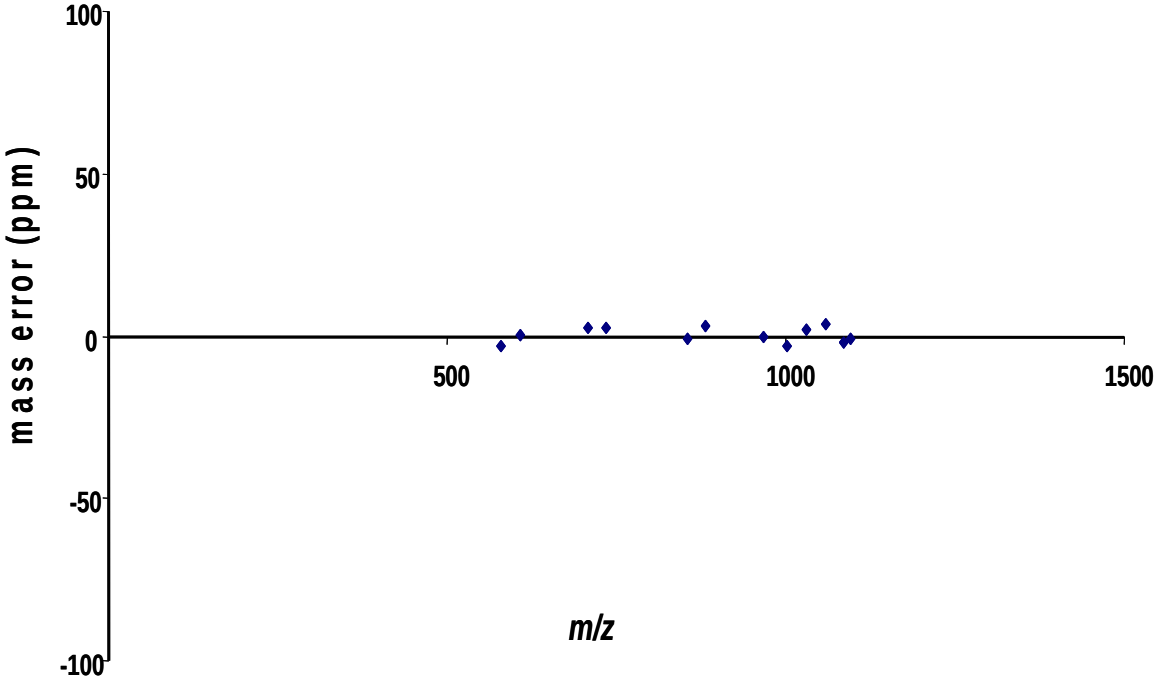

Figure 4. Mass errors of the fragment ions in the MS/MS spectrum of substance P after frequency shift correction with COFI. The average error after calibration is 1.943 ppm.

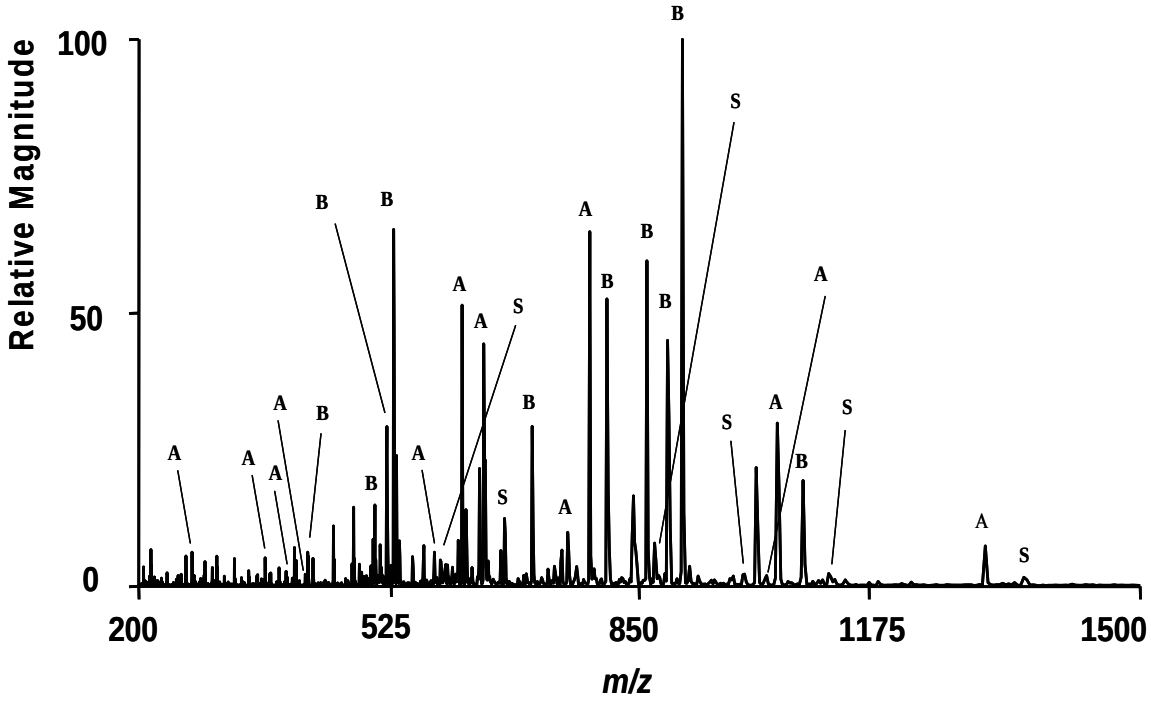

Figure 5. Multiplexed CID spectrum of a three peptide mixture with labeled fragment ions attributed to each individual peptide. The three peptides are bradykinin (B), angiotensin I (A), and substance P (S). Only a-type, b-type, and y-type ions are selected here.

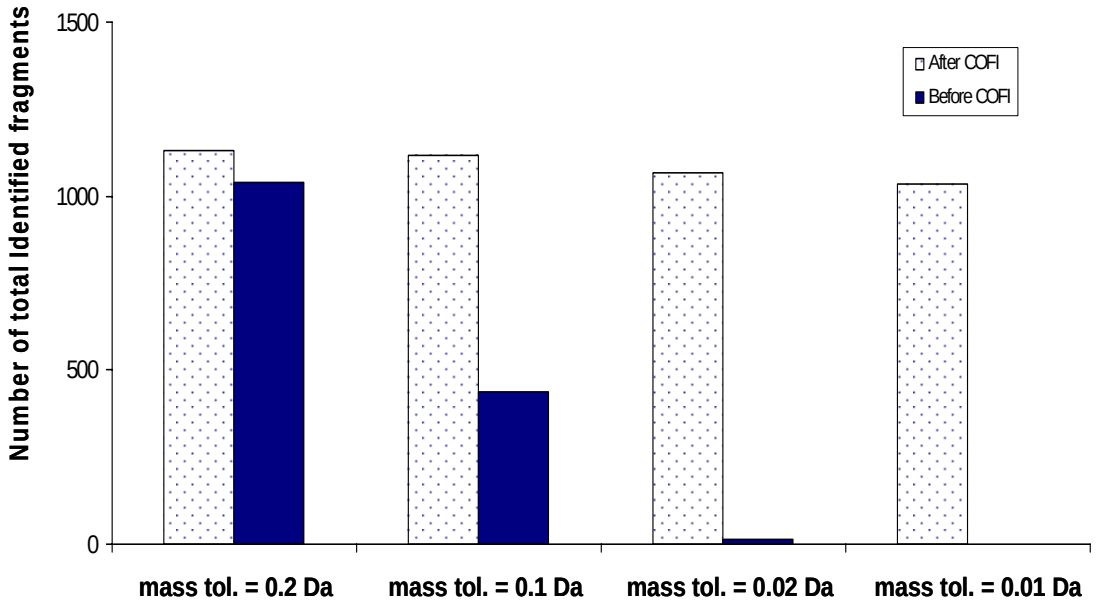

Figure 6. Number of the identified fragments for tryptic digested peptides of BSA during a multiplexed LC-CID-FTICR-MS separation

SUPPLYMENTARY DATA

Table 1. Average mass measurement errors of the identified peptides for tryptic digestion of BSA during a multiplexed LC-CID-FTICR-MS separation (before COFI)

File #	Sequence	mass tol. = 0.2 Da		Mass tol. = 0.1 Da		mass tol. = 0.02 Da	
		No. of fragment	average absoulte error (ppm)	No. of fragment	average absolute error (ppm)	No. of fragment	average absolute error (ppm)
484	FKDLGEEHFK	11	89.2	4	48.47	0	N/D
486	FKDLGEEHFK	8	95.35	2	59.15	0	N/D
488	FKDLGEEHFK	12	88.29	5	53.77	0	N/D
490	FKDLGEEHFK	10	97.49	3	44.27	0	N/D
492	FKDLGEEHFK	10	96.5	3	43.76	0	N/D
494	FKDLGEEHFK	8	99.99	3	55.68	0	N/D
496	FKDLGEEHFK	6	109.6	2	67.36	0	N/D
498	DAFLGSFLYEYSR	2	102.51	0	N/D	0	N/D
498	FKDLGEEHFK	3	103.76	0	N/D	0	N/D
500	DAFLGSFLYEYSR	2	103.36	0	N/D	0	N/D
506	FKDLGEEHFK	2	108.38	0	N/D	0	N/D
508	FKDLGEEHFK	2	67.12	0	N/D	0	N/D
518	FKDLGEEHFK	3	128.61	0	N/D	0	N/D
528	HLVDEPQNLIK	7	86.18	3	45.11	0	N/D
530	HLVDEPQNLIK	9	90.95	4	48.02	0	N/D
532	HLVDEPQNLIK	9	91.33	4	48.36	0	N/D
534	HLVDEPQNLIK	9	90.76	4	48.12	0	N/D
536	HLVDEPQNLIK	9	90.48	5	47.89	0	N/D
538	HLVDEPQNLIK	8	83.46	4	47.81	0	N/D
538	LVVSTQTALA	2	154.1	0	N/D	0	N/D
538	YLYEIAR	2	115.66	0	N/D	0	N/D
540	HLVDEPQNLIK	8	83.2	4	47.73	0	N/D
540	LVVSTQTALA	3	140.52	0	N/D	0	N/D
540	YLYEIAR	2	115.48	0	N/D	0	N/D
542	HLVDEPQNLIK	6	89.31	2	47.54	0	N/D
542	YLYEIAR	3	97.71	2	78.79	0	N/D
544	HLVDEPQNLIK	7	94.77	3	34.88	1	11.49
544	YLYEIAR	3	95.9	2	77.01	0	N/D
546	HLVDEPQNLIK	5	74.68	2	45.97	0	N/D
546	YLYEIAR	3	93.6	2	76.04	0	N/D
548	HLVDEPQNLIK	4	71.95	2	46.54	0	N/D
548	YLYEIAR	3	95.58	2	77.17	0	N/D
552	HLVDEPQNLIK	4	97.26	1	42.11	0	N/D
552	YLYEIAR	3	96.3	2	31.51	0	N/D
554	YLYEIAR	2	118.25	0	N/D	0	N/D

556	LKHLVDEPQNLIK	3	64.07	0	N/D	0	N/D
558	LKHLVDEPQNLIK	3	64.33	0	N/D	0	N/D
558	YLYEIAR	2	77.6	2	77.43	1	3.82
564	HLVDEPQNLIK	3	84.66	0	N/D	0	N/D
566	YLYEIAR	3	95.33	2	76.5	1	4.4
568	KVPQVSTPTLVEVSR	6	65.97	2	38.61	0	N/D
570	KVPQVSTPTLVEVSR	9	73.83	5	40.04	0	N/D
572	KVPQVSTPTLVEVSR	9	61.39	5	39	0	N/D
574	KVPQVSTPTLVEVSR	7	62.93	3	39.3	0	N/D
576	KVPQVSTPTLVEVSR	7	74.59	3	45.04	0	N/D
578	KVPQVSTPTLVEVSR	10	65.1	5	45.6	0	N/D
580	KVPQVSTPTLVEVSR	8	57.62	3	29.87	0	N/D
582	KVPQVSTPTLVEVSR	9	67.44	4	35.04	0	N/D
584	KVPQVSTPTLVEVSR	7	61.2	5	39.61	0	N/D
586	KVPQVSTPTLVEVSR	6	65.49	2	33.99	0	N/D
588	KVPQVSTPTLVEVSR	6	59.69	4	42.94	0	N/D
590	KVPQVSTPTLVEVSR	7	65.8	3	43.19	0	N/D
592	KVPQVSTPTLVEVSR	4	59.9	2	38.04	0	N/D
594	KVPQVSTPTLVEVSR	5	51.96	3	42.52	0	N/D
596	KVPQVSTPTLVEVSR	4	59.84	2	37.73	0	N/D
598	KVPQVSTPTLVEVSR	3	45.84	2	38.07	0	N/D
602	KVPQVSTPTLVEVSR	3	46.09	2	37.92	0	N/D
632	HLVDEPQNLIK	2	79.38	0	N/D	0	N/D
636	HLVDEPQNLIK	2	80.03	0	N/D	0	N/D
642	HLVDEPQNLIK	2	79.95	1	55.32	0	N/D
644	HLVDEPQNLIK	3	95.85	0	N/D	0	N/D
644	LVNELTEFAK	7	78.35	2	37.15	0	N/D
648	LVNELTEFAK	6	81.67	4	42.99	1	3.65
650	LVNELTEFAK	7	75.06	4	46.79	1	4.34
652	LVNELTEFAK	6	81.1	4	37.63	1	4.34
654	LVNELTEFAK	5	96.78	3	37.93	1	4.6
656	LVNELTEFAK	6	86.24	2	54.85	1	2.79
658	LVNELTEFAK	6	81.21	4	56.86	0	N/D
660	LVNELTEFAK	6	81.56	3	37.93	0	N/D
662	LVNELTEFAK	5	97.21	3	38.21	0	N/D
664	LVNELTEFAK	5	96.73	2	55.32	0	N/D
666	LVNELTEFAK	5	96.67	2	54.98	0	N/D
668	LVNELTEFAK	5	100.29	2	54.72	0	N/D
670	LVNELTEFAK	4	107.71	1	56.33	0	N/D
672	LVNELTEFAK	4	107.95	1	56.01	0	N/D
674	KQTALVELLK	9	98.95	2	65.87	0	N/D
674	LVNELTEFAK	4	111.13	1	63.45	0	N/D
676	KQTALVELLK	10	96.48	3	64.35	0	N/D
676	RHPEYAVSVLLR	3	96.22	1	42.33	0	N/D
678	KQTALVELLK	8	109.52	2	55.24	0	N/D
678	LVNELTEFAK	4	116.03	1	43.01	0	N/D
678	RHPEYAVSVLLR	10	74.88	2	30.13	0	N/D
680	KQTALVELLK	8	104	5	50.94	0	N/D
680	RHPEYAVSVLLR	10	72.83	2	32.13	0	N/D
682	KQTALVELLK	6	96.43	3	43.76	0	N/D

682	RHPEYAVSVLLR	10	82.4	2	57.5	0	N/D
684	KQTALVELLK	6	97.29	3	43.27	0	N/D
684	RHPEYAVSVLLR	8	80.62	2	57.72	0	N/D
686	KQTALVELLK	8	103.59	3	53.61	0	N/D
686	RHPEYAVSVLLR	8	70.58	2	58.56	0	N/D
688	KQTALVELLK	7	93.74	3	43.73	0	N/D
688	RHPEYAVSVLLR	11	82.05	3	63.03	0	N/D
690	KQTALVELLK	2	132.11	0	N/D	0	N/D
690	LVNELTEFAK	3	106.31	0	N/D	0	N/D
690	RHPEYAVSVLLR	9	66.9	4	49.85	0	N/D
692	KQTALVELLK	7	96.62	4	47.47	0	N/D
692	RHPEYAVSVLLR	8	70.34	2	57.72	0	N/D
694	RHPEYAVSVLLR	11	81.22	3	43.55	0	N/D
698	KQTALVELLK	6	101.11	2	50.11	0	N/D
698	RHPEYAVSVLLR	8	69.7	4	57.13	0	N/D
700	RHPEYAVSVLLR	8	85.48	4	49.53	0	N/D
702	LVNELTEFAK	2	128.16	0	N/D	0	N/D
702	RHPEYAVSVLLR	9	58.1	2	44.36	0	N/D
704	KQTALVELLK	8	102.6	6	47.35	0	N/D
704	RHPEYAVSVLLR	9	76.37	2	57.85	0	N/D
706	KQTALVELLK	3	95.85	0	N/D	0	N/D
706	RHPEYAVSVLLR	6	91.22	3	43.57	0	N/D
708	RHPEYAVSVLLR	4	72.48	1	47.56	0	N/D
712	RHPEYAVSVLLR	3	109.88	1	42.34	0	N/D
714	RHPEYAVSVLLR	4	112.96	1	53.12	0	N/D
716	HPEYAVSVLLR	3	93.3	1	34.23	0	N/D
716	RHPEYAVSVLLR	7	90.55	2	46.35	0	N/D
718	RHPEYAVSVLLR	3	114.84	1	44.23	0	N/D
720	RHPEYAVSVLLR	3	101.23	1	54.12	0	N/D
728	RHPEYAVSVLLR	2	109.12	0	N/D	0	N/D
730	RHPEYAVSVLLR	2	109.53	0	N/D	0	N/D
734	RHPEYAVSVLLR	2	120.96	0	N/D	0	N/D
746	RHPEYAVSVLLR	2	117.62	0	N/D	0	N/D
754	RHPEYAVSVLLR	3	76.57	2	46.49	1	4.46
774	KQTALVELLK	5	82.33	2	55.65	1	2.24
774	QTALVELLK	4	89.77	2	34.43	1	3.29
776	QTALVELLK	4	89.77	2	63.93	1	2.36
778	QTALVELLK	5	105.87	2	63.79	0	N/D
779	QTALVELLK	2	64.57	2	64.57	0	N/D
782	QTALVELLK	5	103.56	2	64.33	0	N/D
784	QTALVELLK	4	88.73	2	64.03	0	N/D
786	QTALVELLK	5	103.9	2	63.1	0	N/D
806	LGEYGFQNALIVR	5	74.5	2	63.74	0	N/D
810	LGEYGFQNALIVR	11	78.91	3	50.43	0	N/D
812	LGEYGFQNALIVR	7	67.56	3	39.26	0	N/D
814	LGEYGFQNALIVR	8	63.95	5	49.55	0	N/D
816	LGEYGFQNALIVR	10	73.12	6	47.76	0	N/D
822	LGEYGFQNALIVR	10	72.95	3	50.07	0	N/D
824	LGEYGFQNALIVR	5	73.93	3	46.73	0	N/D
826	LGEYGFQNALIVR	5	73.46	3	49.73	0	N/D

828	LGEYGFQNALIVR	6	67.95	3	49.23	0	N/D
952	RHPYFYAPELLYYANK	13	58.73	3	48.99	0	N/D
954	RHPYFYAPELLYYANK	13	58.91	6	37.83	0	N/D
956	RHPYFYAPELLYYANK	13	58.8	5	37.75	0	N/D
958	RHPYFYAPELLYYANK	10	62.7	5	37.63	0	N/D
960	RHPYFYAPELLYYANK	14	61.61	3	34.31	0	N/D
962	RHPYFYAPELLYYANK	14	61.09	5	37.61	0	N/D
964	RHPYFYAPELLYYANK	14	58.25	5	37.24	0	N/D
966	RHPYFYAPELLYYANK	14	61.06	5	37.51	0	N/D
968	RHPYFYAPELLYYANK	14	61.16	5	37.22	0	N/D
970	RHPYFYAPELLYYANK	14	61.19	5	37.4	0	N/D
972	RHPYFYAPELLYYANK	14	61.17	5	37.37	0	N/D
974	RHPYFYAPELLYYANK	12	61.4	5	37.41	0	N/D
976	RHPYFYAPELLYYANK	11	58.13	5	37.7	0	N/D
978	RHPYFYAPELLYYANK	11	53.89	5	37.83	0	N/D
980	RHPYFYAPELLYYANK	12	57.37	5	37.46	0	N/D
982	RHPYFYAPELLYYANK	10	59.7	5	37.41	0	N/D
984	RHPYFYAPELLYYANK	10	66.45	4	38.63	0	N/D
986	RHPYFYAPELLYYANK	10	66.82	4	44.01	0	N/D
988	RHPYFYAPELLYYANK	9	64.99	3	42.79	0	N/D
990	RHPYFYAPELLYYANK	10	66.52	3	42.48	0	N/D
average absolute error (ppm)			**85.03**		**48.02**		**4.32**

Table 2. Average mass measurement errors of the identified peptides for tryptic digestion of BSA during a multiplexed LC-CID-FTICR-MS separation (after COFI)

		mass tol. = 0.1 Da		mass tol. = 0.02 Da		mass tol. = 0.01 Da		
File #	Sequence	No. of fragment	average absolute error (ppm)	No. of fragment	average absolute error (ppm)	No. of fragment	average absolute error (ppm)	frequency shift (*Hz*)
484	FKDLGEEHFK	11	5.07	11	5.07	10	4.66	21.991
486	FKDLGEEHFK	8	4.1	8	4.1	7	3.11	23.297
488	FKDLGEEHFK	12	3.64	12	3.64	12	3.64	22.27
490	FKDLGEEHFK	11	10.31	10	4.18	10	4.18	22.094
492	FKDLGEEHFK	10	3.86	10	3.86	10	3.86	21.93
494	FKDLGEEHFK	8	1.34	8	1.34	8	1.34	22.496
498	DAFLGSFLYEYSR	3	17.75	2	6.65	1	1.15	23.372
498	FKDLGEEHFK	2	3.62	2	3.62	2	3.62	23.372
500	DAFLGSFLYEYSR	3	15.84	2	6.61	1	2.18	22.753
506	FKDLGEEHFK	3	3.5	3	3.5	3	3.5	22.066
508	FKDLGEEHFK	2	6.78	2	6.78	1	3.2	23.627
518	FKDLGEEHFK	2	3.18	2	3.18	2	3.18	22.849
528	HLVDEPQNLIK	8	2.29	8	2.29	8	2.29	22.554
530	HLVDEPQNLIK	11	1.9	11	1.9	11	1.9	22.323
532	HLVDEPQNLIK	10	1.29	10	1.29	10	1.29	22.793
534	HLVDEPQNLIK	11	2.59	11	2.59	11	2.59	22.2
536	HLVDEPQNLIK	11	1.3	11	1.3	11	1.3	22.489
538	HLVDEPQNLIK	10	2.39	10	2.39	10	2.39	22.183
538	LVVSTQTALA	2	2.41	2	2.41	2	2.41	22.183
538	YLYEIAR	2	3.35	2	3.35	2	3.35	22.183
540	HLVDEPQNLIK	10	1.27	10	1.27	10	1.27	22.351
540	LVVSTQTALA	3	1.88	3	1.88	3	1.88	22.351
540	YLYEIAR	2	2.34	2	2.34	2	2.34	22.351
542	HLVDEPQNLIK	7	2.69	7	2.69	7	2.69	22.368
542	YLYEIAR	3	4.23	3	4.23	3	4.23	22.368
544	HLVDEPQNLIK	7	3.3	7	3.3	7	3.3	21.669
544	YLYEIAR	3	5.34	3	5.34	3	5.34	21.669
546	HLVDEPQNLIK	6	0.93	6	0.93	6	0.93	22.072
546	YLYEIAR	3	1.84	3	1.84	3	1.84	22.072
548	HLVDEPQNLIK	5	1.94	5	1.94	5	1.94	21.884
548	YLYEIAR	3	4.08	3	4.08	3	4.08	21.884
552	**HLVDEPQNLIK**	**4**	**23.18**	**1**	**1.15**	**1**	**1.15**	**28.845**
552	**YLYEIAR**	**3**	**24.02**	**1**	**2.35**	**1**	**2.35**	**28.845**
554	YLYEIAR	2	2.33	2	2.33	2	2.33	22.9
556	HLVDEPQNLIK	2	5.2	2	5.2	1	2.62	22.251
556	LKHLVDEPQNLIK	4	15.97	3	4.38	2	3	22.251
558	HLVDEPQNLIK	2	3.08	2	3.08	2	3.08	22.475
558	LKHLVDEPQNLIK	4	15.14	3	2.93	3	2.93	22.475
558	YLYEIAR	2	2.6	2	2.6	2	2.6	22.475
564	HLVDEPQNLIK	4	1.57	4	1.57	4	1.57	22.251
566	**YLYEIAR**	**2**	**76.5**	**0**	**N/D**	**0**	**N/D**	**0**

568	KVPQVSTPTLVEVSR	11	1.57	11	1.57	11	1.57	22.034
570	KVPQVSTPTLVEVSR	11	1.43	11	1.43	11	1.43	23.653
572	KVPQVSTPTLVEVSR	12	4	11	1.18	11	1.18	22.763
574	KVPQVSTPTLVEVSR	12	5.9	12	5.9	6	4.04	21.246
576	KVPQVSTPTLVEVSR	9	1.57	9	1.57	9	1.57	23.603
578	KVPQVSTPTLVEVSR	12	1.14	12	1.14	12	1.14	22.87
580	KVPQVSTPTLVEVSR	12	1.44	12	1.44	12	1.44	22.182
582	KVPQVSTPTLVEVSR	11	1.53	11	1.53	11	1.53	22.667
584	KVPQVSTPTLVEVSR	9	1.56	9	1.56	9	1.56	22.39
586	KVPQVSTPTLVEVSR	11	1.43	11	1.43	11	1.43	21.891
588	KVPQVSTPTLVEVSR	8	0.95	8	0.95	8	0.95	23.1
590	KVPQVSTPTLVEVSR	8	2.55	8	2.55	8	2.55	21.909
592	KVPQVSTPTLVEVSR	7	1.37	7	1.37	7	1.37	21.919
594	KVPQVSTPTLVEVSR	6	1.82	6	1.82	6	1.82	21.758
596	KVPQVSTPTLVEVSR	6	2.52	6	2.52	6	2.52	21.491
598	KVPQVSTPTLVEVSR	4	1.45	4	1.45	4	1.45	22.216
602	KVPQVSTPTLVEVSR	4	1.59	4	1.59	4	1.59	21.711
632	**HLVDEPQNLIK**	**2**	**14.91**	**0**	**N/D**	**0**	**N/D**	**19.693**
636	HLVDEPQNLIK	2	10.03	2	9.33	1	1.03	22.477
642	LVNELTEFAK	4	1.2	4	1.2	4	1.2	22.355
644	HLVDEPQNLIK	3	14.65	1	1.17	1	1.17	21.852
644	LVNELTEFAK	7	10.18	6	2.58	6	2.58	21.852
648	LVNELTEFAK	6	2.31	6	2.31	6	2.31	22.348
650	LVNELTEFAK	7	3.32	7	3.32	6	1.43	22.109
652	**LVNELTEFAK**	**3**	**57.02**	**0**	**N/D**	**0**	**N/D**	42.038
654	LVNELTEFAK	5	1.31	5	1.31	5	1.31	22.257
656	LVNELTEFAK	6	1.41	6	1.41	6	1.41	21.838
658	LVNELTEFAK	6	11.47	5	1.33	5	1.33	22.215
660	LVNELTEFAK	6	13.75	5	4.48	5	4.48	21.352
662	**LVNELTEFAK**	**6**	**25.1**	**2**	**13.21**	**0**	**N/D**	17.487
664	LVNELTEFAK	5	1.22	5	1.22	5	1.22	22.207
666	LVNELTEFAK	5	1.79	5	1.79	5	1.79	21.909
668	LVNELTEFAK	5	10.2	4	2.16	4	2.16	21.583
670	LVNELTEFAK	4	4.39	4	4.39	4	4.39	20.991
672	LVNELTEFAK	4	6.06	4	6.06	3	5.05	20.698
674	KQTALVELLK	10	2.02	10	2.02	10	2.02	22.222
674	LVNELTEFAK	4	1.95	4	1.95	4	1.95	22.222
676	KQTALVELLK	10	0.98	10	0.98	10	0.98	22.974
676	RHPEYAVSVLLR	3	1.15	3	1.15	3	1.15	22.974
678	KQTALVELLK	8	4.99	8	4.99	8	4.99	22.439
678	LVNELTEFAK	4	5.59	4	5.59	4	5.59	22.439
678	RHPEYAVSVLLR	10	6.65	9	3.47	9	3.47	22.439
680	KQTALVELLK	9	1.49	9	1.49	9	1.49	22.862
680	RHPEYAVSVLLR	10	2.21	10	2.21	10	2.21	22.862
682	KQTALVELLK	6	3.06	6	3.06	6	3.06	22.025
682	RHPEYAVSVLLR	10	2.29	10	2.29	10	2.29	22.025
684	KQTALVELLK	6	1.82	6	1.82	6	1.82	22.524
684	RHPEYAVSVLLR	8	1.79	8	1.79	8	1.79	22.524
686	KQTALVELLK	9	2.43	9	2.43	9	2.43	22.545
686	RHPEYAVSVLLR	8	1.42	8	1.42	8	1.42	22.545

688	KQTALVELLK	7	4.44	7	4.44	6	3.62	21.717
688	RHPEYAVSVLLR	11	4.26	11	4.26	9	3.37	21.717
690	KQTALVELLK	3	5.86	3	5.86	3	5.86	21.937
690	LVNELTEFAK	3	3.33	3	3.33	3	3.33	21.937
690	RHPEYAVSVLLR	9	4.14	9	4.14	8	3.45	21.937
692	KQTALVELLK	8	4.58	8	4.58	8	4.58	21.962
692	RHPEYAVSVLLR	8	3.28	8	3.28	7	2.75	21.962
694	RHPEYAVSVLLR	11	2.69	11	2.69	11	2.69	21.927
698	KQTALVELLK	7	3.24	7	3.24	7	3.24	22.075
698	RHPEYAVSVLLR	8	2	8	2	8	2	22.075
700	**RHPEYAVSVLLR**	**4**	**49.53**	**0**	**N/D**	**0**	**N/D**	**0**
702	LVNELTEFAK	2	3.55	2	3.55	2	3.55	22.171
702	RHPEYAVSVLLR	9	2.65	9	2.65	9	2.65	22.171
704	KQTALVELLK	9	3.92	9	3.92	9	3.92	22.019
704	RHPEYAVSVLLR	9	3.25	9	3.25	8	2.37	22.019
706	KQTALVELLK	2	2.66	2	2.66	2	2.66	22.391
706	RHPEYAVSVLLR	6	9.8	5	3.75	4	2.95	22.391
712	RHPEYAVSVLLR	3	16.31	2	4.41	2	4.41	22.288
714	**RHPEYAVSVLLR**	**4**	**46.09**	**0**	**N/D**	**0**	**N/D**	14.513
716	HPEYAVSVLLR	3	3.21	3	3.21	3	3.21	22.416
716	RHPEYAVSVLLR	7	3.12	7	3.12	7	3.12	22.416
718	RHPEYAVSVLLR	3	5.69	3	5.69	3	5.69	21.314
720	RHPEYAVSVLLR	3	3.38	3	3.38	3	3.38	24.587
728	RHPEYAVSVLLR	2	4.8	2	4.8	2	4.8	21.958
730	RHPEYAVSVLLR	2	3.78	2	3.78	2	3.78	21.555
734	**RHPEYAVSVLLR**	**2**	**38.28**	**0**	**N/D**	**0**	**N/D**	30.288
746	RHPEYAVSVLLR	2	2.21	2	2.21	2	2.21	21.9
754	**RHPEYAVSVLLR**	**2**	**46.49**	**0**	**N/D**	**0**	**N/D**	0
772	QTALVELLK	2	5.92	2	5.92	1	1.4	20.743
774	KQTALVELLK	6	3.16	6	3.16	6	3.16	21.664
774	QTALVELLK	4	3.12	4	3.12	4	3.12	21.664
776	QTALVELLK	4	3.18	4	3.18	4	3.18	21.648
778	QTALVELLK	5	2.45	5	2.45	5	2.45	22.296
780	QTALVELLK	5	1.4	5	1.4	5	1.35	22.276
782	QTALVELLK	5	1.35	5	1.35	4	2.47	22.239
784	QTALVELLK	4	2.47	4	2.47	2	1.44	21.573
786	QTALVELLK	5	2.72	5	2.72	5	2.72	21.804
806	LGEYGFQNALIVR	7	1.6	7	1.6	7	1.6	22.115
810	LGEYGFQNALIVR	15	4.3	14	2.65	13	2.3	22.325
812	LGEYGFQNALIVR	9	3.67	9	3.67	8	3.11	21.835
814	LGEYGFQNALIVR	10	1.05	10	1.05	10	1.05	22.435
816	LGEYGFQNALIVR	13	3.15	12	1.46	12	1.46	22.882
822	LGEYGFQNALIVR	12	3.47	11	1.58	11	1.58	22.407
824	**LGEYGFQNALIVR**	**3**	**44.56**	**0**	**N/D**	**0**	**N/D**	1.2102
826	**LGEYGFQNALIVR**	**6**	**20.2**	**2**	**10.13**	**1**	**1.98**	16.871
828	LGEYGFQNALIVR	7	2.81	7	2.81	7	2.81	21.492
952	RHPYFYAPELLYYANK	16	1.82	16	1.82	16	1.82	21.781
954	RHPYFYAPELLYYANK	17	2.15	17	2.15	17	2.15	21.814
956	RHPYFYAPELLYYANK	16	1.72	16	1.72	16	1.72	21.881
958	RHPYFYAPELLYYANK	11	2.93	11	2.93	11	2.93	21.354

960	RHPYFYAPELLYYANK	17	2	17	2	17	2	21.784
962	RHPYFYAPELLYYANK	16	1.3	16	1.3	16	1.3	21.797
964	RHPYFYAPELLYYANK	16	2.03	16	2.03	15	2.13	21.874
966	HPYFYAPELLYYANK	17	1.1	17	1.1	17	1.1	21.878
968	HPYFYAPELLYYANK	16	1.75	15	1.2	15	1.2	21.883
970	HPYFYAPELLYYANK	16	2.31	16	2.31	15	1.99	21.6
972	HPYFYAPELLYYANK	15	1.68	15	1.68	15	1.68	21.721
974	HPYFYAPELLYYANK	12	2.15	12	2.15	12	2.15	21.744
976	HPYFYAPELLYYANK	12	2.1	12	2.1	12	2.1	21.797
978	HPYFYAPELLYYANK	13	2.16	13	2.16	13	2.16	21.652
980	HPYFYAPELLYYANK	12	2.5	12	2.5	12	2.5	21.422
982	HPYFYAPELLYYANK	11	1.86	11	1.86	11	1.86	21.653
984	HPYFYAPELLYYANK	10	1.03	10	1.03	10	1.03	21.746
986	RHPYFYAPELLYYANK	10	1.8	10	1.8	10	1.8	21.546
988	HPYFYAPELLYYANK	9	1.1	9	1.1	9	1.1	22.281
990	HPYFYAPELLYYANK	10	4.1	10	4.1	9	3.58	20.677
	average absolute error (ppm)		**6.43**		**2.89**		**2.49**	

CHAPTER THREE

A Hybrid LC-Gel-MS Method for Proteomics Research and Its Application to Protease Functional Pathway Mapping

Si Wu, Xiao-Ting Tang, William F. Siems, and James E. Bruce*

Department of Chemistry

Washington State University

PO BOX 644630, Pullman, WA 99164-4630

Keywords: multidimensional protein profiling; SAX; SDS-PAGE; BACE; mass spectrometry

*Correspondence: James E. Bruce
Department of Chemistry
Washington State University
PO BOX 644630
Pullman, WA 99164-4630
Fax: 509-335-8867
Email: james_bruce@wsu.edu

Published at *Journal of Chromatograph B Analyt Technol Biomed Life Sci 2005*;822:98-111.

ABSTRACT

Two-dimensional (2D) gel electrophoresis is the most common protein separation method in proteomics research. It can provide high resolution and high sensitivity. However, 2D gel methods have several limitations, such as labor-intensive procedures, poor reproducibility, and limited dynamic range of detection. In fact, many investigators have returned to couple the one-dimensional (1D) SDS-PAGE with mass spectrometry for protein identification. The limitation of this approach is the increased protein complexity in each one-dimensional gel band. To overcome this problem and provide reproducible quantitative information, we describe here a 2D method for protein mixture separation using a combination of high performance liquid chromatography (HPLC) and 1D SDS-PAGE. The study shows that the step-gradient fractionation method we have applied provides excellent reproducibility. In addition, high mass accuracy of LC-FTICR-MS can allow more confident protein identifications by high resolution and ultra-high mass measurement accuracy. This approach was applied to *comparative proteomics* since protein abundance level changes can be easily visualized with side-by-side vertical comparison in one gel. Furthermore, separation of multi-samples in the same gel significantly reduces run-to-run variation, as is shown with differential image gel electrophoresis (DIGE). Finally, this approach readily incorporates immunological methods to normalize relative abundances of multiple samples within a single gel. This paper presents the results of our developments and our initial application of this strategy for mapping protease function of beta amyloid cleaving enzyme (BACE) in biological systems.

INTRODUCTION

The proteome contains information critical to an improved comprehension of life, biological organisms and achieving the paradigm shift now known as "systems biology" [1,2]. Proteomics research technologies are rapidly changing our understanding of complex and dynamic biological systems by providing information relevant to functionally-associated changes in protein abundances, protein-protein interactions, and posttranslational modifications [3-7]. Current proteomics research demands highly efficient analytical systems that are high resolution, high sensitivity, high throughput and robust. The overall challenge of proteomics research is the assignment of function to the large fraction of genes whose functions are currently not known [8,9]. Although several facets of proteomics research currently exist related to the assignment of functional elements, the primary goals of such research can be classified into two categories including the visualization of changes that occur at the protein level in biological systems and the identification of protein species involved in these changes [7,9,10]. As such, protein separation and mass spectrometry technologies have become integral components in much of what is today's proteomics research. However, each of these components places constraints upon the other and proteomics research is only facilitated with integration of the two.

Gel electrophoresis has for some time been the method of choice of biologists and biochemists when faced with the task of protein separation. Gels represent relatively simple technology that can be used for stable, spatial separation of proteins that can then be visualized with a number of stains and dyes [11,12]. The development of immobilized pH gradient (IPG) strips has made 2D gel electrophoresis a reproducible and viable technique that can allow stable separation of thousands of proteins in a single gel image [6,13-16]. This capability has

significantly impacted the newly emerging field of proteomics, since it allows high resolution, relatively robust separation of protein mixtures [13]. However, due to the limitation presented by the amount of protein that can be loaded for the IEF separation stage, the identification of low abundance proteins is more difficult [3,17]. For example, for normal analytical 2D gels used for comparative analysis, as with difference image gel electrophoresis (DIGE) analysis [18,19], the recommended protein loading amount is limited to several hundred micrograms of total protein. Additionally, this much protein must be loaded in a restricted volume, placing additional constraints on the applications of 2D gels. These factors place significant limitations on the ability to accurately visualize and quantitate proteins, as well as on the subsequent protein identification strategies. To some extent, these limitations result in proteomics research only being applicable to more abundant proteins, and significantly limit the dynamic range of current proteomics capabilities [16,20-22].

The approach for efficient protein separation presented here involves coupling liquid chromatography as the first dimension, as opposed to isoelectric focusing, followed by additional stages of chromatography and/or SDS-PAGE [21,23,24]. This strategy provides a powerful, flexible and reproducible method to more rapidly separate the large number of proteins present in the proteomes of mammalian cells. The combination of separation techniques exploits the high loading capacity and excellent reproducibility of liquid chromatographic separations [21,25], combined with the attractive features of gel electrophoresis that allow stable spatial separation of proteins that can then independently be visualized for relative quantitation and identification. It has been reported [26] that significant enrichment was obtained for individual proteins by using MonoQ anion exchange chromatography before 1D or 2D PAGE. The feasibility to detect low abundance proteins by combining HPLC and 1D SDS-PAGE has also been demonstrated by

Nawarak et al [17]. This approach also provides the opportunity to gather sample separation information during the first dimension of analysis that can then be used to determine which samples, if any, are subjected to additional stages of liquid chromatography prior to gel analysis. Finally, the last dimension gel analysis also exploits the attractive feature of DIGE that allows multiple samples to be run in the same gel, minimizing difficulties that arise from gel-to-gel comparisons. Because the new approach presented here can allow proteome comparisons for larger numbers of samples, the present methodology will be highly applicable to time-resolved or multi-point proteomics analyses where the protein expression profiles from samples collected at a multitude of time points, dosages, or other parameters are to be compared.

We demonstrate this new approach with proteomics analysis for improved characterization of the Alzheimer's disease-relevant protease, Beta Amyloid Cleaving Enzyme or BACE [27]. BACE and a closely related enzyme BACE2 are two newly identified proteases which are involved in proteolysis of amyloid precursor protein (APP) [28-31]. BACE is a recognized enzyme that initiates generation of beta amyloid peptides, the major components of amyloid plaques found in postmortem brains of Alzheimer's disease patients. Characterization of BACE and BACE2 activity and involvement in Aβ generation in cells is critical to improved understanding of these proteases. In this paper, we present the initial application of our novel profiling system to the study of overexpression of BACE and BACE2 in HEK 293 cells. The initial results showed that this new separation strategy provides more reproducible visualization of protein abundance level changes and offers much greater flexibility for comparative analysis of biological systems.

EXPERIMENTAL

Chemicals and reagents

The HEK 293 cell line used for these studied was obtained from Clontech (Palo Alto, CA, USA). Antibiotics G418 from GibcoBrl, Lipofectamine2000, and pcDNA3 vector were purchased from Invitrogen (Carlsbad, CA, USA). BACE and BACE2 overexpressing pcDNA3 plasmids were kindly provided by Dr. Michael Farzan, Harvard Medical School. Plasmid Midi Kit was purchased from QIAGEN (Valencia, CA, USA). Competent cells JM109, reporter gene β-gal, porcine trypsin, and 5 × cell lysis buffers were from Promega (Madison, WI, USA). Antibody anti-1D4 was purchased from Chemicon (Temecula, CA, USA). DMEM, iodoacetamide, DTT, PMSF, and protein inhibitor mixture were purchased from Sigma-Aldrich (St. Louis, MI, USA). FBS was from HyClone (Logcen, UT, USA). Goat anti-mouse HRP-conjugated secondary antibody, protein assay reagent, and gel staining buffer were from Bio-Rad (Hercules, CA, USA). Western Lightning Chemiluminescence reagent was from PerkinElmer (Wellesley, MA, USA). Precast SDS-PAGE gels were either from Bio-Rad or from Invitrogen as indicated below. Sample buffer, running buffer, and gel electrophoresis instruments were from these two companies correspondingly.

Stable transfection on HEK 293 cells

HEK 293 cells were maintained in DMEM supplemented with 10% FBS. BACE and BACE2 encoded pcDNA3 vectors were tagged by 1D4 which is a 10 amino-acid C-terminal tag derived from bovine rhodopsin [28]. All these vectors were transformed on JM109 cells and purified by using Plasmid Midi Kit. Transfection was carried out using Lipofectamine2000

based on the manufacturer's protocols. BACE, BACE2 constructs and pcDNA3 plasmid were transfected in HEK 293 cells with a DNA to Lipofectamine2000 ratio of 1 μg/ 10 μl. Fresh growth medium was replaced 24 hours after transfection. Selective medium containing 0.5 mg/ml G418 was added the following day. Medium was continually exchanged every 1-2 days for 1 week for the neomycin to act on the non-transfected cells. Stable transfected cells were maintained in growth medium with 0.5 mg/ml G418.

Western blot analysis

Cells that stably express BACE and BACE2 each contained in a 10-cm diameter dish were detached and briefly centrifuged. Half of the cell pellet was re-suspended in Laemmli sample buffer (Invitrogen, Carlsbad, CA, USA) to get the whole cell lysate. Lysates were separated by a 4 -12% SDS-PAGE gel (Invitrogen, Carlsbad, CA, USA) and then transferred to a PVDF membrane (Imobilon-P, Millipore, Billerica, MA, USA) with a semidry transfer system Semi-Phor TE-77 (Hoefer, San Francisco, CA, USA). After transferring, membranes were blocked with 5% nonfat milk in PBS overnight followed by incubating with the primary antibody anti-1D4 (1:500) for 1 h at room temperature. The membrane was then probed by HRP-conjugated secondary antibody and labeled by Western Lightning Chemiluminescence reagent.

BACE and BACE2 activity assay

Cells were detached from culture dishes and washed with cold PBS buffer 3 times. Harvested cells were lysed in 0.3 ml of 0.5% NP-40/0.5 M NaCl/phosphate buffer, pH 7.4, containing protease inhibitor mixture and 0.5 μM PMSF, and incubated for 2 h at room temperature with 1D4 antibody which was bound to Ultralink Immobilized protein G beads

(Pierce, Rockford, IL, USA). Samples were washed four times with lysis buffer and twice with incubation buffer (2.5% acetic acid/ammonium acetate, pH 5.5). Immunoprecipitates bound to 1D4-protein G beads were mixed with 100 µl of incubation buffer containing 50 µM synthetic peptides, and incubated at 37°C for 2 h. Protein G beads were removed by centrifugation and the supernatant was analyzed by LC/MS/MS with an Esquire HCT ion trap mass spectrometer (Bruker Daltonics, Billerica, MA, USA). Nano-HPLC separation was performed with an LC packings Ultimate Nano-HPLC system equipped with a Famos micro autosampler and a Swichos micro column switching module (Dionex, Sunnyvale, CA, USA). Reverse phase solvents were (A) 0.1 % TFA in water and (B) 0.1% TFA in 95% acetonitrile. Samples were first injected by the autosampler and loaded onto a micro trap column (C18 PepMap, 300 µm × 1mm, 5µm, LC packings) at a flow rate of 50 µl/min with solvent A. The loaded sample was continuously washed with solvent A for 3 minutes to remove salts. Peptides were then eluted at a flow rate of 300 nL/min to an analytical column (C18 PepMap, 75µm × 150mm, 3µm, 100 Å, LC packings) and separated using the following gradient: 0% B for 0-3 min, 20-70% B for 3-45 min, 90% B for 45-55 min, and 0% B for 55-65 min. The eluant from the analytical column was sprayed on-line with a nano-spray emitter to the mass spectrometer. The nano-spray emitter was made in house by etching 20 µm × 360 µm fused silica capillary with HF. The spray potential was set as 1300-1500 volts. LC/MS/MS mass spectra were acquired using Hystar software (version 2.3, Bruker Daltonics, Billerica, MA, USA). MS/MS data acquisition was set in automatic mode with active exclusion based on peak intensity and a selection of exclusion peak lists. Data analysis and processing were using Bruker Daltonics DataAnalysis software (version 3.1).

SAX (strong anion exchange)-HPLC separation

Cell lysates were collected as described above and total protein concentration was detected by Bradford assay. Analysis of cell lysates was performed using a SAX HPLC column (4.6 mm × 100 mm, Source 15Q, Amersham, Piscataway, NJ, USA) attached to the DIONEX Auto-Ion HPLC instrument with a 2-ml sample injection loop. UV absorbance signals (280 nm) were collected by 757 Absorbance Detector (Applied Biosystems, Foster City, CA, USA) and were translated to digital signals using a LabJack U12 (LabJack, Lakewood, CO, USA). Buffer A (20 mM Tris buffer, pH 7.0) and buffer B (1 M NaCl, 20 mM Tris buffer, pH 7.0) were used as mobile phases for all samples. Fractions were collected using SF-2120 fraction collector (Advantic MFS, Inc., CA, USA).

For reproducibility experiments, three 1 mg aliquots of HEK 293 cell lysate were used. In each experiment, the sample was diluted to total injection volume of 1.5 ml and then loaded to the column. A linearly increased step-gradient from 100 % buffer A to 100% buffer B at a flow rate of 1.0 ml/min was used. After injection, the column was equilibrated in buffer A for 5 minutes. Fraction 1 was collected from 2-5 min during equilibration time. Then fraction 2 to fraction 11 were collected by increasing elution buffer B concentration from 10%, 20% to 100% with 10% increase in each step. Future studies will employ non-linear step gradients to maximize separation resolution. Each fraction corresponded to one elution condition and was collected in a 3-min interval. The total elution time was 35 minutes. 1 ml of each fraction was used for TCA precipitation and resuspended in 20 μl sample buffer. For reproducibility comparison, 3 replicate fractions were loaded onto a 4-12% SDS-PAGE gel (Invitrogen, Carlsbad, CA, USA) in neighboring lanes to allow rapid visual comparison.

For BSA spiking experiments, 10 μg and 20 μg BSA were spiked into 1 mg pcDNA3-transfected HEK 293 cell lysate separately. For ovalbumin spiking experiments, 1 μg, 5 μg, 10

μg, and 20 μg ovalbumin were spiked into 1 mg pcDNA3-transfected HEK 293 cell lysate separately. The SAX HPLC (4.6 mm × 100 mm, Poros QE, PerSeptive Biosystems, Foster City, CA) was used at the flow rate of 2.0 ml/min. Each sample was diluted to total injection volume of 1.5 ml. A linearly increased step-gradient from 100% buffer A to 100% buffer B at a flow rate of 2.0 ml/min was used. Fractions were collected as described before. Each fraction corresponded to one elution condition and was collected in 6 ml total volume. 1 ml of each fraction was used for TCA precipitation and re-suspended in 20 μl sample buffer. Corresponding fractions of individual samples were loaded on neighboring lanes on 4-12% SDS-PAGE gel (Invitrogen, Carlsbad, CA, USA).

For BACE, BACE2 overexpressing cells and pcDNA3-transfected cells comparison experiments, 2 mg of each cell lysate was used. Each sample was diluted to total injection volume of 1.5 ml. After injection, the column was equilibrated in buffer A for 5 minutes. A linearly increased step-gradient described as before was used and the flow rate was set at 2.0 ml/min. Fractions were collected as described before. Each fraction corresponded to one elution condition and was collected in 6 ml total volume. 1 ml of each fraction was used for TCA precipitation and re-suspended in 20 μl sample buffer. Corresponding fractions of individual samples were loaded on neighboring lanes on 8-16% SDS-PAGE gel (Bio-Rad, Hercules, CA, USA).

SDS-PAGE analysis

SDS-PAGE was carried out by the method of Laemmli under denatured conditions in different gradient polyacrylamide gels; each sample (after TCA precipitation) was dissolved in 20 μl sample buffer followed by heating 10 minutes at 70 ^{o}C. Gels were run at a constant

voltage of 200 V. After completion of electrophoresis, the gels were stained with Coomassie G-250 stain buffer. Bio-Rad precision plus protein standards were used as standard molecular weight markers. After staining and destaining, gels were scanned by a laser scanning densitometer (ImageQuant Densitometer, Molecular Dynamics, Sunnyvale, CA, USA) and analyzed by ImageQuaNT software.

In-gel tryptic digestion

The gel bands for protein identifications were cut and destained in 50% methanol/ 5% acetic acid solution overnight, followed by treatment with DTT for reduction of disulfide bonds and iodoacetamide for alkylation[32]. After equilibration in 100 mM NH_4HCO_3 solution, the gel bands were dehydrated in acetonitrile. The remaining solvent was evaporated by using CentriVap (Labconco, Kansas City, MO, USA). Trypsin solution was added with the concentration of 20 ng/μl and allowed to react with the gels overnight at 37 ^{o}C. Peptide extraction solutions were concentrated and desalted using C18 ziptip (Millipore, Billerica, MA, USA). Solution A (0.1% TFA in deionized water) was used for washing and solution B (0.1% TFA and 50 % acetonitrile) was used for elution.

Mass spectrometry and protein identification

1 μl concentrated peptide solution was mixed with 1 μl matrix solution (α-CHCA saturated in solution of 0.1% TFA and 50% acetonitrile) and then was spotted on a 7×7 sample target. OmniFlex MALDI-TOF mass spectrometer (Bruker Daltonics, Billerica, MA, USA) was used for analysis. The spectrum was externally calibrated by angiotensin I, ACTH clip (1-17), and ACTH clip (18-39), and analyzed by Bruker FlexAnalysis software. MASCOT was used for

peptide mass mapping by searching NCBRnr database. The database search was performed based on following parameters: taxonomy (Homo Sapiens), enzyme (trypsin), missing cleavage (1), mass tolerance (0.1 - 0.3 Da), modification (carbamidomethylation for cysteine and oxidation for methionine).

In-gel digestion of gel bands of interest of BSA spiking sample were also analyzed by ESI-FTICR-MS/MS experiment. A Bruker Daltonics Apex-Q 7T FTICR mass spectrometer was used to acquire the mass spectral data using Xmass as the data acquisition software program. The voltage on the capillary of ESI was set between 2050V and 2350V. A syringe pump used to introduce the solutions was set between 15-25 μl/h. The ions enter the instrument through a glass capillary and then pass through a hexapole followed by a quadrupole then a second hexapole. The quadrupole was used to select the specific *m/z* ions of interest to be fragmented. These ions were accumulated and were activated by CAD in the second set of hexapoles (collision cell energy was set to 30 eV) between 1-2 seconds to acquire MS/MS data. The ions were then sent to the ICR cell using electrostatic lenses. The FTICR data were processed using ICR-2LS software package [33].

RESULTS AND DISCUSSION

Overexpression of BACE and BACE2 in cells and BACE activity assay

C-terminal tagged BACE and BACE2 were subcloned into pcDNA3 separately and were stably transfected into HEK 293 cells. HEK 293 cell lines were employed here since BACE was discovered in HEK 293 expression library analysis [27]. Thus, BACE likely fulfills some natural functional roles in HEK 293 cells. Additionally, HEK 293 cells were used previously to identify BACE and to analyze its proteolytic function by many other reported studies [27,28,30,31] . After transfection, all cells were grown in the culture media containing 0.5 mg/ml G418. Untransfected HEK 293 cells and cells transfected with pcDNA3 vector were prepared as control for cells stably expressing BACE and BACE2. Expression of BACE and BACE2 was identified by Western blot analysis (Figure 1) using the anti-1D4 antibody for C-terminal 10 amino acid tag [28]. The C-terminal labeling enables the detection of the exogenous protein and consequently facilitates the detection of differences in its amount in different cells by one Western blot analysis. For example, only one band corresponding to a molecular mass of about 70 kDa was detected in BACE overexpressing cells and was not found in all other cells. Furthermore, only one band corresponding to a molecular mass of about 50 kDa was detected in BACE2 overexpressing cells and was not found in all other cells. Both of them are close to their expected masses [28]. These data illustrate stable overexpression of BACE and BACE2 in these newly developed cell lines.

To demonstrate that BACE and BACE2 in transfected cells are active, lysates of cells transfected with plasmids encoding tagged BACE, BACE2, or vector alone were incubated with 1D4-protein G beads. Beads were washed extensively and incubated with peptide

SEVNLDAEFR which is a well-known BACE substrate. This peptide was then analyzed by LC/MS/MS. As shown in Figure 2, peptides incubated with 1D4-protein G beads from vector only cell lysates exhibited a $(M+2H)^{2+}$ peak at *m/z* 590.2, corresponding to the full-length peptide (Figure 2B). The same peptide incubated with beads from BACE overexpressing cell lysates has produced a $(M+H)^{+}$ peak at *m/z* 561.2 as well as a $(M+2H)^{2+}$ peak at *m/z* 590.0. The peak at *m/z* 561.2 agrees well with the mass of the peptide, DAEFR, the expected C-terminal fragment ($(M+H)^{+}$ = 561.612) resultant from BACE hydrolysis of the incubated substrate. Figure 2C is the MS/MS spectrum of peak 561.2 which indicates that the sequence of this peak is DAEFR. No peak at *m/z* 561.2 was found when the peptide was incubated with 1D4-protein G beads from vector only cell lysates. The same fragment peak was also obtained from peptide incubated with BACE2 (data not shown here) as expected since both proteases have been shown to cleave this substrate [31].

Method development

A schematic representation of this method is illustrated in Figure 3. In the initial implementation, cell lysates are fractionated off a strong anion exchange (SAX) column and fractions are then run on a 1D gel for relative quantitation. This approach allows a lane-by-lane comparison of samples for relatively easy identification of changes in protein abundance, either visually or with computer analysis. Since much larger total protein amounts can be loaded on the SAX column as compared with IPG strips, much greater amounts of protein are available on the gel for improved quantitation and protein identification.

For this study, we used the cell lysis method described above to collect the protein sample from HEK 293 untreated cells. Figure 4A illustrates the UV chromatograms during SAX

fractionation of this cell lysate. Also shown in this figure are the elution buffer concentration steps employed for fractionation. These data indicate the qualitative nature of the UV chromatogram, since most fractions that showed strong UV peaks also showed a lot of bands on corresponding lanes in gels. However, in some cases, for example in fraction 7, very little protein was detected on the gel or by Bradford assays (data not shown), indicating UV absorbance in the fraction was dominated by non-protein species.

After SAX fractionation, samples were concentrated and desalted by TCA precipitation. During TCA precipitation, protein loss might have occurred due to the acetone wash. However, previous studies [34] reported the effects of protein precipitation methods on sample preparation. Their results with 2D gel electrophoresis showed all spots detected before TCA precipitation were also detected after TCA precipitation, including low M.W. IgG light chain proteins (M.W. about 20 KDa).

Figure 4B illustrates corresponding gel separation for the fractions resultant from SAX fractionation shown in Figure 4A. Most proteins eluted from fraction 1 to fraction 6. After comparing with the gel image of unfractionated sample, we found that the sample complexity of fractions was reduced after the SAX fractionation. Also, different fractions have significantly different band patterns, which indicate substantially different proteins are present in each fraction. These data showed that SAX fractionation can clearly divide the proteome into several less complicated protein mixtures.

Reproducibility study

We also used untransfected HEK 293 cell lysates to demonstrate the reproducibility of this new approach. After protein concentration measurement, 3 mg of total protein was used

and diluted with buffer A into 4.5 ml total volume. Three 1.5 ml aliquots were injected separately to test the reproducibility of this new method. After each run, the column was washed with a large amount of buffer B and then equilibrated by buffer A. The analysis of blank injections verified that no signals were resultant from carryover between each sample.

Figure 5A illustrates the UV absorption chromatogram acquired with triplicate analysis of the HEK 293 cell lysate described above. We evaluated the reproducibility of retention times based on the major peaks marked in Figure 5A. Calculated reproducibility of retention times is listed in table 1, and the average RSD value of 1.3% is obtained. For stepwise gradient LC separations, there is a standard deviation of the time of individual steps formation (instrumental parameter) [35]. This constant deviation can result in a small deviation of peak elution time related to the beginning of particular gradient step which elutes this peak. The deviation of peak elution time can have some impact on the band intensity in the SDS-PAGE gel. However, since we use relatively long elution time (3 minutes) for each step, this impact should be relatively small. Figure 5B shows the gel image of individual fraction comparison of these triplicate samples. We also evaluated the reproducibility of the gel band intensity. Figure 5C demonstrated the quantitative data (average intensity and standard deviation) of the marked gel bands in Figure 5B. After comparison of both UV chromatograms and SDS-PAGE images, we found both components showed excellent reproducibility. These results show that step-gradient fractionation can provide excellent reproducibility. We also did continuous gradient fractionation (data not shown here), but that approach turned out to be more difficult to get comparable reproducibility since slight changes in conditions, such as buffer pH or timing of fraction collection, can cause the whole elution pattern to systematically shift. Step-gradient

fractionation significantly decreased the variability of continuous gradient fractionation, resulting in significantly improved performance.

Standard protein spiking experiments

We spiked BSA at two levels into control cell lysates and injected half of the protein mixtures onto the SAX column. Spiked BSA was eluted at fraction 4 and was observed in both the UV chromatogram signals and the SDS-PAGE images of SAX fractions (Figure 6). The bands circled were cut and digested with trypsin. We identified BSA from band circled in Figure 6B "BSA2" sample using MALDI-TOF peptide fingerprint mapping (Figure 7A) and ESI-FTICR-MS/MS. Figure 7A was MALDI-TOF spectrum and peptide fingerprint mapping using MASCOT method. Figure 7B shows the ESI-FTICR-MS/MS of *m/z* 653.3 identified as BSA tryptic digest peptide using the same in-gel digestion solution, which confirms the protein identification using MALDI peptide fingerprint mapping. The average mass measurement accuracy of these identified fragments is 3.8 ppm.

We used another half of the samples for the second SDS–PAGE gel and performed Western blot analysis of the internal control protein, beta actin, as shown in Figure 6C. Band intensity was measured with ImageQuant software. Figure 6C also shows the relative intensity ratio of the three bands circled in Figure 6B after normalization with the internal control beta actin. Since the employed cell culture medium contained bovine serum albumin, we also identified the band in control cell lysate as BSA. We used control band intensity as background and subtracted it from bands observed in the BSA spiked samples. After subtraction, we found that the relative intensity ratio between 10 μg BSA spiked sample and 20 μg BSA spiked was about 1:1.9, in good agreement with the expected ratio of 1:2.

Since control samples contained relatively large amount of BSA, we chose another standard protein ovalbumin to demonstrate the range for the quantitative study. Figure 8A is the SDS-PAGE image of SAX fractions which contained ovalbumin. Spiked ovalbumin also eluted in fraction 4. Four different spiking concentration of ovalbumin were chosen: 1 μg/mg cell lysate, 5 μg/mg cell lysate, 10 μg/mg cell lysate, and 20 μg/mg cell lysate. Intensity of gel bands corresponding to ovalbumin increased when spiked ovalbumin concentration increased, as shown in box 1 in Figure 8A. Also, another set of band intensities (box 2 in Figure 8A) increased corresponding to the spiked concentration. The M.W. of this set of bands is about two times larger than the M.W. of ovalbumin, which probably contain ovalbumin dimer. Here we only quantitatively analyzed the bands in box 1. Band intensities were measured with ImageQuant software. We used control band intensity as background and subtracted it from bands observed in the ovalbumin spiked samples. After subtraction, we calculated the relative intensities of each band compared to the intensity of 1 μg/mg cell lysate spiking sample. The relative intensity comparison was shown in Figure 8B by average value and standard deviation. The data in Figure 8B show that in general, the relative intensities of the detected bands correlated well with the amount of ovalbumin protein that was spiked into the cell lysates. The relatively low observed intensity of the band resultant from spiking 20 μg/mg ovalbumin may be resultant from overloading of ovalbumin on the gel. Overall, the results from spiking experiments suggest that this method can be used for quantitative comparison.

SAX-HPLC analysis of BACE, BACE2 overexpressing cells and vector control cells

The following study focused on the following 3 cell lines that include BACE overexpressing HEK cells, BACE2 overexpressing HEK cells, and cells transfected by pcDNA3

vector only as control. The SAX-HPLC separation of these three different cell lysates demonstrated different UV chromatogram profiles (Figure 9A). All three of these chromatograms showed a majority of proteins eluted in the range of 20% to 50% buffer B. With comparison of these chromatograms, we found that they showed similar peak patterns but reproducible differences were observed. For example, as compared with control cell lysates, BACE and BACE2 overexpressing cell lysates have greater similarity. At present, these data are currently used to produce a relatively qualitative picture of protein separation, but will be used in future studies to optimize fractionation and determine which fractions are subjected to additional LC methods. A better comparison of proteins present in each cell lysate is shown in gel separation as described below.

SDS-PAGE gel comparison

The SDS-PAGE gels were used to further separate proteins present in fractions resultant from SAX. The corresponding fractions of different cell lysates showed similar band patterns. In fact, a majority of protein bands appeared identical among samples. However, we were also able to visually identify many differences among the samples. In Figure 9B, bands marked with circles are found up-regulated in both BACE and BACE2 overexpressing cell lysates relative to vector-only control cell lysate. These differences are resultant from overexpression of BACE and BACE2, and are targets for protein identification as described below. There are also differences between BACE and BACE2 overexpressing cells (marked as square boxes). For example, bands marked with square box in fraction 4 were only found in fraction 1 were only found of BACE2 but not in BACE or control sample. Since BACE but not BACE2 has been

identified as being expressed at high levels in brain [29 ,31], these bands may shed light on the different functional roles held by these very similar proteases.

Protein identification

Data from MALDI-TOF-MS were used to search protein databases for protein identification. 25 gel bands were excised as marked in Figure 9B. Protein identification results were considered significant with $p < 0.05$. Some proteins that were identified in this study using MALDI-TOF peptide mass fingerprint are listed in Table 2.

Our initial efforts have resulted in protein identification for many spots that were changed in abundance between samples. A separated publication is under preparation to present all proteins identified and a discussion of the significance of these new results. However, among initial results, HSP70 (heat shock protein 70) that we observed to be increased in abundance as a result of BACE expression, was also reported previously to be increased in abundance in AD brain tissue [36]. Rab3D, whose up-regulation was only found in BACE but not BACE2 overexpressing cells, is a member of the Ras family of GTPases that is a key regulator of intracellular vesicle transport during exocytosis [37,38]. In addition, several other GTPase proteins have been found previously to be altered in abundance in AD brain tissue [39]. Therefore, both Rab3D and BACE are members of the secretory pathway and the present results suggest that some cooperativity exists between BACE activity and Rab3D expression. EBNA-2 co-activator p100 was found to be increased in abundance in both BACE and BACE2 overexpressing cells. This protein is involved in co-activation of gene expression relevant to Epstein-Barr antigen 2 [40]. Its relationship to BACE or BACE2 overexpression is unclear.

CONCLUSIONS

The results presented in this paper highlight the utility that new strategies for protein separation hold for *comparative proteomics* research. Additionally, the new approach has shown much greater flexibility for protein separation as well as sample loading. We used SAX chromatography as the first dimension of protein separation, which has a capacity as large as 25 mg. Since much more protein can be loaded on the first dimension, as compared to conventional gel-based IEF separation, the demands on mass spectrometry performance at the protein ID stage are reduced. Furthermore, greater loading also provides increased ability to visualize and identify low abundance proteins by increasing total sample loading amount into SAX column. Also, reverse phase HPLC can be added as another dimension for more separation as needed. Flexibility also exists in the second dimension of our approach. For example, with SDS-PAGE separations, we can get better separation on larger molecular weight samples by increasing gel running time or capture of low molecular weight proteins by decreasing gel running time to keep low molecular weight proteins in the gel. This was useful for the present study; for example, the molecular weights of several proteins are below 30 KDa. For high concentration of polyacryamide gel as normally used to separate low MW proteins, it is more difficult to extract peptides out of the gel, which means larger amounts of protein are required for identification of small MW proteins. Recently more attention was put towards large molecular weight protein identification since it was difficult to get good separation from 2D gel. This new approach also shows some advantage for identification of large MW proteins.

Reproducibility experiments have shown that step-gradient fractionation can provide excellent reproducibility. An additional advantage of this method is that protein abundance level

changes can be easily visualized with side-by-side vertical comparison in one gel. Separation of multi-samples in the same gel significantly reduces run-to-run variation as well, as is shown with DIGE. Since samples are loaded into one gel, it can provide more reliable and reproducible data than is obtained by visual comparison of large numbers of 2D gels. This method allows analysis of virtually any number of samples in parallel, as shown here for control, BACE, and BACE2 samples. Furthermore, we expect that this approach will enable successful identification of much lower abundance proteins and greater dynamic range as a result of the greater sample loading amount. With dynamic range and sensitivity representing two of the most challenging aspects of proteomics research, the present method promises to significantly extend our capabilities to more interesting, less abundant and in some cases, more biologically significant proteins. High performance FTICR-MS can be applied to in-gel digestion sample to resolve more than one protein in a single gel band. Finally, since the first dimension chromatographic step can be tailored to many different types of separation techniques, we anticipate this approach and derivatives resultant from it, will significantly expand proteomics research to classes of proteins not readily tractable by current methodology.

ACKNOWLEDGEMENTS

We are grateful to Dr. Michael Farzan (Harvard Medical School) for providing us with pcDNA3 vectors encoding 1D4-tagged BACE or BACE2. Dr. Michael Grisword kindly provided us the HEK 293 cell line. We also thank Dr. Ying Li and Dr. Shisheng Li for help with cell transfections, and thank Gordon A. Anderson from PNNL for providing the software ICR-2LS used for FTICR data analysis. This work was supported by grants from The Murdock Charitable trust and NIH-NCRR Grant 1 S10 RR017805-01.

ABBREVIATIONS

AD, Alzheimer's disease; HPLC, high pressure liquid chromatography; PAGE, polyacrylamide gel electrophoresis; TCA, trichloroacetic acid; SAX, strong anion exchange; FTICR-MS, Fourier Transform Ion Cyclotron Resonance mass spectroscopy; MALDI, Matrix-assisted Laser Desorption/Ionization; TOF, time of flight; DMEM, Dulbecco's modified Eagle's medium; FBS, Fetal Bovine Serum; PMSF, phenyl methyl sulfonyl fluoride); MW, molecular weight; DIGE, differential image gel electrophoresis.

REFERENCES

[1] T. Ideker, T. Galitski, L. Hood, Annu Rev Genomics Hum Genet 2 (2001) 343.

[2] H. Kitano, Science 295 (2002) 1662.

[3] J.R. Yates, 3rd, Trends Genet 16 (2000) 5.

[4] R. Aebersold, B. Rist, S.P. Gygi, Ann N Y Acad Sci 919 (2000) 33.

[5] J.L. Harry, M.R. Wilkins, B.R. Herbert, N.H. Packer, A.A. Gooley, K.L. Williams, Electrophoresis 21 (2000) 1071.

[6] L. Tonella, B.J. Walsh, J.C. Sanchez, K. Ou, M.R. Wilkins, M. Tyler, S. Frutiger, A.A. Gooley, I. Pescaru, R.D. Appel, J.X. Yan, A. Bairoch, C. Hoogland, F.S. Morch, G.J. Hughes, K.L. Williams, D.F. Hochstrasser, Electrophoresis 19 (1998) 1960.

[7] A. Pandey, M. Mann, Nature 405 (2000) 837.

[8] M.P. Washburn, D. Wolters, J.R. Yates, 3rd, Nat Biotechnol 19 (2001) 242.

[9] J.R. Yates, 3rd, J.K. Eng, A.L. McCormack, D. Schieltz, Anal Chem 67 (1995) 1426.

[10] B. Cooper, D. Eckert, N.L. Andon, J.R. Yates, P.A. Haynes, J Am Soc Mass Spectrom 14 (2003) 736.

[11] B. Schulenberg, B. Arnold, W.F. Patton, Proteomics 3 (2003) 1196.

[12] L.R. Williams, Biotech Histochem 76 (2001) 127.

[13] T. Rabilloud, Proteomics 2 (2002) 3.

[14] M. Traini, A.A. Gooley, K. Ou, M.R. Wilkins, L. Tonella, J.C. Sanchez, D.F. Hochstrasser, K.L. Williams, Electrophoresis 19 (1998) 1941.

[15] H. Boucherie, F. Sagliocco, R. Joubert, I. Maillet, J. Labarre, M. Perrot, Electrophoresis 17 (1996) 1683.

[16] R. Joubert, P. Brignon, C. Lehmann, C. Monribot, F. Gendre, H. Boucherie, Yeast 16 (2000) 511.

[17] J. Nawarak, S. Sinchaikul, C.Y. Wu, M.Y. Liau, S. Phutrakul, S.T. Chen, Electrophoresis 24 (2003) 2838.

[18] M. Unlu, M.E. Morgan, J.S. Minden, Electrophoresis 18 (1997) 2071.

[19] R. Tonge, J. Shaw, B. Middleton, R. Rowlinson, S. Rayner, J. Young, F. Pognan, E. Hawkins, I. Currie, M. Davison, Proteomics 1 (2001) 377.

[20] G.L. Corthals, V.C. Wasinger, D.F. Hochstrasser, J.C. Sanchez, Electrophoresis 21 (2000) 1104.

[21] H. Wang, S. Hanash, J Chromatogr B Analyt Technol Biomed Life Sci 787 (2003) 11.

[22] X. Zuo, L. Echan, P. Hembach, H.Y. Tang, K.D. Speicher, D. Santoli, D.W. Speicher, Electrophoresis 22 (2001) 1603.

[23] K. Wagner, K. Racaityte, K.K. Unger, T. Miliotis, L.E. Edholm, R. Bischoff, G. Marko-Varga, J Chromatogr A 893 (2000) 293.

[24] N.G. Ahn, J.S. Campbell, R. Seger, A.L. Jensen, L.M. Graves, E.G. Krebs, Proc Natl Acad Sci U S A 90 (1993) 5143.

[25] D.B. Wall, M.T. Kachman, S. Gong, R. Hinderer, S. Parus, D.E. Misek, S.M. Hanash, D.M. Lubman, Anal Chem 72 (2000) 1099.

[26] A. Butt, M.D. Davison, G.J. Smith, J.A. Young, S.J. Gaskell, S.G. Oliver, R.J. Beynon, Proteomics 1 (2001) 42.

[27] R. Vassar, B.D. Bennett, S. Babu-Khan, S. Kahn, E.A. Mendiaz, P. Denis, D.B. Teplow, S. Ross, P. Amarante, R. Loeloff, Y. Luo, S. Fisher, J. Fuller, S. Edenson, J. Lile, M.A.

Jarosinski, A.L. Biere, E. Curran, T. Burgess, J.C. Louis, F. Collins, J. Treanor, G. Rogers, M. Citron, Science 286 (1999) 735.

[28] M. Farzan, C.E. Schnitzler, N. Vasilieva, D. Leung, H. Choe, Proc Natl Acad Sci U S A 97 (2000) 9712.

[29] R. Yan, J.B. Munzner, M.E. Shuck, M.J. Bienkowski, J Biol Chem 276 (2001) 34019.

[30] B. Nawrot, S. Antoszczyk, M. Maszewska, G. Rebowski, T. Kuwabara, M. Warashina, K. Taira, W.J. Stec, Nucleic Acids Res Suppl (2002) 105.

[31] D. Andrau, C. Dumanchin-Njock, E. Ayral, J. Vizzavona, M. Farzan, M. Boisbrun, P. Fulcrand, J.F. Hernandez, J. Martinez, S. Lefranc-Jullien, F. Checler, J Biol Chem 278 (2003) 25859.

[32] A. Shevchenko, M. Wilm, O. Vorm, M. Mann, Anal Chem 68 (1996) 850.

[33] G.A. Anderson, J.E. Bruce , S. R.D., in, Pacific Northwest National Laboratory, Richmond, WA, 1996.

[34] L. Jiang, L. He, M. Fountoulakis, J Chromatogr A 1023 (2004) 317.

[35] M. Hutta, R. Gora, J Chromatogr A 1012 (2003) 67.

[36] B.C. Yoo, R. Vlkolinsky, E. Engidawork, N. Cairns, M. Fountoulakis, G. Lubec, Electrophoresis 22 (2001) 1233.

[37] A.L. Millar, N.J. Pavios, J. Xu, M.H. Zheng, Histol Histopathol 17 (2002) 929.

[38] D. Riedel, W. Antonin, R. Fernandez-Chacon, G. Alvarez de Toledo, T. Jo, M. Geppert, J.A. Valentijn, K. Valentijn, J.D. Jamieson, T.C. Sudhof, R. Jahn, Mol Cell Biol 22 (2002) 6487.

[39] S. Greber, G. Lubec, N. Cairns, M. Fountoulakis, Electrophoresis 20 (1999) 928.

[40] I. Callebaut, J.P. Mornon, Biochem J 321 (Pt 1) (1997) 125.

Table 1. Reproducibility of the retention time based on the major peaks in Figure 5A.

Peak no.	retention time (min)					
	1st	2nd	3rd	Average	SD	RSD (%)
1	3.02	3.03	3.02	3.02	0.0096	0.32
2	10.65	10.27	9.85	10.06	0.4010	3.99
3	11.4	11.17	10.88	11.02	0.2587	2.35
4	17.32	17.30	17.32	17.31	0.0096	0.056
5	20.57	20.42	20.58	20.50	0.0918	0.45
6	22.83	22.70	22.98	22.84	0.1417	0.62

Table 2. Part of identified proteins and their physiological function.

Band number	Protein	Observed mass (kDa)	Reported mass (kDa)	Accession number	MASCOT score
1	Chain A, Heat-Shock 70kDa Protein 42kDa ATPase N-Terminal Domain	75	41827	gi|6729803	75
2	Mitochondrial ribosomal protein S10	17	23163	gi|16554607	65
3	RAB3D, member RAS oncogene family;	26	24267	gi|4759000	107
	Similar to Zinc finger protein 180 (HHZ168)		24137	gi|30155719	
4	EBNA-2,co-activator (100kDa)	110	99671	gi|33869218	71

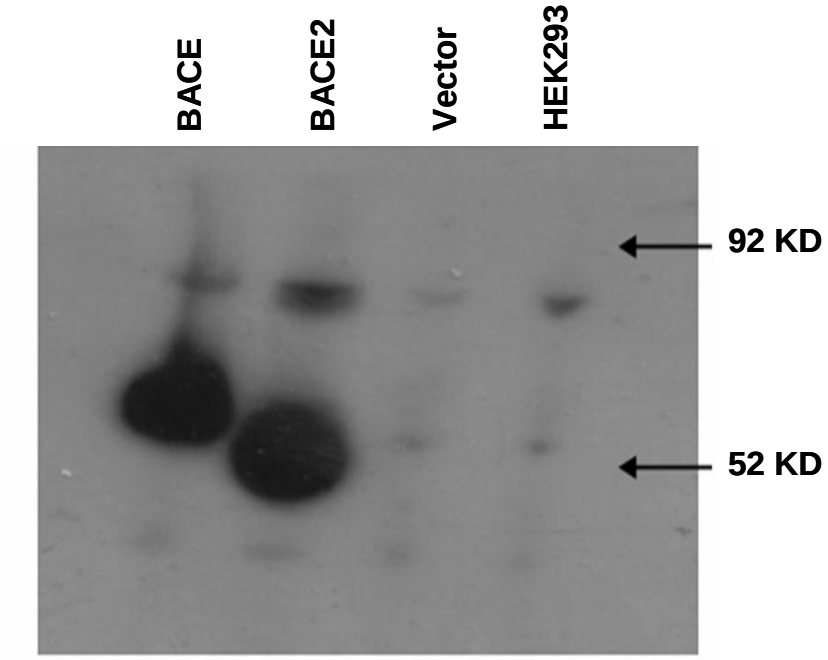

Figure 1. Western blot analysis of BACE overexpression and BACE2 overexpression in HEK 293 cells versus controls of vector-transfected HEK 293 cells and untransfected HEK 293 cells.

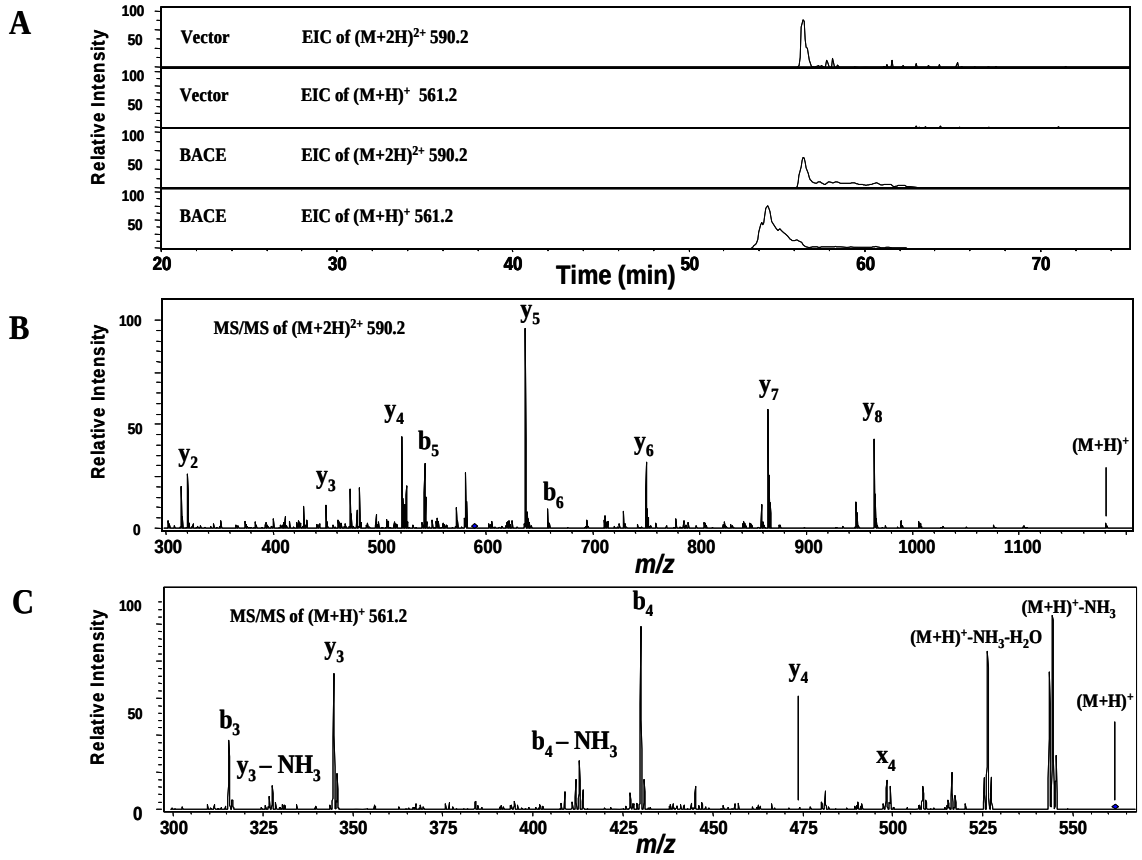

Figure 2. LC/MS/MS analysis of enzyme assay reaction mixture. (A) Extracted ion chromatogram (EIC) of full length peptide ($(M+2H)^{2+}$ at 590.2) and N-terminal product ($(M+H)^{+}$ at *m/z* 561.2) for vector control and BACE, respectively; (B) MS/MS mass spectrum of full length peptide; (C) MS/MS spectrum of N-terminal product.

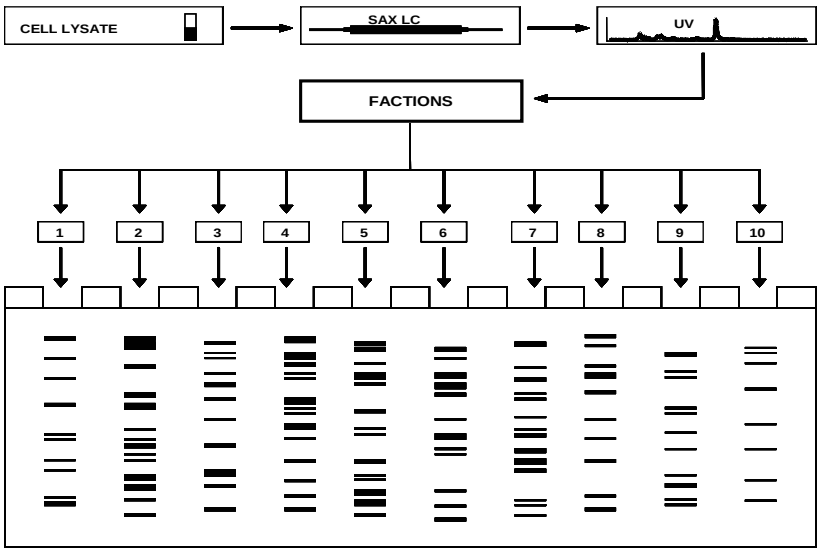

Figure 3. Schematic diagram illustrating combined liquid chromatography gel electrophoresis separation of proteins.

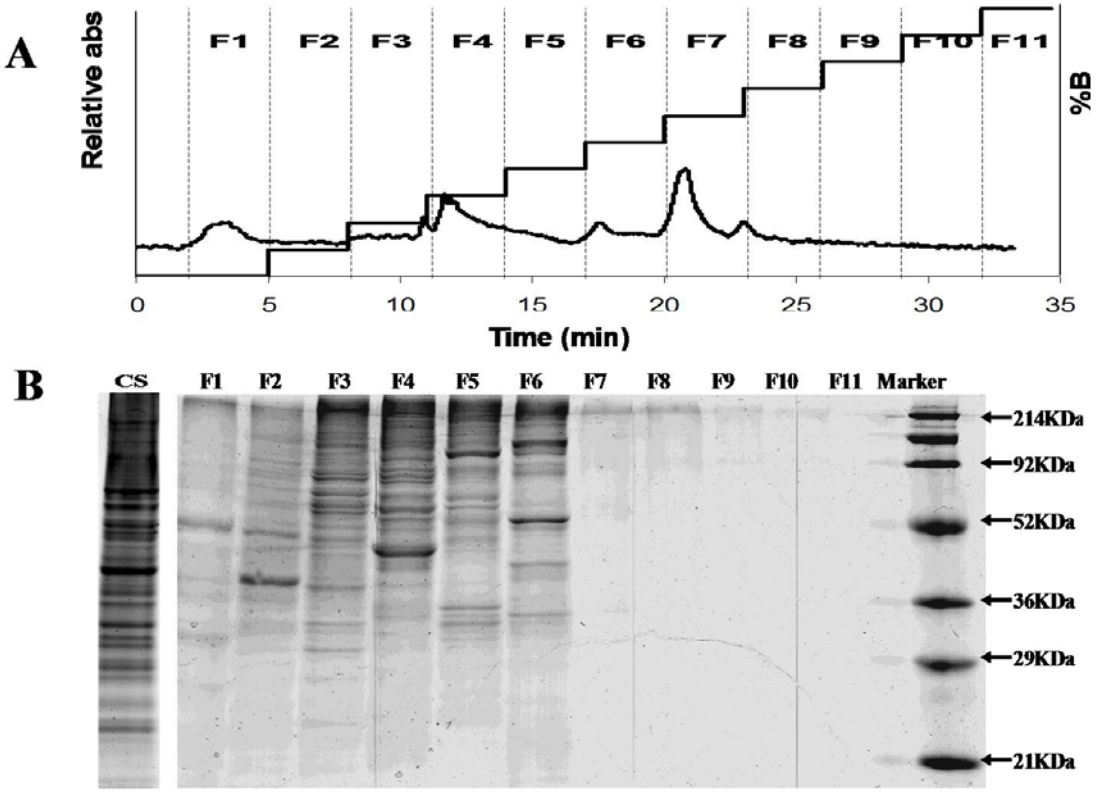

Figure 4. SAX HPLC on protein separation and gel separation of fractions. (A) UV chromatogram. The step-gradient elution profile is shown here. F1 to F11 represented the fractions collected at 3 minute intervals corresponding to different elution condition, and CS represented unfractionated cell lysate; (B) 8-16% SDS-PAGE gel (Bio-Rad) image of individual fractions.

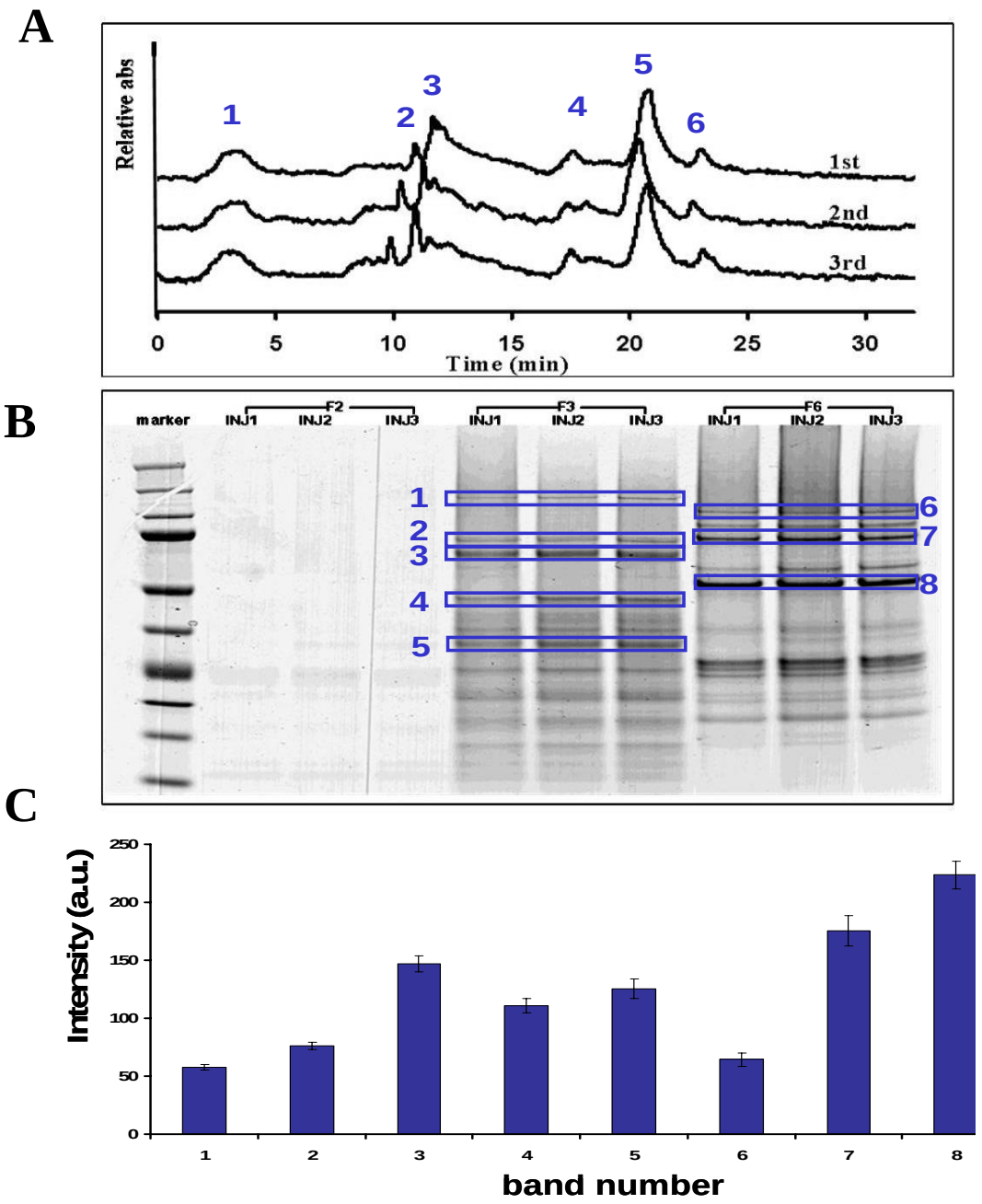

Figure 5. Multiple analyses of HEK 293 cell lysates with SAX HPLC and gel separation of fractions. (A) UV chromatograms; marked peaks are used to evaluate the reproducibility of retention time (in Table 1). (B) 4-12% SDS-PAGE gel (Invitrogen) image of individual fractions from triplicate analyses; (C) Quantitative data (average and standard deviation) of sets of gel bands marked in (B).

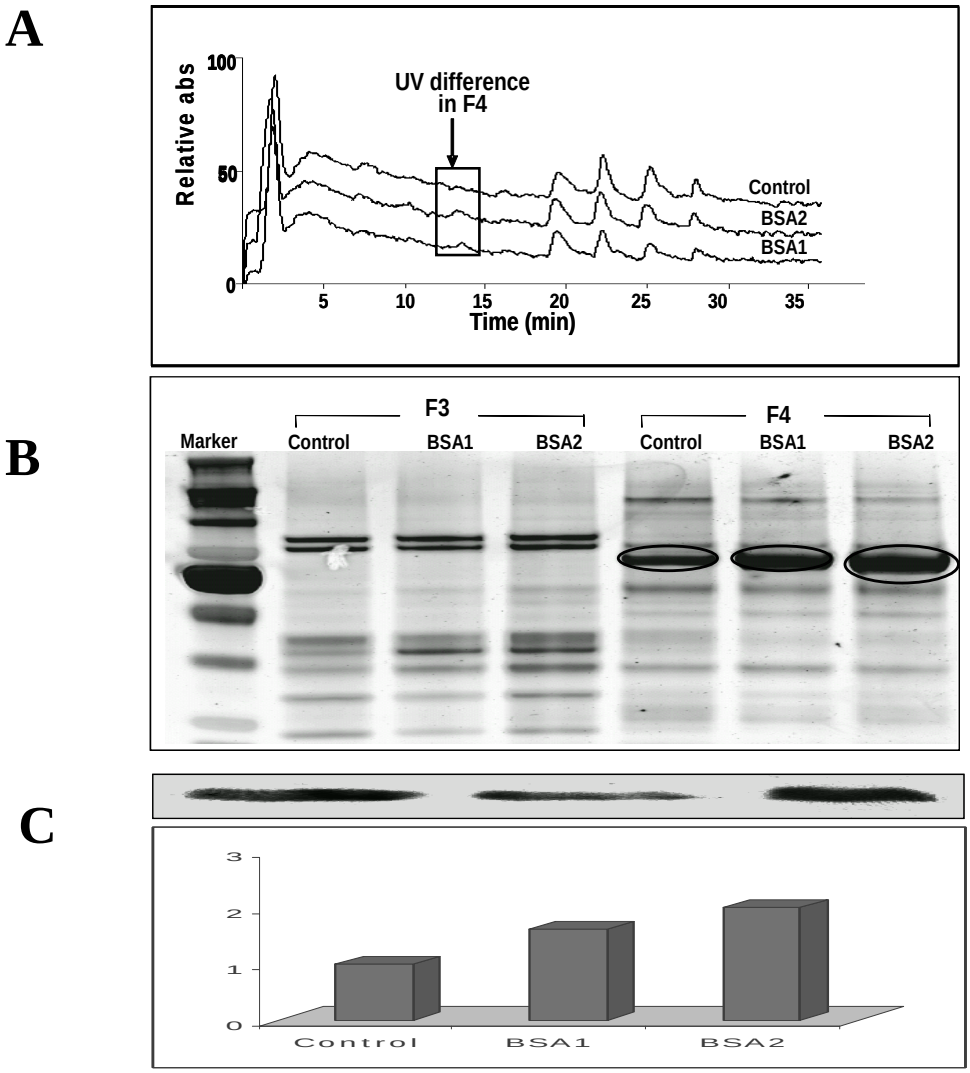

Figure 6. BSA spiking in control HEK 293 cell lysates. (A) UV chromatograms; (B) 4-12% SDS-PAGE gel (Invitrogen) image of individual fraction; (C) Intensity ratio after normalization by Western blot of internal control beta-actin on the same gel. "BSA1" refers to cell lysate spiked 10 μg BSA and "BSA2" refers to cell lysate spiked 20 μg BSA.

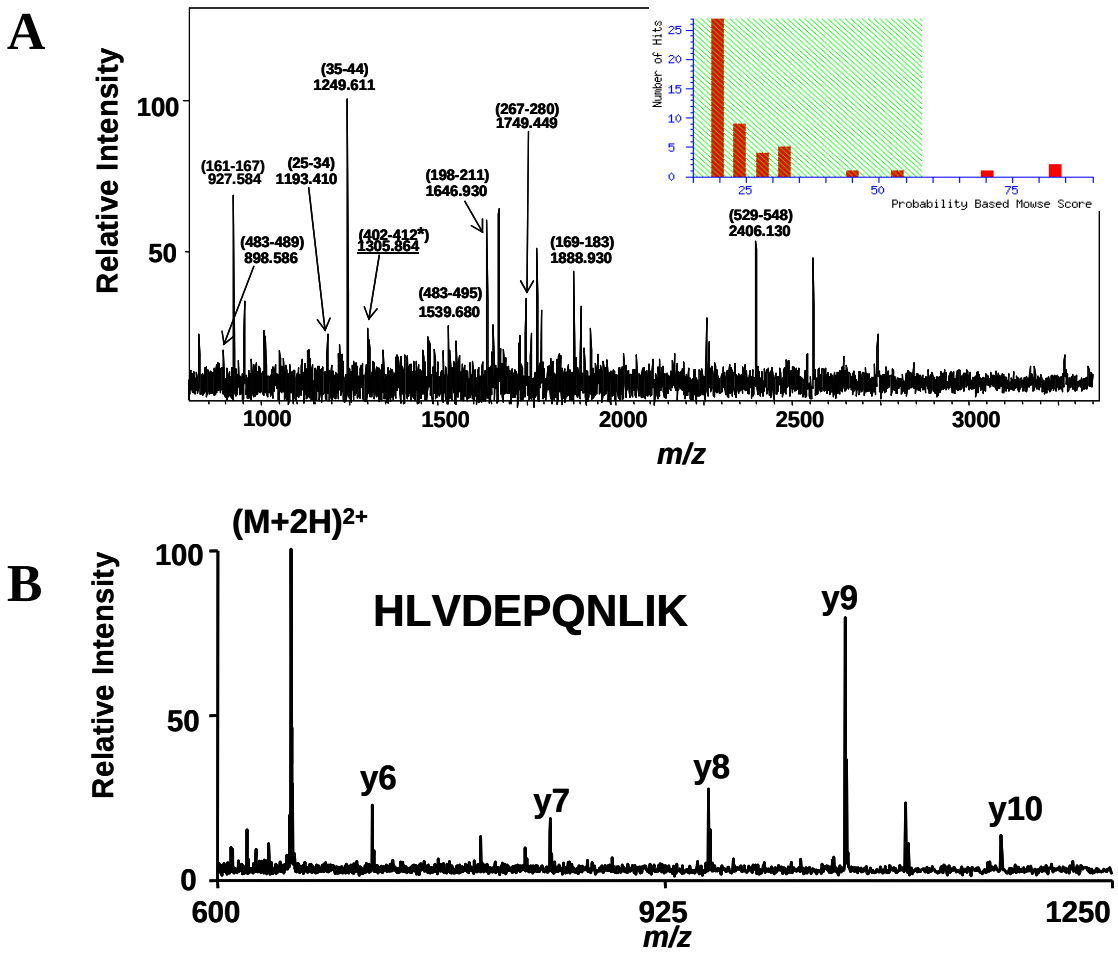

Figure 7. Mass spectra from in-gel tryptic digestion of band circled in Figure 6B "BSA2" sample. (A) MALDI-TOF based peptide mass fingerprint; the identified peptides are labeled by using their $(M+H)^+$ and sequence range. (B) ESI-FTICR-MS/MS spectrum of the 2+ charge state ions of the peptide denoted with an asterisk in Figure 7A. The observed y-series ions confirm the sequence of this BSA tryptic fragment.

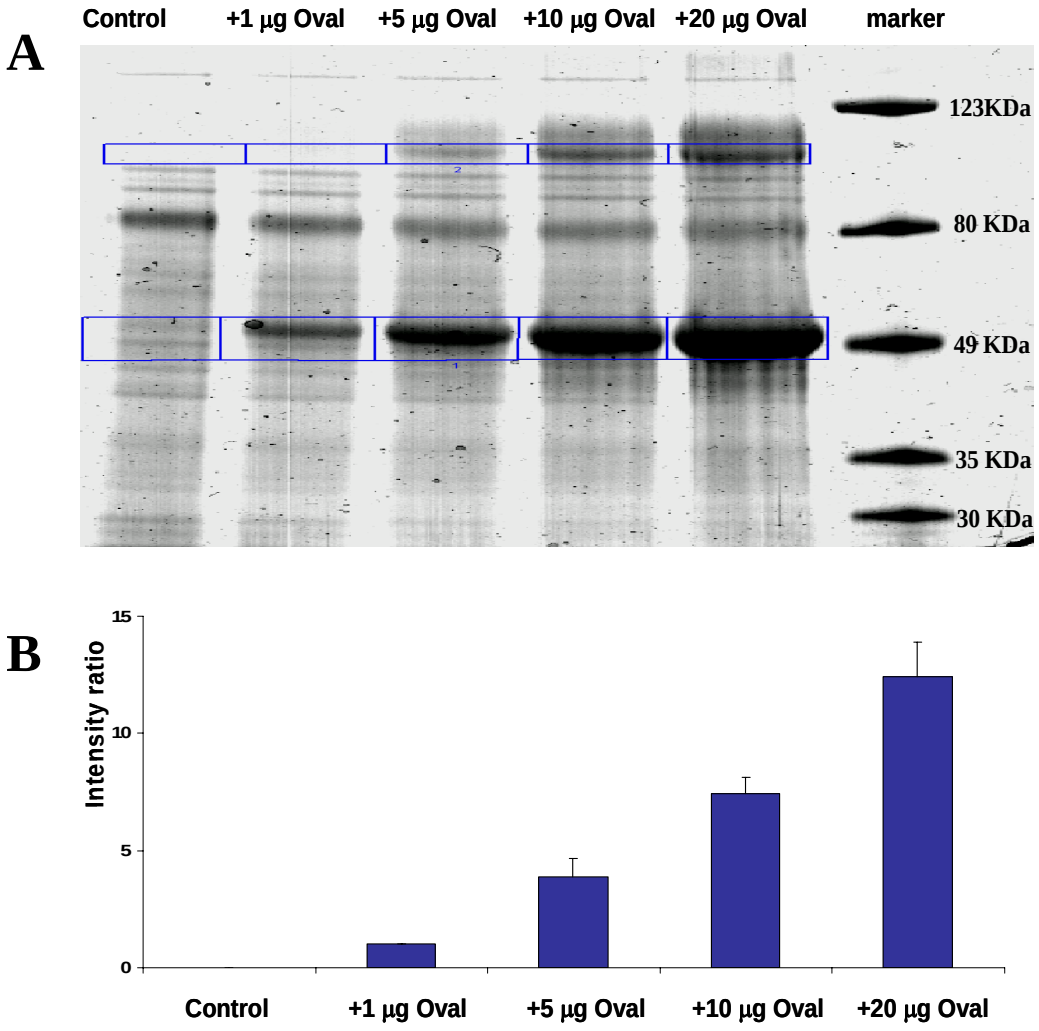

Figure 8. Ovalbumin spiking in control HEK 293 cell lysates. (A) 4-12% SDS-PAGE gel (Invitrogen) image; (B) Intensity ratio after subtracting control as the background. Quantitative data are shown here with average values and standard deviations.

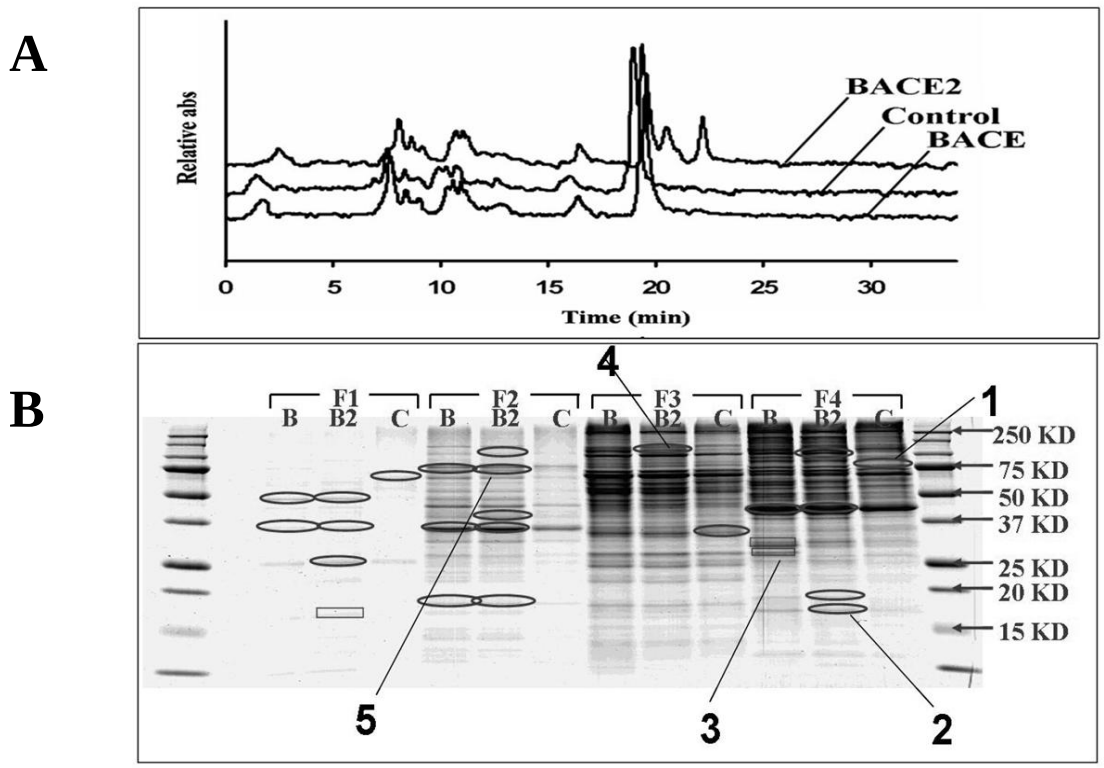

Figure 9. Comparison of BACE and BACE2 overexpressing cells with pcDNA3-transfected control cells. (A) UV chromatograms; (B) 8-16% SDS-PAGE gel (Bio-Rad) image of individual fractions (B = BACE, B2 = BACE2, C = control). The bands marked with numbers are the identified proteins shown in Table 2.

CHAPTER FOUR

Incorporation of a Flared Inlet Capillary Tube on a Fourier Transform Ion Cyclotron Resonance Mass Spectrometer

Si Wu[1], David C. Prior[2], Kai Zhang[1], Nathan K. Kaiser[1]

Gordon A. Anderson[2], James E. Bruce[1*]

[1] Department of Chemistry, Washington State University, Pullman, WA 99164;

[2] Environmental Molecular Sciences Laboratory, Pacific Northwest National Laboratory, Richland, WA 99352

Running title: Atmospheric pressure ionization methods with a flared inlet capillary tube on a FTICR mass spectrometer

*Corresponding author: James E. Bruce
Washington State University
Department of Chemistry
P.O. Box 644630
Pullman, WA, 99164-4630
Fax: (509) 335-8867
Email: james_bruce@wsu.edu

Published at *Journal of the American Society for Mass Spectrometry 2006*;17:772-9.

ABSTRACT

Flared inlet capillary tubes have been coupled with a Fourier transfer ion cyclotron resonance mass spectrometer (FTICR-MS) to help the ion transmission from the atmospheric pressure to the first vacuum region. We investigated different types of atmospheric pressure ionization methods using flared inlet tubes. For most of the ionization methods, such as ESI and DESI, increased ion current transmitted from the atmospheric pressure ion source to the first stage vacuum system was observed with the use of our enhanced ion inlet designs. The corresponding ion intensity detected on a FTICR-MS was also observed to increase ~ 2-5 fold using ESI or DESI with the flared tube inlet. Moreover, increased spray tip positional tolerance was observed with implementation of the flared inlet tube. We also include our preliminary results obtained by coupling AP-MALDI with flared inlet tube in this paper. For AP-MALDI, the measured ion current transferred through the flared inlet tube was about 2-3 times larger than the ion current through the control non-flared inlet tube.

INTRODUCTION

A number of atmospheric pressure ionization sources, such as electrospray ionization (ESI) and atmospheric pressure matrix-assisted laser desorption/ionization (AP-MALDI), have been widely used with mass spectrometry for proteomics study [1-5]. Desorption electrospray ionization (DESI) is an exciting new atmospheric pressure desorption ionization method introduced by Cooks et al. [6,7] Charged solvent droplets are sprayed directly onto an analyte surface through a pneumatically-assisted electrospray ion source. This new method is very attractive due to its utility for direct analysis of different compounds on a variety of surface types [6-8] and will enable application of mass spectrometry to more diverse, more challenging analytical problems. For all these ionization methods, the ions generated under ambient conditions are transferred through an atmospheric pressure interface such as an inlet tube or an orifice followed by several stages of differential pumping and then ions are sent to the MS detector [1-3].

A common hurdle encountered in the implementation of any atmospheric ion source is related to the transfer of ions produced at atmospheric pressure to the low vacuum mass analyzer. For all these atmospheric pressure ion sources, the gas-phase ions produced at atmospheric pressure are transferred to the lower pressure regions through conductance limits such as a metal capillary or an orifice [9,10]. For electrospray ionization, it has been reported that gas-phase collisions and charge-charge repulsion after ion formation lead to an expansion of the ion cloud [3,11]. In AP-MALDI and DESI, ions are also dispersed once created at atmospheric pressure. Since ions must enter the MS through a small aperture or capillary with limited cross section, the ion cloud expansion and dispersion can significantly decrease the ion transmission to the lower

pressure region, and thus decrease the sensitivity of the analysis. It has also been reported that the ion transmission efficiency between the ESI emitter and the inlet of the mass spectrometer is only 0.01-0.1% [3,12,13]. For AP-MALDI, even with precise aperture alignment and source positioning, sampling efficiency is generally lower than the sampling efficiency in ESI [14]. Several approaches have been developed to improve ion transmission efficiencies between the ion source and the mass spectrometer as outlined below.

Smith et al. [9,15-17] have developed an electrodynamic ion funnel interface for electrospray ionization mass spectrometry, which applies rf and dc electric fields to a series of ring electrodes with successively smaller inner diameter apertures. The ion funnel can be situated immediately after the atmospheric pressure interface of the MS. The use of the ion funnel leads to more effective ion transmission to the analyzer region. This development has been reported to increase ion transmission efficiencies up to 23-fold. However, as the pressure in the ion funnel region increases, the required rf peak-to-peak potential for efficient ion focusing increases correspondingly [9]. Due to this, the ion funnel has not achieved widespread implementation in the atmospheric pressure region between the electrospray tip and ion sampling interface, where most ion losses may occur [3].

A new dynamic focusing technique called pulsed dynamic focusing (PDF) has been developed and applied to the AP-MALDI ion source to improve ion transmission into a mass spectrometer [14,18]. Other atmospheric pressure electrostatic lenses that improve ion transmission efficiencies in the high pressure region have also been reported [19-21]. However, these conventional ion optic devices are not very effective in avoiding or reversing ion-cloud expansion generated by gas-phase collisions and Coulombic repulsion in high pressure regions.

Other efforts to improve ion transmission efficiencies in the high pressure region include nebulization gas to assist in desolvation. Henion et al. [22] reported an "ion spray" device in which an increase of about 30% in ion signal intensity was obtained as compared to that obtained with a lower flow rate. An intersecting gas flow device developed by Covey et al. [23] can provide an increase in sensitivity of more than a factor of 10, and can significantly lower the background in the resulting mass spectra. Recent studies by Lee et al. [24] and Muddiman et al. [13] have shown large increases in ion abundance resultant from the implementation of a commercial air amplifier or a modified venturi device in the high pressure region. They also reported that these devices generated a concentric high-velocity converging gas flow around the electrospray tip to reduce spreading of the electrospray plume and improve the conduction of ions to the sampling orifice of the MS. They reported an impressive 18-fold increase in ion abundance and a 34-fold reduction in the detection limit. These advancements were achieved without any aperture or capillary entrance modifications, as described here, and could likely be further enhanced with the design described below.

Recently, we have developed a flared inlet capillary tube to replace the conventional straight metal capillary inlet tube which is widely used by different kinds of mass spectrometers [25]. Glish et al. [26] developed a new glass ion sampling device which also included a larger inner diameter inlet of the capillary. Both reports showed that a larger cross section of the capillary entrance can allow more ions to enter the MS using electrospray ionization. Similar to the Venturi device [13,24], the convergence of the gas flow toward the smaller end of the capillary tube can also help to reduce the spreading of the ion cloud and help to transfer more ions into the low pressure region. We observed that ion current from ESI could be improved by nearly a factor of three with flared inlet tubes as compared with non-flared control tubes. Ion

signal measured by a TOF spectrometer was similarly improved. Building on the initial report [25], we incorporated the flared inlet tube onto a 7T FTICR-MS instrument for a more comprehensive study on ion transmission efficiency under different kinds of atmospheric pressure ionization methods such as ESI, DESI, and AP-MALDI. Improved ion transmission by coupling the flared inlet tube with different ionization methods was demonstrated by the increase in both the observed ion abundances in the FTICR mass spectra and the ion current measured beyond the capillary exit. Also, we observed a weaker dependence on ESI spray position relative to the capillary central axis. The results with ESI-FTICR-MS and DESI-FTICR-MS and our initial data illustrating the benefits of coupling an AP-MALDI ion source with flared inlet tubes are reported here.

EXPERIMENTAL

Chemicals

Substance P and angiotensin II were purchased from Sigma (St. Louis, MO) and used without further purification. 10 mM stock solutions of each standard peptide were prepared in purified water (18 MΩ*cm) using a Nanopure ultra-purified water system from Barnstead International (Dubuque, IA). Analytical standards were prepared by dilution using 50/50 (v/v) methanol/water with 0.1% acetic acid.

Flared inlet tubes for the atmospheric pressure interface

The flared inlet tube was implemented in our FTICR-MS instrument as shown in the Figure 1. A set of prototype ion inlet tubes were produced either in-house or from Small Parts Inc. (Miami Lakes, FL) with various inlet sizes and configurations. The inlet tube was designed with a larger flared end which pointed towards the ion source to receive ions. In Figure 1, different angles of the flared tubes were made with 0.015" or 0.02" interior diameter. Outer diameter of the unflared end was either 0.03" or 1/16". Non-flared tubes with the same i.d. and length were used for control studies to demonstrate the improvements of the flared tube. The lengths of both the flared tubes and non-flared tubes were variable from 6" to 10". Two different types of flared tubes were used in the ESI, DESI, and ESSI experiments reported in this paper: one set was 0.02" i.d. and 1/16" o.d. at the unflared end, and was flared 10 degrees from the center line to ~ 3 mm o.d. at the larger end; The other set was 0.015" i.d. and 0.03" o.d. at the unflared end, and was flared with a 45 degree angle from the center line to ~ 2.2 mm o.d. at the larger end. Both types of the flared tubes were placed into a ¼" stainless steel tube which is

interchangeable with the commercial glass capillary tube originally in our FTICR-MS instrument. All the capillary inlet tubes were maintained at a temperature of 220 °C during experiments.

Atmospheric pressure ionization sources

We investigated the ion transmission efficiency of flared ion inlet tubes with ESI and other atmospheric pressure ion sources such as DESI. For ESI experiments, the spray tips were made by etching a 20-μm-i.d., 360-μm-o.d. fused-silica capillary with 49% HF. Solutions of the peptides were prepared by dilution of stock solutions using 50:50 MeOH:H_2O with 0.1% acetic acid. Infusion was performed with a syringe pump at a flow rate of 250 nl/min. A potential up to 4 kV was applied to the sample solution through a copper alligator clip attached to the metal union before the spray tip. For ESI, the position of the spray tip was controlled by a 3D linear stage from Newport (Irvine, CA). The setup used for DESI was similar to the setup previously described by Cooks et al. [6,7]. For DESI, a potential of 2.5-3.5 kV was applied to the spray solution through a copper alligator clip attached to the stainless steel syringe tip used for sample infusion. The spray emitter was mounted about 0.5-1 mm from the sample surface at about 50 degrees (similar to the optimal conditions reported by Cooks et al. [6] and Van Berkel et al. [8]). A polytetrafluoroethylene (PTFE) surface was used in the DESI experiments and its surface area was about 20 mm^2, and the position of the sample target was controlled by the 3D linear stage mentioned above. DESI solvent flow rate was about 0.5-1μl/min. Other optimal operation conditions were similar to those reported by Cooks et al. [6,7]. We also investigated the implementation of electrosonic spray ionization method (ESSI) by comparing the flared inlet tube and the non-flared control inlet tube. The homebuilt ESSI ion source was similar to the setup previously described ESSI ion source by Takats et al.[27]

AP-MALDI

The AP-MALDI ion source described here was designed as a component of a novel high sensitivity AP-MALDI-FTICR mass spectrometer which is currently under development in our lab. Several stages of differential pumping are incorporated in the vacuum system of this mass spectrometer. The first pumping stage (between the capillary exit and the skimmer) was evacuated by an Edwards E2M30 mechanical pump (Wilmington, MA) to 2-4 torr. For AP-MALDI, a pulsed nitrogen laser (model VSL337, Spectra-Physics, Irvine, CA), at a wavelength of 337.1 nm was employed. The laser output was attenuated using a circular variable neutral density filter, and was focused onto a small copper target plate (approximately 2 mm x 3 mm in size) by a 10 cm focal length UV grade fused silica precision plano-convex lens SPX022 from Newport (Irvine, CA). Laser firing was externally triggered at a 3-Hz repetition rate by an arbitrary function waveform generator, model 33120A from Hewlett Packard (Palo Alto, CA). The AP-MALDI source was coupled with several types of capillary inlet tubes. The position of the sample plate relative to the interface of the inlet tube was optimized by adjustment of the 3D linear stage described above. No high voltage was applied to the sample target. We compared the ion transmission efficiency of different inlet tubes by measuring the ion current on the skimmer from each laser pulse. The generated ion current was amplified by a Keithley current amplifier Model 428 (Cleveland, OH) and then recorded by a digital storage oscilloscope model TDS 2024 from Tektronix (Richardson, TX). Samples for AP-MALDI were prepared on the sample target by mixing 2 μl 100 μM substance P with 2 μl matrix solution (saturated 2,5-dihydroxybenzoic acid in 50:50:0.1 of acetonitrile:H_2O:TFA).

Instrumentation

A Bruker Daltonics (Billerica, MA) Apex-Q 7T FTICR mass spectrometer was used to acquire the mass spectral data. The ions entered the instrument through the flared inlet tube, and then passed through a hexapole followed by a mass-selective quadrupole and then a second hexapole. After accumulation in the second set of hexapole rods for the duration of 0.5-2 seconds, the ions were then sent toward the ICR cell using an electrostatic ion guide. The ions were trapped in the ICR cell using a low energy sidekick potential [28] to keep the ions close to the central *z* axis of the cell. All data sets acquired were 128k points. The mass spectral data were acquired using Xmass 7.0.6 as the data acquisition software program. The external calibration was done using a mixture solution of standard peptides. All the FTICR-MS data were analyzed using ICR-2LS software package [29].

RESULTS AND DISCUSSION

Electrospray ionization

Ion intensity comparison

As shown in the patent by Prior et al.[25], measured ion current can be increased 3-fold or more using the flared inlet tube. The original data compared the ion signal from the magnetic-bottle time of flight photoelectron spectrometer using ESI with flared inlet tube or with non-flared control tube. Here we applied the flared inlet tube on our FTICR-MS instrument with a variety of ion sources. We evaluated total ion signal intensity for each mass spectrum. We also measured the ion current transmitted through the capillary tube by placing an aluminum plate ~ 3 mm beyond the capillary exit. Figure 2 shows the total ion intensity measurements as a function of spray potential with or without the flared inlet tube. The flared inlet tube used for this research was 0.015" i.d. and 0.03" o.d. at the unflared end, and was flared with a 45 degree angle from the center line to ~ 2.2 mm o.d. at the larger end. A 10 μM substance P solution was used for both sets of experiments, and the MS operating parameters and infusion rates were held constant. The distance between the spray tip and the capillary was 1 mm for both cases, and the tip was aligned to the capillary center with careful adjustments. With ESI, the ion signal intensity is generally dependent on the high voltage applied to the spray tip. Most of the time, the ion signal will be initiated at some minimum voltage and will increase with increasing voltage until the signal intensity reaches some maximum value [3]. Figure 2 shows that this maximum ion intensity value was achieved at the spray potential of 2.2 kV with or without the flared inlet tube. However, we observed nearly a 2-fold increase in ion intensity with the implementation of the flared inlet tube. From the measurement of current via the aluminum plate

beyond the exit of the capillary tube, we also observed a ~ 3-fold increase in the ion current transmitted through the capillary. Since both ion current and measured ion signal are increased, we believe that the flared inlet tube significantly improves the ion transmission from atmospheric pressure to the first vacuum stage, and therefore improves the ion signal intensity detected with the mass spectrometer. These improvements are likely related the convergence of the gas flow and larger angle of acceptance of the flared tubes as compared with the conventional ion inlet tubes. When using the non-flared inlet tube, only a small portion of the ions in the plume can be transferred due to the small inner diameter of the inlet tube. With the flared inlet tube, the much larger entrance and acceptance angle can help to transfer a much larger portion of the ions in the plume.

Dependence of tip position

The location of the spray tip relative to the capillary central axis is very critical to achieve the optimum ion transmission when using a non-flared control capillary inlet tube. To determine the dependence of the tip position relative to the capillary central axis with the flared inlet tube, we did a series of experiments where the distance between the spray tip and inlet interface (distance Z in Figure 1) was varied, or the distance that the spray tip is away from the inlet tube center (distance X in Figure 1) was varied. The flared tube used in these experiments was 0.015" i.d. and 0.03" o.d. at the smaller end with a flared 45 degree angle at the larger end from the center line to ~ 2.2 mm i.d. (the distance from the center to the edge was about 1.1 mm).

Direct infusion of 10 μM substance P solution was used for the determination of spray tip position effects on signal intensities. As mentioned above, we evaluated the total ion intensity for each spectrum. Figure 3 shows the total ion intensity of substance P ions from the FTICR-

MS as a function of the distance between the spray tip and inlet surface (distance Z). As shown in Figure 3, when we moved the spray tip further from the inlet interface, the ion intensity started to decrease at about 2 mm with the flared inlet tube or with the non-flared control tube. However, the *initial* rate of decrease of ion intensity with the non-flared ion inlet tube was found to be much higher than that observed with the flared ion inlet tube. Ion signal intensity decreased by 50% within the distance Z of 5 mm when using the non-flared tube. For the flared tube, the ion signal intensity decreased much slower. This may result from the fact that a larger electrospray plume due to charge-charge repulsion is present with ESI at longer tip-to-entrance distances. With the use of the flared tube, the convergence of the gas flow toward the smaller end of the capillary tube can help to reduce the spreading of the ion cloud, resulting in a smaller decrease in the ion intensity.

Figure 4 demonstrates the observed change in the total ion intensity of substance P ions observed when the relative position of the spray tip and the inlet center (distance X) was varied. A spray potential of 3 kV was applied for both cases, which was optimal for both the flared capillary tube and the non-flared capillary tube. With a constant distance Z of 1mm with the non-flared tube, we found that the ion intensity decreased quickly with increasing distance X and ion signal was completely gone when distance X was 0.8 mm. However, when we employed the flared tube (distance Z = 1 mm), the ion intensity measured by FTICR-MS was observed to be constant without significant decrease when the distance X was increased as large as 1.2 mm. When we increased the distance X greater than 1.2 mm, ion signal started to decrease and the signal-to-noise ratio of the peak approached 1 at the distance X of 2.0 mm. Since the diameter of the flared inlet interface is about 2.2 mm, when we moved the spray tip to the distance X of 1.2 mm, the tip position is near the outer edge of the flared inlet interface. These results showed that

we can observe constant ion signal when we keep the spray tip in any position inside the interface area (distance Z=1 mm). Similar results were also observed when we increased the distance Z to 10 mm (Figure 4B). As mentioned above, with the longer distance Z, the larger ion plume of ESI spray can be formed due to the longer time for charge-charge repulsion to result in ion dispersion prior to capillary entrance. Thus, the longer distance leads the smaller portion of ions transferred through the capillary tube. However, the larger ion plume results in less dependence on the spray tip position relative to the inlet center. Therefore, we expect the ion signal to decrease slower by increasing the distance X using longer distance Z. As shown in Figure 4B, even with the non-flared inlet tube, ion signal was observed when the distance X was smaller than 10 mm. However, with the flared inlet tube, this distance increased to 20 mm. Therefore, ion signal was observed to be less dependent on the spray tip position with the use of the flared inlet tube. Overall, the increase of the spray tip positional tolerance observed with the flared inlet tube can significantly increase sensitivity and reduce the efforts required to optimize spray performance, as compared with a non-flared control inlet tube.

Desorption Electrospray Ionization (DESI) and Electrosonic Spray Ionization (ESSI)

A series of angiotensin II solutions with various analyte concentration values were analyzed with flared and non-flared inlet tubes to determine if the flared inlet tube can improve the ion transmission efficiency using DESI. Five different solutions of angiotensin II were used for sampling on a PTFE surface with an average surface sample concentration of 10, 50, 100, 500 and 1000 fmol/mm^2 (we adopted the average surface concentration concept as published by Cooks et al. [6]). For each spot, a series of scans with 1s ion accumulation time was acquired. As shown in Figure 5A, for a 500 fmol/mm^2 sample, the highest ion intensity among all the

scans collected for a single spot using the non-flared tube is about 3-4 times less than the highest ion intensity using flared tube. For each spot, the average of 10 highest total ion intensities was plotted as a function of sample concentration, as shown in Figure 5B. The error bars in Figure 5B represent the standard deviation resultant from three independent spot analyses. To demonstrate the improvements using the flared inlet tube, we calculated the average intensity ratio of the flared inlet tube to the non-flared control inlet tube at each concentration. While comparing with the standard inlet tube, we found an overall 2.5-fold increase in the average ion intensity with use of the flared tube with DESI. In addition, the lowest surface sample concentration that produced measurable ion signals with DESI-FTICR-MS was 50 fmol/mm^2 with the use of the non-flared inlet tube. However, the lowest surface sample concentration observable with DESI decreased to 10 fmol/mm^2 with the use of the flared tube. These results show a factor of 2.5-5 improvement in both S/N and limit of detection (LOD) with the use of the flared inlet tube with DESI. As with the studies of coupling ESI and the flared inlet tubes described above, we also found that the sample target positional tolerance relative to the capillary tube was increased with the implementation of the flared inlet (data not shown here).

We have also evaluated the measured ion current and the corresponding ion intensity for mass spectra acquired with the flared inlet tube and with the non-flared control inlet tube using ESSI [27]. However, no significant improvement of total ion signal was observed with the flared inlet tube (data not shown here) when we aligned the tip very carefully to the capillary center. This was different from ESI and DESI results described above, and may result from the greater overall charge and repulsion of ions with ESI that leads to greater radial dispersion of ions as compared with ESSI [27,30].

Coupling the flared inlet tube with AP-MALDI

To investigate the effects of the flared inlet tube on the transmission of ions produced by AP-MALDI, we used an inlet tube which was 0.03" i.d. and 1/16" o.d. at the unflared end, 9.3" total length, and was flared 30 degrees from the center line to ~ 3 mm o.d. at the larger end. The corresponding control non-flared inlet tube we used was 0.03" i.d. and 1/16" o.d. with a total length of 10". The choice of larger diameter inlet tube here was made to allow us to record and compare the ion current from AP-MALDI ion source. In general, the ion current generated by AP-MALDI was much smaller that the ion current generated by ESI [14] and with smaller i.d. capillaries, became difficult to measure. We recorded output of the current amplifier with a digital oscilloscope and synchronized the scope to the laser firing by triggering the oscilloscope using the same triggering signal from the functional waveform generator which was used to fire the laser pulse. The ion current for each sample spot was measured on the skimmer and was recorded by averaging 16 scans of current signals corresponding to 16 laser pulses. We found the ion current arrival time at the skimmer was slightly delayed for the non-flared tube compared to the flared inlet tube, which is expected due to the fact that the inlet tube lengths of the flared and non-flared tubes were slightly different (9.3" v.s. 10"). However, since the overall lengths of the tubes were similar, as was the measured pressure near the capillary exit (4.0 torr v.s. 3.6 torr), we believed that the measured ion current values are still comparable. To demonstrate the differences observed with AP-MALDI, we overlaid the ion current profiles with the flared inlet tube and with the control tube. Figure 6 is the overlay comparison of the recorded ion current responses with the flared inlet tube and with the non-flared inlet tube. The error bars indicated on the peak values of each profile illustrate the standard deviation resultant from peak current measurements from 3 sample spots. We observed approximately a 3-fold increase in ion current

measured on the skimmer with implementation of the flared inlet tube. Ion current peak width of the laser pulse with the flared tube was slightly smaller than the peak width with the control tube. The calculated average peak area with the flared tube was 2.4 times larger than the calculated average peak area with the non-flared tube. Although the ion current we measured hitting on the skimmer likely included many matrix ions other than gas phase analyte ions, this current is anticipated to be proportional to the analyte ion signal detected by the mass spectrometer. Based on these preliminary results, in the future we will design a new AP-MALDI ion source for the Bruker 7T FTICR mass spectrometer and incorporate with the flared inlet tube as the atmospheric pressure interface. We expect similar improvements in the measured ion signal intensities, as we have observed with most other atmospheric ion sources.

CONCLUSIONS

A new type of atmospheric pressure interface with FTICR-MS was employed with a flared inlet tube. The flared inlet tube can efficiently focus ions at atmospheric pressure from a variety of ion sources, including ESI, DESI and AP-MALDI. The application of a flared inlet tube to nano-electrospray ionization resulted in a 2-fold increase of the measured ion intensity. Also, our studies on the tip position relative to the inlet tube showed relative tip-inlet position adjustment was less critical for optimal performance with the flared tubes, as compared with conventional non-flared inlet tubes. With the application of the flared inlet tube to DESI, we also observed a significant increase in the measured ion intensity. The lowest surface sample concentration which can be successfully detected with DESI on our instrument also decreased to 10 fmol/mm^2, a 5-fold improvement in LOD with the use of the flared inlet tube. Our preliminary studies with an AP-MALDI ion source with the flared inlet tube demonstrated that more ions can be transferred through the flared inlet tube. In future work, we will implement the AP-MALDI ion source with our 7T FTICR-MS by coupling with the flared inlet tube.

In addition to greater ion current, another advantage of the flared inlet tube is that standard capillary tubes can be easily replaced with flared inlet tubes without additional significant instrument modifications. This makes the flared inlet tube very attractive, since it is readily combined with other atmospheric pressure or high pressure ion focusing techniques. For example, a possible combination is to incorporate the Venturi device described by Lee et al. [24] and Muddiman et al. [13] with the flared inlet tube. Coupling with the flared inlet tube can potentially further improve the performance of the Venturi device due to the larger cross section area of the flared tube. Another area where the flared inlet tube will likely significantly benefit

analysis is in the coupling of atmospheric pressure gas phase separation techniques like IMS [31] or FAIMS [32,33]. Williams et al. [34] have demonstrated significant decrease in background chemical noise possible with FAIMS-FTICR-MS coupling that significantly enhances dynamic range. These efforts can likely be even further improved with methods that allow more efficient transmission of ions from atmospheric pressure to the first stage of the vacuum system, as is possible with the flared inlet. Finally, the combination of the flared inlet with the ion funnel introduced by Smith et al. [15], and adopted in other groups as well [35], is also likely to produce greater sensitivity since these devices show significant improvement in ion focusing in the vacuum stage after the capillary tube. By combining the flared inlet tube with the ion funnel, we anticipate that more ions can be transferred to the detector, and even greater sensitivity can be achieved.

ACKNOWLEDGEMENTS

This work was supported by grants from the M.J. Murdock Charitable Trust; the Directorate of Biological Sciences, National Science Foundation, Grant No.DBI-0352451; and the Office of Science (BER), U.S. Department of Energy, Grant No. DE-FG02-04ER63924. We are also grateful to PNNL for providing the software ICR-2LS used for data analysis.

REFERENCES

1. Fenn, J. B.; Mann, M.; Meng, C. K.; Wong, S. F.; Whitehouse, C. M. Electrospray Ionization for Mass Spectrometry of Large Biomolecules. *Science* **1989**, *246*, 64-71.

2. Whitehouse, C. M.; Dreyer, R. N.; Yamashita, M.; Fenn, J. B. Electrospray Interface for Liquid Chromatographs and Mass Spectrometers. *Anal. Chem.* **1985**, *57*, 675-679.

3. Cech, N. B.; Enke, C. G. Practical Implications of Some Recent Studies in Electrospray Ionization Fundamentals. *Mass Spectrom. Rev.* **2001**, *20*, 362-387.

4. Laiko, V. V.; Baldwin, M. A.; Burlingame, A. L. Atmospheric Pressure Matrix-Assisted Laser Desorption/Ionization Mass Spectrometry. *Anal. Chem.* **2000**, *72*, 652-657.

5. Laiko, V. V.; Moyer, S. C.; Cotter, R. J. Atmospheric Pressure Maldi/Ion Trap Mass Spectrometry. *Anal. Chem.* **2000**, *72*, 5239-5243.

6. Takats, Z.; Wiseman, J. M.; Gologan, B.; Cooks, R. G. Mass Spectrometry Sampling under Ambient Conditions with Desorption Electrospray Ionization. *Science* **2004**, *306*, 471-473.

7. Takats, Z.; Cotte-Rodriguez, I.; Talaty, N.; Chen, H.; Cooks, R. G. Direct, Trace Level Detection of Explosives on Ambient Surfaces by Desorption Electrospray Ionization Mass Spectrometry. *Chem. Commun. (Camb)* **2005**, 1950-1952.

8. Van Berkel, G. J.; Ford, M. J.; Deibel, M. A. Thin-Layer Chromatography and Mass Spectrometry Coupled Using Desorption Electrospray Ionization. *Anal. Chem.* **2005**, *77*, 1207-1215.

9. Shaffer, S. A.; Tolmachev, A.; Prior, D. C.; Anderson, G. A.; Udseth, H. R.; Smith, R. D. Characterization of an Improved Electrodynamic Ion Funnel Interface for Electrospray Ionization Mass Spectrometry. *Anal. Chem.* **1999**, *71*, 2957-2964.

10. Burlingame, A. L.; Boyd, R. K.; Gaskell, S. J. Mass Spectrometry. *Anal. Chem.* **1998**, *70*, 647R-716R.

11. Dodonov, A.; Kozlovsky, V.; Loboda, A.; Raznikov, V.; Sulimenkov, I.; Tolmachev, A.; Kraft, A.; Wollnik, H. A New Technique for Decomposition of Selected Ions in Molecule Ion Reactor Coupled with Ortho-Time-of-Flight Mass Spectrometry. *Rapid Commun. Mass Spectrom.* **1997**, *11*, 1649-1656.

12. Mann, M. In *Ion Formation from Organic Solids V*; Hedin, A., Sundqvist, B., Benninghoven, A., Ed.; John Willey and Sons: New York, 1990, pp 139-144.

13. Hawkridge, A. M.; Zhou, L.; Lee, M. L.; Muddiman, D. C. Analytical Performance of a Venturi Device Integrated into an Electrospray Ionization Fourier Transform Ion Cyclotron Resonance Mass Spectrometer for Analysis of Nucleic Acids. *Anal. Chem.* **2004**, *76*, 4118-4122.

14. Kellersberger, K. A.; Tan, P. V.; Laiko, V. V.; Doroshenko, V. M.; Fabris, D. Atmospheric Pressure Maldi-Fourier Transform Mass Spectrometry. *Anal. Chem.* **2004**, *76*, 3930-3934.

15. Shaffer, S. A.; Prior, D. C.; Anderson, G. A.; Udseth, H. R.; Smith, R. D. An Ion Funnel Interface for Improved Ion Focusing and Sensitivity Using Electrospray Ionization Mass Spectrometry. *Anal. Chem.* **1998**, *70*, 4111-4119.

16. Belov, M. E.; Gorshkov, M. V.; Udseth, H. R.; Anderson, G. A.; Smith, R. D. Zeptomole-Sensitivity Electrospray Ionization--Fourier Transform Ion Cyclotron Resonance Mass Spectrometry of Proteins. *Anal. Chem.* **2000**, *72*, 2271-2279.

17. Belov, M. E.; Gorshkov, M. V.; Udseth, H. R.; Anderson, G. A.; Tolmachev, A. V.; Prior, D. C.; Harkewicz, R.; Smith, R. D. Initial Implementation of an Electrodynamic Ion Funnel with Fourier Transform Ion Cyclotron Resonance Mass Spectrometry. *J. Am. Soc. Mass Spectrom.* **2000**, *11*, 19-23.

18. Tan, P. V.; Laiko, V. V.; Doroshenko, V. M. Atmospheric Pressure Maldi with Pulsed Dynamic Focusing for High-Efficiency Transmission of Ions into a Mass Spectrometer. *Anal. Chem.* **2004**, *76*, 2462-2469.

19. Schneider, B. B.; Douglas, D. J.; Chen, D. D. Multiple Sprayer System for High-Throughput Electrospray Ionization Mass Spectrometry. *Rapid Commun. Mass Spectrom.* **2002**, *16*, 1982-1990.

20. Schneider, B. B.; Douglas, D. J.; Chen, D. D. An Atmospheric Pressure Ion Lens That Improves Nebulizer Assisted Electrospray Ion Sources. *J. Am. Soc. Mass Spectrom.* **2002**, *13*, 906-913.

21. Feng, X.; Agnes, G. R. Single Isolated Droplets with Net Charge as a Source of Ions. *J. Am. Soc. Mass Spectrom.* **2000**, *11*, 393-399.

22. Henion, J. D.; Covey, T. R.; Bruins, A. P.: US patent 4,861,988, 1989.

23. Covey, T. R.: U.S. Patent 5,412,208, 1995.

24. Zhou, L.; Yue, B.; Dearden, D. V.; Lee, E. D.; Rockwood, A. L.; Lee, M. L. Incorporation of a Venturi Device in Electrospray Ionization. *Anal. Chem.* **2003**, *75*, 5978-5983.

25. Prior, D. C.; Price, J.; Bruce, J. E.: US patent 6,455,846, 2002.

26. Glish, G. L.; Danell, R. M.: US patent 6,703,611, 2004.

27. Takats, Z.; Wiseman, J. M.; Gologan, B.; Cooks, R. G. Electrosonic Spray Ionization. A Gentle Technique for Generating Folded Proteins and Protein Complexes in the Gas Phase and for Studying Ion-Molecule Reactions at Atmospheric Pressure. *Anal. Chem.* **2004**, *76*, 4050-4058.

28. Polfer, N. C.; Haselmann, K. F.; Zubarev, R. A.; Langridge-Smith, P. R. Electron Capture Dissociation of Polypeptides Using a 3 Tesla Fourier Transform Ion Cyclotron Resonance Mass Spectrometer. *Rapid Commun. Mass Spectrom.* **2002**, *16*, 936-943.

29. Anderson, G. A.; Bruce , J. E.; Smith , R. D.; ICR-2LS, Version 2.18 ed.; Pacific Northwest National Laboratory: Richmond, WA, 1996.

30. Hirabayashi, A. A Novel Nanoflow Interface for Atmospheric Pressure Ionization Mass Spectrometry. *Rapid Commun. Mass Spectrom.* **2003**, *17*, 391-394.

31. Hill, H. H., Jr.; Siems, W. F.; St Louis, R. H.; McMinn, D. G. Ion Mobility Spectrometry. *Anal. Chem.* **1990**, *62*, 1201A-1209A.

32. Guevremont, R.; Ding, L.; Ells, B.; Barnett, D. A.; Purves, R. W. Atmospheric Pressure Ion Trapping in a Tandem Faims-Faims Coupled to a Tofms: Studies with Electrospray Generated Gramicidin S Ions. *J. Am. Soc. Mass Spectrom.* **2001**, *12*, 1320-1330.

33. Purves, R. W.; Barnett, D. A.; Ells, B.; Guevremont, R. Gas-Phase Conformers of the [M + 2h](2+) Ion of Bradykinin Investigated by Combining High-Field Asymmetric Waveform Ion Mobility Spectrometry, Hydrogen/Deuterium Exchange, and Energy-Loss Measurements. *Rapid Commun. Mass Spectrom.* **2001**, *15*, 1453-1456.

34. Robinson, E. W.; Williams, E. R. Multidimensional Separations of Ubiquitin Conformers in the Gas Phase: Relating Ion Cross Sections to H/D Exchange Measurements. *J. Am. Soc. Mass Spectrom.* **2005**, *16*, 1427-1437.

35. Julian, R. R.; Mabbett, S. R.; Jarrold, M. F. Ion Funnels for the Masses: Experiments and Simulations with a Simplified Ion Funnel. *J. Am. Soc. Mass Spectrom.* **2005**, *16*, 1708-1712.

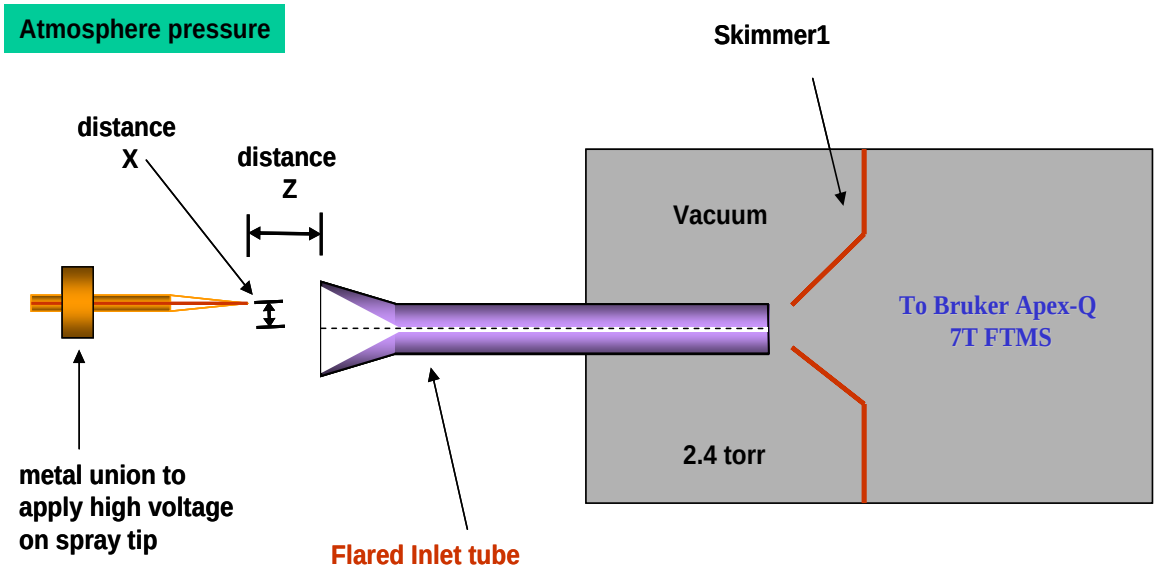

Figure 1. Schematic diagram of the implementation of the flared inlet tube. Distance Z is the distance between the spray tip and the inlet interface. Distance X is the distance that the spray tip is away from the inlet tube center. When the spray tip is aligned with the center of the inlet tube, distance X is 0.

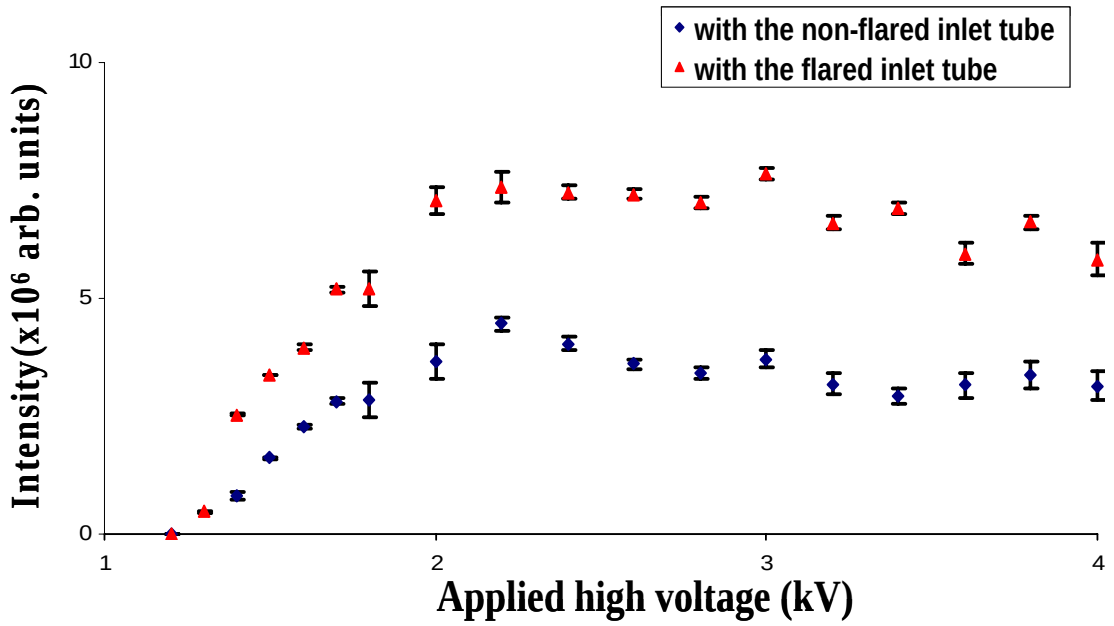

Figure 2. Total ion intensity of substance P as a function of spray potential. 10 μM substance P solution was prepared in 50:50 MeOH:H_2O with 0.1% acetic acid. Infusion was performed using a syringe pump with a flow rate of 250 nl/min.

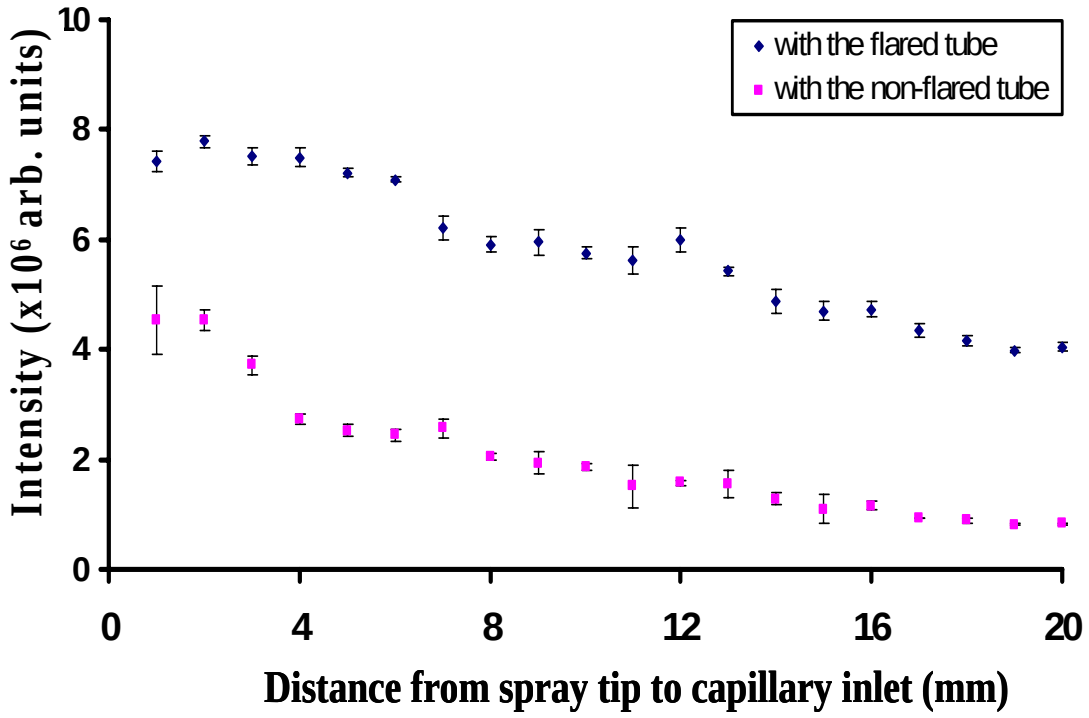

Figure 3. Total ion intensity of substance P as a function of the distance between spray tip and inlet interface (distance Z). Ion intensities were normalized individually using the most intense peak with or without flared inlet tube. 10 μM substance P solution was prepared in 50:50 MeOH:H_2O with 0.1% acetic acid. Infusion was performed using a syringe pump with a flow rate of 250 nl/min.

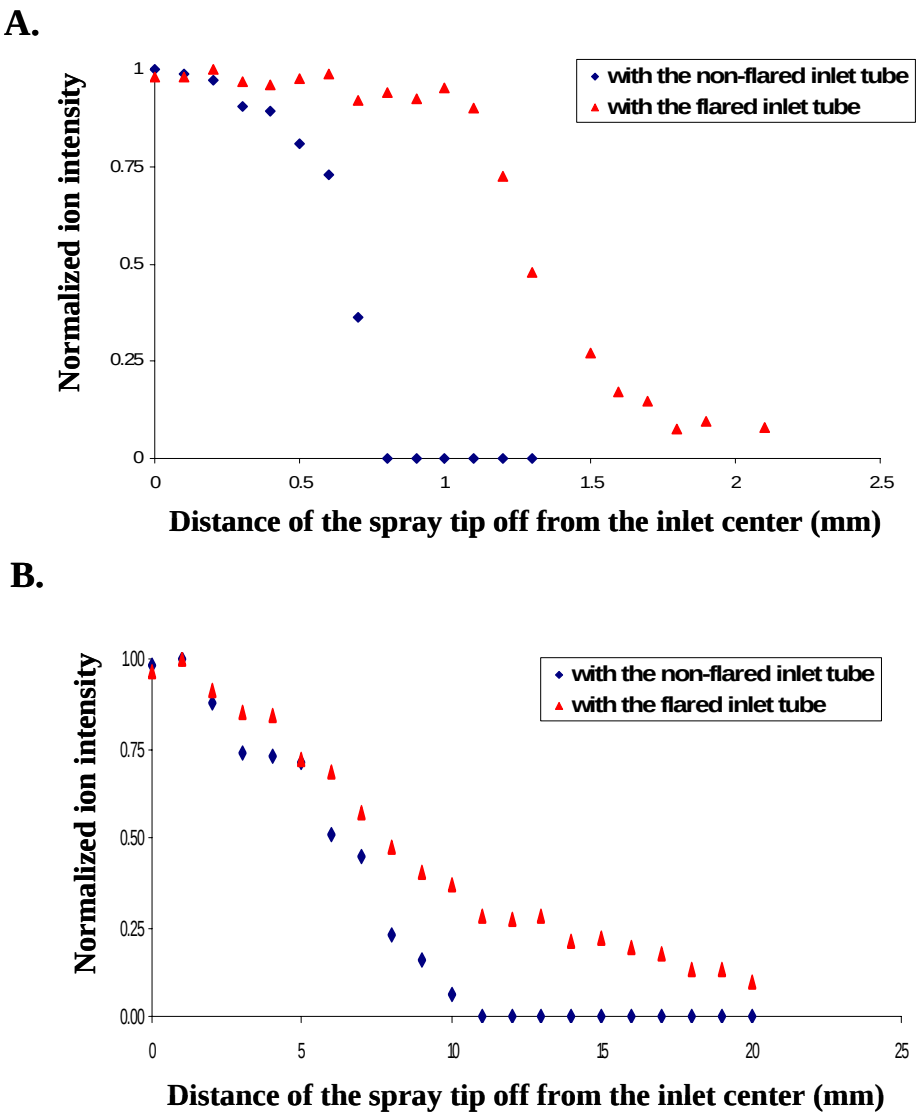

Figure 4. Normalized total ion intensity of substance P as a function of the distance that the spray tip was away from the inlet tube center (distance X). Ion intensities were normalized individually using the most intense peak with or without flared inlet tube. A 10 μM substance P solution was infused at a flow rate of 250 nl/min. **(A)** The distance between spray tip and inlet interface (distance Z) is 1mm. **(B)** The distance between spray tip and inlet interface (distance Z) is 10 mm.

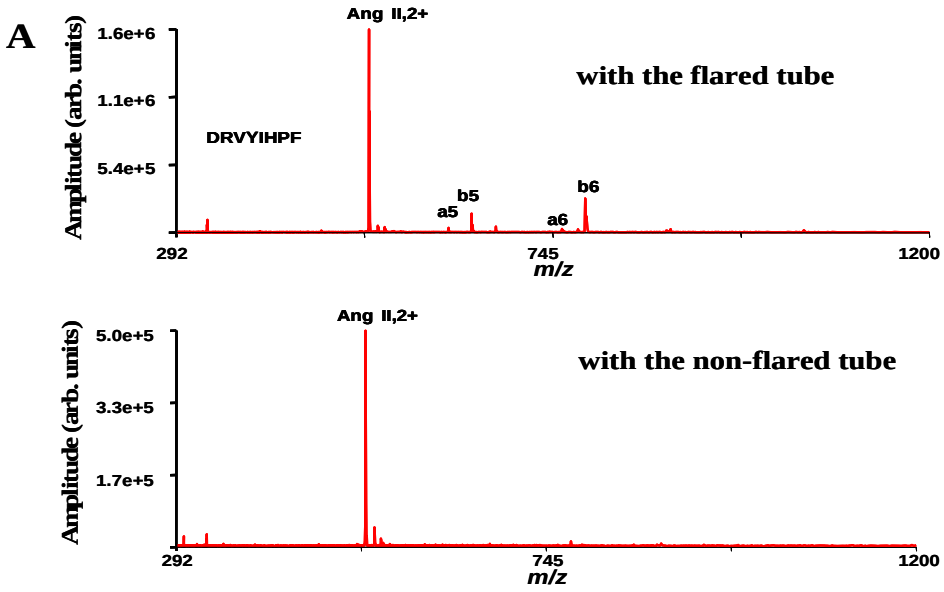
A
Ang II,2+
with the flared tube
DRVYIHPF
b5
a5
b6
a6
Amplitude (arb. units)
1.6e+6
1.1e+6
5.4e+5
292
745
1200
m/z
Ang II,2+
with the non-flared tube
5.0e+5
3.3e+5
1.7e+5

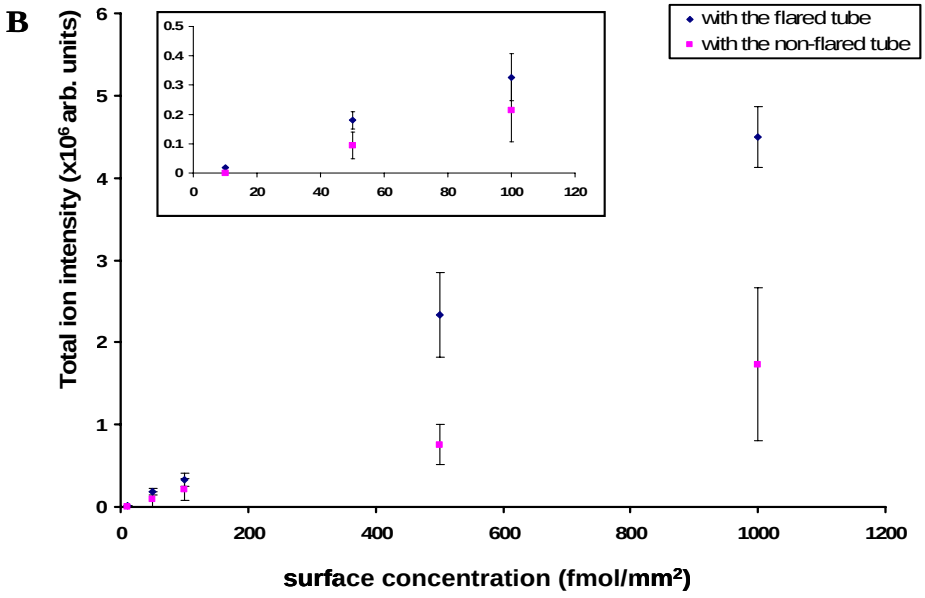
B
with the flared tube
with the non-flared tube
Total ion intensity (x10⁶ arb. units)
surface concentration (fmol/mm²)
0
200
400
600
800
1000
1200
1
2
3
4
5
6

Figure 5. DESI of angiotensin II on the PTFE surface. **(A)** DESI spectra with the highest ion intensity among 300 spectra with the flared inlet tube or with the non-flared control inlet tube. The average surface concentration of angiotensin II was 500 fmol/ mm^2. Each spectrum was accumulated 0.5 seconds and a total of 300 spectra were collected for one spot. **(B)** Plot of mass spectral total ion intensity versus the amount of angiotensin II spotted on the same sample holder with disposable surface. The average of 10 highest intensities achieved from each spot was compared. Triplicate experiments were performed for each sample concentration. Inset illustrates the data in the low concentration region.

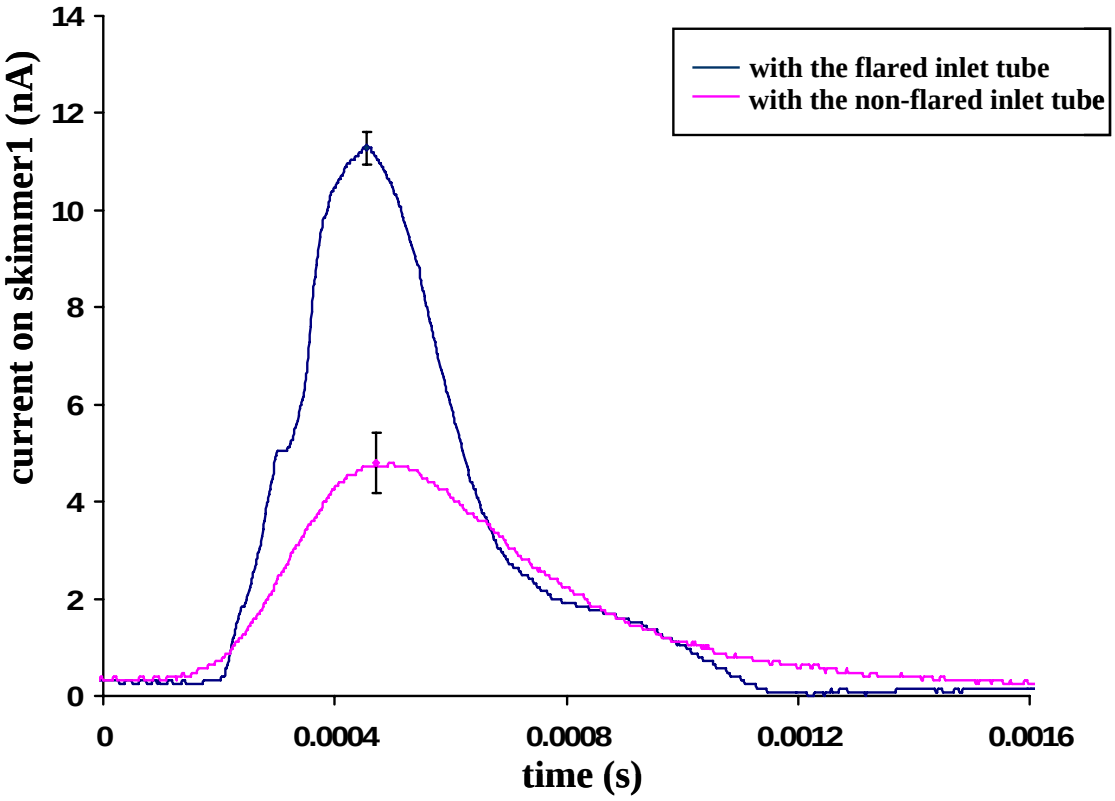

Figure 6. Average ion current profiling on the skimmer1 using AP-MALDI ion source. Each plot is an average of 16 laser shots on the same sample spot. The error bars represent the standard deviation of the peak measured ion current from three different sample spots.

CHAPTER FIVE

Integration of a New Atmospheric Pressure Interface with Atmospheric Pressure Ionization Methods

Si Wu[1], Kai Zhang[1], Nathan K. Kaiser[1], Gunnar Skulason[1], Li Zhou[2],

Milton L. Lee[2], David C. Prior[3], Gordon A. Anderson[3], and James E. Bruce[1*]

1. Department of Chemistry, Washington State University, Pullman, WA 99164;

2. Department of Chemistry and Biochemistry, Brigham Young University, Provo, Utah;

3. Environmental Molecular Sciences Laboratory, Pacific Northwest National Laboratory, Richland, WA 99352

*Corresponding author: James E. Bruce
Washington State University
Department of Chemistry
P.O. Box 644630
Pullman, WA, 99164-4630
Phone: (509) 335-2116
Fax: (509) 335-8867
Email: james_bruce@wsu.edu

ABSTRACT

A venturi air amplifier has been applied in the atmospheric pressure region which can significantly improve ion transmission efficiency using electrospray ionization. We have previously demonstrated that ion transmission efficiency from the atmospheric pressure stage to the first vacuum region can be improved using flared inlet capillary tubes coupled with a Fourier transform ion cyclotron resonance (FTICR) mass spectrometer. Here we report our investigations of the hybrid atmospheric pressure interface which couples an air amplifier with a flared inlet tube. Different atmospheric pressure ionization methods such as ESI and AP-MALDI have been used to investigate the improvements of this new interface. Using nano-ESI and the new interface, the comparisons on the ion current measurements and ion intensity from mass spectra were made with and without the high-velocity gas flow. Increased ion signals were confirmed using the new interface with the high velocity gas flow. We also found better desolvation using the new interface while comparing the ion current responses. Using AP-MALDI with the air amplifier, we observed more than a 5-fold increase in measured ion current with the flared inlet tube compared to the non-flared tube. About 3-fold increase in the measured ion current was found while using the new interface compared to the standard inlet tube interface. A two nano-electrosprayer device has also been coupled with the hybrid air amplifier-flared inlet tube. Internal calibrant can be easily introduced by using this setup, while the ratio of the calibrant and the analytes can be tunable by changing the relative position of the two-sprayer device to the acceptance region of the air amplifier. By using substance P as the internal standard, the absolute average mass error of the BSA digest peaks from direct infusion decreased to 2.2 ppm.

INTRODUCTION

Different atmospheric pressure ionization methods have been developed and applied to the proteomics research, such as electrospray ionization (ESI) and atmospheric pressure matrix-assisted laser desorption/ionization (AP-MALDI) [1-5]. For all these atmospheric pressure ion sources, the gas-phase ions are produced at the atmospheric pressure, and then transferred to the mass analyzer in a lower pressure region through several conductance limits and pumping regions. A verity of conductance limits can be used between the atmospheric pressure region and the first vacuum region, such as a metal capillary or an orifice[3]. It has been reported that the ion transmission efficiency between the ESI emitter and the inlet of the mass spectrometer is only 0.01-0.1% [3,6,7]. For AP-MALDI, even with precise aperture alignment and source positioning, sampling efficiency is generally lower than the sampling efficiency in ESI [8].

Different approaches have been developed to improve ion transmission efficiencies between the ion source and the mass spectrometer which use either electrofocusing or gas dynamically focusing methods. Smith et al. [9-12] incorporated an electrodynamic ion funnel interface right after the atmospheric interface for electrospray ionization mass spectrometry, which applies rf and dc electric fields to a series of ring electrodes with successively smaller inner diameter apertures. Close to 100% ion transmission efficiency into the mass analyzer was achieved for the analytically relevant ions which can be transferred through the electrospray ionization interface. However, with the pressure in the ion funnel region increases, the required rf peak-to-peak potential for efficient ion focusing increases correspondingly [10]. Therefore, the ion funnel has not been practically applied to the atmospheric pressure region between the electrospray tip and the ion sampling interface, where most ion losses may occur. A new

dynamic focusing technique called pulsed dynamic focusing (PDF) has been developed and applied to the AP-MALDI ion source to improve the ion transmission into a mass spectrometer [8,13]. Up to 2 fold more ions from a given laser shot can be transferred into the MS. Other atmospheric pressure electrostatic lenses that improve ion transmission efficiencies in the high pressure region have also been reported [14-16]. However, ion-cloud expansion resulted from the gas-phase collisions and Coulombic repulsion in high pressure regions can not be effectively avoided or reversed.

Gas dynamically focusing approaches such as nebulizing gas assisted method can also improve ion transmission efficiencies and ion desolvation in the high pressure region. Covey et al. [17] developed an ESI source in which a heated gas flow was directed at an angle toward the flow axis of a nebulizer-assisted electrospray source and intersected the droplet flow in a region upstream of the orifice of the MS. This intersecting flow device can provide an increase in sensitivity of more than a factor of 10, and can significantly lower the background in the resulting mass spectra. This may be due to better desolvation for the electrospray source. Henion et al. [18] reported an "ion spray" device in which a high-velocity sheath flow nebulizing gas was directed past the electrospray aperture tip. By optimizing the flow rate for desolvating the ions generated from the electrospray, an increase of about 30% in ion signal intensity was obtained as compared to that obtained with a lower flow rate.

Recent studies by Lee et al. [19] and Muddiman et al. [7] have shown large increases in ion abundance resultant from the implementation of a commercial air amplifier or a modified venturi device in the high pressure region. They also reported that these devices generated a concentric high-velocity converging gas flow around the electrospray tip to reduce spreading of the electrospray plume and improve the conduction of ions to the sampling orifice of the MS.

They reported an 18-fold increase in ion abundance and a 34-fold reduction in the detection limit. Better desolvation for the protein ions using the air amplifier has also been demonstrated by the Cooks group[20]. We developed a flared inlet capillary tube to replace the conventional straight metal capillary inlet tube which is widely used by different kinds of mass spectrometers [21]. Glish et al. [22] developed a new glass ion sampling device which also included a larger inner diameter inlet of the capillary. Both reports showed that a larger cross section of the capillary entrance can allow more ions to enter the MS. We have incorporated the flared inlet tube in a 7T FTICR-MS instrument to study ion transmission efficiency under different kinds of atmospheric pressure ionization methods such as ESI, APMALDI, and DESI [23]. We found that the flared inlet tube can efficiently focus ions at atmospheric pressure from a variety of ion sources. Also, the studies on the tip position relative to the inlet tube showed that ion intensities were less dependent on the central axis position of the spray tip. Since in both the venturi device [7,19] and the flared inlet tube, the convergence of the gas flow can help to reduce the spreading of the ion cloud and help to transfer more ions into the low pressure region. Therefore, we incorporated the venturi air amplifier and the flared inlet tube as a new type of the atmospheric pressure interface. Different ionization methods have also been investigated. Better ion transmission efficiency and better desolvation have been demonstrated.

Internal calibration can produce more accurate peak assignments than most of the other calibration methods. In FTICR-MS, single calibrant can serve as the "lock mass" to achieve accurate mass measurement [24]. Typically for the internal calibration, a calibration solution is added into the analyte solution before it is ionized. However, when electrospray solution contains both calibrant and analyte ion species, ionization suppression can occur since sometimes one of the ion species is more easily ionized, and therefore may cause the signal

suppression of other species. This signal suppression problem can potentially be reduced (or avoided) by spraying the calibrant and the analyte separately using dual-electrosprayers. Different groups have been trying to incorporate the multi-electrosprayers into their electrospray ionization devices [22,25-28]. The Moini group [26] coupled the multi-electrosprayers with the multi-nozzle interface. Each sprayer pointed to a separate nozzle, which can help reduce interaction between the reference standard and the analyte of interest. They demonstrated the accurate mass measurements of organic compounds using TOF-MS. However, multi-nozzle interface may increase the pressure in the first pumping region, therefore additional pumps or pumping stages may be needed. The Muddiman group [25] introduced a dual electrospray ionization source combined with hexapole accumulation for high mass accuracy in FTICR-MS. Their setup allows the sequential accumulation and gated trapping of an analyte and internal mass standard for attaining accurate mass measurements by internal calibration. Since the analyte and the internal calibrant did not spray simultaneously, additional pulse control was required for positioning the spray tips and the ion accumulation in the hexapole. Due to the small distance between the spray tip and the inlet orifice (several millimeters), dual sprayer setup for nano-electrospray can be more difficult. When the two spray tips are positioned too close to each other, their ion plumes seem to interfere with each other. Glish et al. [22] demonstrated the possibility of using the dual nano-electrosprayers with their glass sampling device which had a larger inner diameter inlet of the capillary. However, the ion source parameters need to be very carefully tuned, and sample from one sprayer may still be dominated. Here we applied the dual nano-electrosprayers to our hybrid air amplifier-flared inlet tube interface. Since this interface has much larger sample acceptance region than the standard inlet interface, the electrospray

spray has relatively larger positional alignment tolerances which are capable of two or more nano-electrospray tips.

EXPERIMENTAL

Chemicals

BSA, substance P, and angiotensin II were purchased from Sigma (St. Louis, MO) and used without further purification. 10 mM solutions of each standard peptide were prepared in purified water (18 MΩ*cm) using a Nanopure ultra-purified water system (Barnstead International, Boston, MA). Analytical standards were prepared by dilution using 50/50 (v/v) methanol/water with 0.1% acetic acid. Sequencing grade modified trypsin was purchased from Promega (Madison, WI).

Hybrid air amplifier-flared inlet tube interface

The hybrid air amplifier-flared inlet tube interface was implemented in our FTICR-MS instrument as shown in the Figure 1A. For the flared inlet tubes, they were produced either in-house or from Small Parts Inc. (Miami Lakes, FL) with various inlet sizes and configurations. The flared inlet tube was designed with a larger flared end which pointed towards the ion source to receive ions. The figures of the flared tubes were described in the text. Non-flared tubes with the same i.d. and length were used for control studies. All the flared tubes were placed into a ¼" stainless steel tube which is interchangeable with the commercial glass capillary tube originally in our FTICR-MS instrument. Unless otherwise indicated, capillary inlet tubes were maintained at a temperature of 220 °C during experiments. The venturi air amplifier used in this study was the modified version as described by Hawkridge et al. [7], and the main parts of the air amplifier were held ground for all the experiments. The nitrogen pressure was maintained at about 20 psi.

Atmospheric pressure ionization sources

We investigated the ion transmission efficiency and other properties of the new hybrid interface with atmospheric pressure ion sources such as ESI and AP-MALDI. For ESI experiments, the spray tips were made by etching a 20-μm-i.d., 360-μm-o.d. fused-silica capillary with 49% HF. Solutions of the peptides were prepared by dilution of stock solutions using 50:50 MeOH:H_2O with 0.1% acetic acid. Direct infusion was performed with a syringe pump at a flow rate of 500 nl/min. For most experiment, a high voltage at 3 kV was applied to sample solution through a copper alligator clip attached to the syringe needle. For ESI, the position of the spray tip was controlled by a 3D linear stage from Newport (Irvine, CA).

For the AP-MALDI ion source, a pulsed nitrogen laser at a wavelength of 337.1 nm was used in the study (model VSL337, Spectra-Physics). As we described before, the nitrogen laser was focused onto a small replaceable copper target plate (approximately 2 mm x 3 mm in size). For most of the experiments, laser firing was externally triggered at a 3-Hz repetition rate by a functional arbitrary waveform generator (33120A, Hewlett Packard). For the current scanning experiments, laser was held at a 20-Hz constant repetition rate. The AP-MALDI source was then interfaced to different kinds of capillary inlet tubes. Positioning of the sample plate relative to the interface of the inlet tube was optimized by adjustment of the 3D linear stage. A 2 kV potential was applied to the sample target. As shown in Figure 1B, while coupling the AP-MALDI source with the new interface, the sample target was placed ~4-5 mm inside the air amplifier, and was nearly coaxial toward the inlet tube. We compared the ion transmission efficiency of different interfaces by measuring the ion current on skimmer1 (Figure 1A) from each laser pulse. Samples for AP-MALDI were prepared on the sample target by mixing 2 μl

100mM substance P with 2 μl matrix solution (saturated 2,5-dihydroxybenzoic acid in 50:50:0.1 of acetonitrile:H_2O:TFA).

Instrumentation

All the mass spectral data were collected using a Bruker Daltonics Apex-Q 7T FTICR mass spectrometer. The ions entered the instrument through the flared inlet tube, and then passed through a hexapole followed by a mass selective quadrupole and then a second hexapole. After accumulation in the second set of hexapole rods for the duration of 0.5-2 seconds, the ions were then sent toward the ICR cell using an electrostatic ion guide. The ions were trapped in the ICR cell using a low energy sidekick potential to keep the ions close to the central *z* axis of the cell. All data sets acquired were 128k points. The mass spectral data were acquired using Xmass 7.0.6 as the data acquisition software program. The external calibration was done using a mixture solution of standard peptides. All the FTICR-MS data were analyzed using ICR-2LS software package [29].

RESULTS AND DISCUSSION

Electrospray ionization

Ion intensity and ion current comparison

The Lee group [7,19] has demonstrated that the air amplifier can efficiently focus ions generated from electrospray ionization. The measured ion abundance can be significantly increased while using the air amplifier. We have developed a flared inlet capillary tube to replace the conventional straight metal capillary inlet tube which is widely used by different kinds of mass spectrometers [21,23]. As shown in the patent by Prior et al.[21], measured ion current can be increased 3-fold or more using the flared inlet tube. The flared inlet tubes have also been applied on our FTICR-MS instrument using nano-electrospray ionization source [23]. The application of the flared inlet tube resulted in a 2-fold increase of the measured ion intensity. Here we incorporated the flared inlet tube with the air amplifier, and evaluated the measured ion intensity and ion current using this hybrid atmospheric interface.

We evaluated the ion current measured on the skimmer1. The generated ion current was amplified by a Keithley current amplifier (Model 428, Keithley) and then recorded by a digital storage oscilloscope (TDS 2024, Tektronix). To demonstrate that the new hybrid interface can help the ion desolvation, the capillary was not heated. Four different interfaces were applied here: the flared inlet tube without the air amplifier, the flared inlet tube with the air amplifier (N_2 pressure was 20 psi), the flared inlet tube with the air amplifier (no gas flow), and the standard inlet tube. The flared inlet tube we used here was 0.03" i.d. and 1/16" o.d. at the unflared end, 9.3" total length, and was flared 30 degrees from the center line to ~ 3 mm o.d. at the larger end.

A 10 μM substance P solution was used for all sets of experiments with the flow rate of 500 nl/min.

The measured current comparison results are shown in Figure 2. We found that the average ion current measured using the flared inlet tube with the air amplifier (new interface, 20 psi) was about 2 times larger than the average ion current using the standard inlet tube. The average ion current had the improvement of more than 10 comparing with the high velocity gas in the air amplifier than without gas in the air amplifier. This result was similar to the results reported by other groups, which indicated that the high velocity gas can efficiently focus the ions passing through the air amplifier. We also compared the FTICR mass spectra (the capillary was heated to 220 ^{o}C, data not shown here). The flared inlet tube we used was 0.02" i.d. and 1/16" o.d. at the unflared end, and was flared 10 degrees from the center line to ~ 3 mm o.d. at the larger end. Similar results were observed: about 2 fold increase in the measured ion intensity can be found by using the new interface (20 psi) comparing to the standard inlet tube; a 10 times increase in the signal intensity was observed using the high velocity gas flow compared to no gas flow. For all these experiments, the potential on the air amplifier was set as 0. As demonstrated by Lee et al., the high potential gradient on the modified air amplifier should help focus the ions even better.

Another observation in Figure 2 was that the ion current measured from the flared inlet tube without the air amplifier was slightly larger than the ion current measured from the hybrid air amplifier and flared inlet tube interface. However, it was very unstable and fluctuated over a wide range. The fluctuant range of the ion current was about 30% using the flared inlet tube without the air amplifier. Similar fluctuation was found using the standard tube without the air amplifier. When we heated the flared capillary tube to 220 ^{o}C, the fluctuant range of the ion

current decreased to about 10% to 15% (data not shown here). These results suggest the fluctuation in the measured current may be due to poor ion desolvation, or the pressure decrease by the increase of temperature. While using the air amplifier, the measured ion current was much more stable. The fluctuant range was less than 10% using the flared inlet tube and the air amplifier (20 psi). Therefore, the high velocity N_2 gas in the air amplifier may also help the desolvation of the ions.

Two-tip experiment

Since the air amplifier has relatively large sampling area, simultaneous nanoelectrospray ionization of multiple samples is enabled using multiple spray tips. The schematic of the dual electrospray source is presented in Figure 3. The spray tips were fixed parallel on an aluminum plate. Both the spray tips were connected to metal unions which were electrically-connected with the Al plate. The high voltage (3 kV) was applied on the Al plate which can be applied to both spray tips. The distance between the spray tips was about 5 mm. The positions of the tips were manually controlled by a 3D linear stage from Newport (Irvine, CA). This dual-tip setup was incorporated with either the standard inlet tube interface or the hybrid air amplifier and flared inlet interface. For both cases, we applied 10 μM angiotensin II to the spray tip 1 and 10 μM substance P to the spray tip 2. Separate syringe pumps were used for the sample infusion, and flow rate was 500 nl/min.

When coupling with the standard inlet tube, we fixed the vertical distance between both tips and the interface as about 2-3 mm. It has been reported that the signal from one spray tip will dominate the spectrum if the distance is less than 2 mm from one tip to another tip [22]. This is likely due to the electric field perturbations resultant from the overlap of the ion plumes

from the two tips. We set the distance between the two tips at 5 mm, where we observed no interference between the tips. We gradually adjusted the distance X in Figure 3A to pull tip 1 toward the sampling axis first, and then did the same with spray tip 2. The results are plotted in Figure 3A. As expecting, we observed the ions from angiotensin II came out firstly, and then the ions form substance P. We also observed no overlap between these two analytes. For both analytes, there was an optimum position where the ion intensity was maximized. The distance between the optimum position of angiotensin II and the optimum position of substance P was about 5 mm, which was close to the distance between the spray tips. Therefore, while using the standard inlet interface, it would be very difficult to set the dual-tip device for introducing the internal calibrant.

We then applied the dual-tip device to the hybrid air amplifier-flared inlet tube interface. The spray tips were placed slightly inside the air amplifier entrance (2-3 mm) where we found that the measured ion intensity was close to the peak value. We also set the distance between the two tips at 5 mm as we used above for the standard inlet tube experiments. At the initial position, the spray tip 1 was close to the central axis of the entrance, and the spray tip 2 was near the surface of the air amplifier (as shown in Figure 3B). The spray tips were gradually moved using the 3D linear stage until the spray tip 1 reached the other end surface of the air amplifier. In Figure 3B illustrates that the angiotensin II ion intensity was stable near the maximum value for ~ 0.4 cm and then decreased until it reached zero. The ion intensity of substance P (from the other tip) started near 0, and increased until it reached its maximum value. Overlapping areas for the angiotensin ions and the substance P ions existed between 0.2 and 0.6 cm. The spectra corresponding to the position *a*, position *b*, and position *c* in the Figure 3B were shown in Figure 4. The ion intensity of angiotensin II at the position *a* was close to the maximum ion intensity

using a single sprayer for the angiotensin II. The ion intensity of substance P at the position *c* was close to the maximum ion intensity using a single sprayer for the substance P. At the position b which was in the overlapping region of these two type ions, the ion intensity of angiotensin II and the ion intensity of substance P were close to each other. Therefore, this dual-tip setup can be used as the sprayer for angiotensin II, or the sprayer for substance P, or for both ion species. The distance X in the Figure 3B can be adjusted to optimize either signal as shown. Since the distance between the tips was relatively big (5 mm), the overlapping of these two kinds of ions can not reach the maximum value for both of them. This can be potentially solved by decreasing the distance between the tips (less than 5 mm while larger than 2 mm). Additional, if this dual-tip setup was used for introducing the internal standard, the ion intensity ratio of calibrant to analyte can be easily tuned changing the distance X in Figure 3B.

We applied the BSA digest and substance P simultaneously using the dual-tip device, as shown in Figure 5. Both the tryptic digested peptide peaks from BSA and the peaks of substance P were found in the same spectrum. We adjusted the position of the two-tip setup until the $(M+2H)^{2+}$ ion intensity of substance P was slightly larger to the average peak intensity from BSA tryptic digested peptides. We used the substance P as the internal standard for the calibration of the peaks from BSA digest. Table 1 lists the mass measurement errors of BSA peaks with the internal calibration and the external calibration. External calibration resulted in an average mass error of 29.2 ppm. While using the internal calibration on the same spectra, we found that the average mass error decreased to 2.2 ppm. Therefore, this two-sprayer setup can help to achieve the better mass measurement accuracy.

Coupling the new atmospheric pressure interface with AP-MALDI

The AP-MALDI ion source described here was designed as a component of a novel high sensitivity AP-MALDI-FTICR mass spectrometer which is currently under development in our lab. Several stages of differential pumping are incorporated in the vacuum system of this mass spectrometer. The first pumping stage (between the capillary exit and the skimmer) was evacuated by an Edwards E2M30 mechanical pump (Wilmington, MA) to 2-4 torr. The overall AP-MALDI source and the interface setup were shown in Figure 1B. We triggered the oscilloscope using the same triggering signal from the functional waveform generator which was used to fire the laser pulse. The ion current for each sample spot was measured on skimmer1 (-5 V negative bias was applied to the skimmer 1) and was recorded using two different kinds of methods: by averaging 16 scans of current signals corresponding to 16 laser pulses (Figure 6), or by scanning the current signals with the time scale (Figure 7). Similar to the work we did before, we used the inlet tube which was 0.03" i.d. and 1/16" o.d. at the unflared end, 9.3" total length, and was flared 30 degrees from the center line to ~ 3 mm o.d. at the larger end. The corresponding non-flared control inlet tube we used was 0.03" i.d. and 1/16" o.d. with a total length of 10".

As shown in Figure 6A, when using the air amplifier at 20 psi N_2 gas flow, we found that more than 5 fold ion current increase with the flared inlet tube relative to the standard inlet tube. This result was close to the result we reported before without using the air amplifier. While using the air amplifier, we found the ion current peak width significantly increased. In Figure 6B, the half peak width without the air amplifier was about 3 ms, while the half peak width with the air amplifier was about 12 ms. The enlargement of the peak half width was due to the longer distance between the ion source and the sampling orifice which allows more collisions with the neutral gas molecules. When we compared the peak areas with and without the air amplifier, we

found that ion peak areas from these two setups were very close to each other. The hybrid air amplifier-flared inlet interface can give an improvement of 3 on the ion current relative to the standard inlet interface (no air amplifier). We performed current measurements without the gas flow in the air amplifier. In this case, no observable ion current was measured. From the experiments, we found that less solid clusters were attached to the skimmer1 while doing laser ablation for a long period of time using the air amplifier (20 psi). The possible explanation is that the high flow rate of N_2 from air amplifier can help ion declustering in AP-MALDI. Although the ion current we measured hitting on the skimmer did include many ions other than the gas phase analyte ions, it should be proportional to the analyte ion signal detected by the mass spectrometer.

We also did the current scanning at the skimmer1, as shown in Figure 7. The laser repetition frequency we applied was 20 Hz. We found that the period between the peaks in both cases (Figure 5) was 0.05 s, which indicated that each measured current peak was generated from one laser ablation on the sample target. We found that the average ion current from each laser shot was about 3 times larger than with the implement of the flared inlet tube as compared with a standard inlet tube, in agreement with the results we reported previously. We also found that the peak-to-peak reproducibility with the flared inlet tube was much better than with observed with the standard inlet tube. The possible reason might be due to the larger position tolerance using the flared inlet tube since it had a larger acceptance angle. If so, the peak-to-peak reproducibility should also be improved with the use of the hybrid air amplifier-flared inlet tube as the interface.

CONCLUSIONS

We have investigated the hybrid air amplifier-flared inlet tube interface using atmospheric pressure ion sources such as ESI and AP-MALDI. Comparing to the standard inlet, the application of this new interface to nano-electrospray ionization source resulted in a about 2-fold increase in both the measured current and the total ion intensity obtained using FTICR-MS. We also found evidence of better desolvation of ions using the current measurements, which may be due to the high velocity of the nitrogen gas. A dual-electrosprayer device was incorporated to this new interface, which allows us to introduce an internal standard into the mass spectrometer. The ratio of the calibrant and the analytes can be tunable by changing the relative position of the two-electrosprayer device to the acceptance region of the air amplifier. This setup can be used as either two-electrosprayer device or single-tip sprayer device without any changes. Coupling of AP-MALDI ion source also demonstrated the feasibility to focus the ions using the new interface. The large acceptance area of the air amplifier also help reduce the possibility of arcing in the standard AP-MALDI setup due to the close distance between the sample target and the conventional atmospheric pressure interface.

ACKNOWLEDGEMENTS

This work was supported by grants from the M.J. Murdock Charitable Trust, the Directorate of Biological Sciences, National Science Foundation, Grant No. DBI-0352451, and the Office of Science (BER), U.S. Department of Energy, Grant No. DE-FG02-04ER63924. We are also grateful to PNNL for providing the software ICR-2LS used for data analysis.

REFERENCES

[1] J.B. Fenn, M. Mann, C.K. Meng, S.F. Wong, C.M. Whitehouse, Science 246 (1989) 64.

[2] C.M. Whitehouse, R.N. Dreyer, M. Yamashita, J.B. Fenn, Anal. Chem. 57 (1985) 675.

[3] N.B. Cech, C.G. Enke, Mass Spectrom. Rev. 20 (2001) 362.

[4] V.V. Laiko, M.A. Baldwin, A.L. Burlingame, Anal. Chem. 72 (2000) 652.

[5] V.V. Laiko, S.C. Moyer, R.J. Cotter, Anal. Chem. 72 (2000) 5239.

[6] M. Mann, in A. Hedin, Sundqvist, B., Benninghoven, A. (Editor), Ion formation from Organic Solids V, John Willey and Sons, New York, 1990, p. 139.

[7] A.M. Hawkridge, L. Zhou, M.L. Lee, D.C. Muddiman, Anal. Chem. 76 (2004) 4118.

[8] K.A. Kellersberger, P.V. Tan, V.V. Laiko, V.M. Doroshenko, D. Fabris, Anal. Chem. 76 (2004) 3930.

[9] S.A. Shaffer, D.C. Prior, G.A. Anderson, H.R. Udseth, R.D. Smith, Anal. Chem. 70 (1998) 4111.

[10] S.A. Shaffer, A. Tolmachev, D.C. Prior, G.A. Anderson, H.R. Udseth, R.D. Smith, Anal. Chem. 71 (1999) 2957.

[11] M.E. Belov, M.V. Gorshkov, H.R. Udseth, G.A. Anderson, R.D. Smith, Anal. Chem. 72 (2000) 2271.

[12] M.E. Belov, M.V. Gorshkov, H.R. Udseth, G.A. Anderson, A.V. Tolmachev, D.C. Prior, R. Harkewicz, R.D. Smith, J. Am. Soc. Mass Spectrom. 11 (2000) 19.

[13] P.V. Tan, V.V. Laiko, V.M. Doroshenko, Anal. Chem. 76 (2004) 2462.

[14] B.B. Schneider, D.J. Douglas, D.D. Chen, Rapid Commun. Mass Spectrom. 16 (2002) 1982.

[15] B.B. Schneider, D.J. Douglas, D.D. Chen, J. Am. Soc. Mass Spectrom. 13 (2002) 906.

[16] X. Feng, G.R. Agnes, J. Am. Soc. Mass Spectrom. 11 (2000) 393.

[17] T.R. Covey, in, U.S. Patent 5,412,208, 1995.

[18] J.D. Henion, T.R. Covey, A.P. Bruins, in, US patent 4,861,988, 1989.

[19] L. Zhou, B. Yue, D.V. Dearden, E.D. Lee, A.L. Rockwood, M.L. Lee, Anal. Chem. 75 (2003) 5978.

[20] P. Yang, R.G. Cooks, Z. Ouyang, A.M. Hawkridge, D.C. Muddiman, Anal Chem 77 (2005) 6174.

[21] D.C. Prior, J. Price, J.E. Bruce, in, US patent 6,455,846, 2002.

[22] G.L. Glish, R.M. Danell, in, US patent 6,703,611, 2004.

[23] S. Wu, K. Zhang, N.K. Kaiser, J.E. Bruce, D.C. Prior, G.A. Anderson, J Am Soc Mass Spectrom 17 (2006) 772.

[24] R.D. Burton, K.P. Matuszak, C.H. Watson, J.R. Eyler, Journal of the American Society for Mass Spectrometry 10 (1999) 1291.

[25] J.C. Hannis, D.C. Muddiman, J Am Soc Mass Spectrom 11 (2000) 876.

[26] L. Jiang, M. Moini, Anal Chem 72 (2000) 20.

[27] T. Kim, K. Tang, H.R. Udseth, R.D. Smith, Anal Chem 73 (2001) 4162.

[28] T. Kim, H.R. Udseth, R.D. Smith, Anal Chem 72 (2000) 5014.

[29] G.A. Anderson, J.E. Bruce , R.D. Smith in, Pacific Northwest National Laboratory, Richmond, WA, 1996.

Table 1. Measured mass errors for the BSA in-solution digested peptides using external and internal calibration

peaks in Figure 5	charge state	theoretical ***m/z***	sequence	before internal calibration (ppm)	after internal calibration (ppm)
1	1	545.3406	VASLR	-23.81	-1.702
2	2	571.8608	KQTALVELLK	-23.096	-0.076
3	2	625.3142	FKDLGEEHFK	-23.594	0.553
4	2	653.3617	HLVDEPQNLIK	-22.659	-3.204
5	1	689.3729	AWSVAR	-27.72	2.802
6	1	712.3737	SEIAHR	-38.866	-3.49
7	2	720.4095	RHPEYAVSVLLR	-22.369	-0.518
8	1	733.4203	VLTSSAR	-25.423	-1.888
9	2	740.4014	LGEYGFQNALIVR	-20.88	-2.625
10	2	784.375	DAFLGSFLYEYSR	-42.252	-6.911
11	1	789.4716	LVTDLTK	-26.827	0.117
12	1	818.4254	ATEEQLK	-22.591	3.558
13	2	820.4725	KVPQVSTPTLVEVSR	-35.005	1.855
14	1	922.488	AEFVEVTK	-38.1	-3.53
15	1	927.4934	YLYEIAR	-38.05	0.143
16	2	944.9671	HPYFYAPELLYYANK	-29.225	-1.533
17	1	974.4578	DLGEEHFK	-27.771	2.028
18	2	978.4835	DAIPENLPPLTADFAEDK	-24.957	1.157
19	1	1002.583	ALKAWSVAR	-30.31	-3.752
20	1	1014.6194	QTALVELLK	-30.12	-3.887
21	2	1023.0176	RHPYFYAPELLYYANK	-31.096	1.8
22	1	1163.6307	LVNELTEFAK	-37.309	-1.488

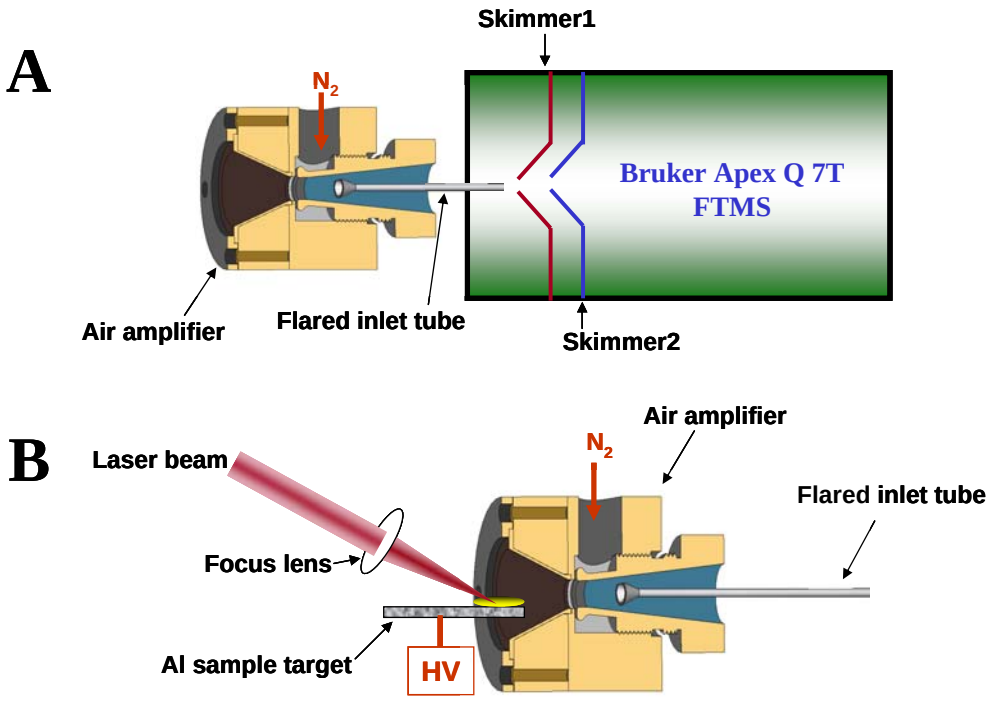

Figure 1. Schematic of the new interface which couples an air amplifier with a flared inlet tube. (A) Implement of the new interface with the FTICR-MS instrument; (B) Incorporation the AP-MALDI source with the new interface.

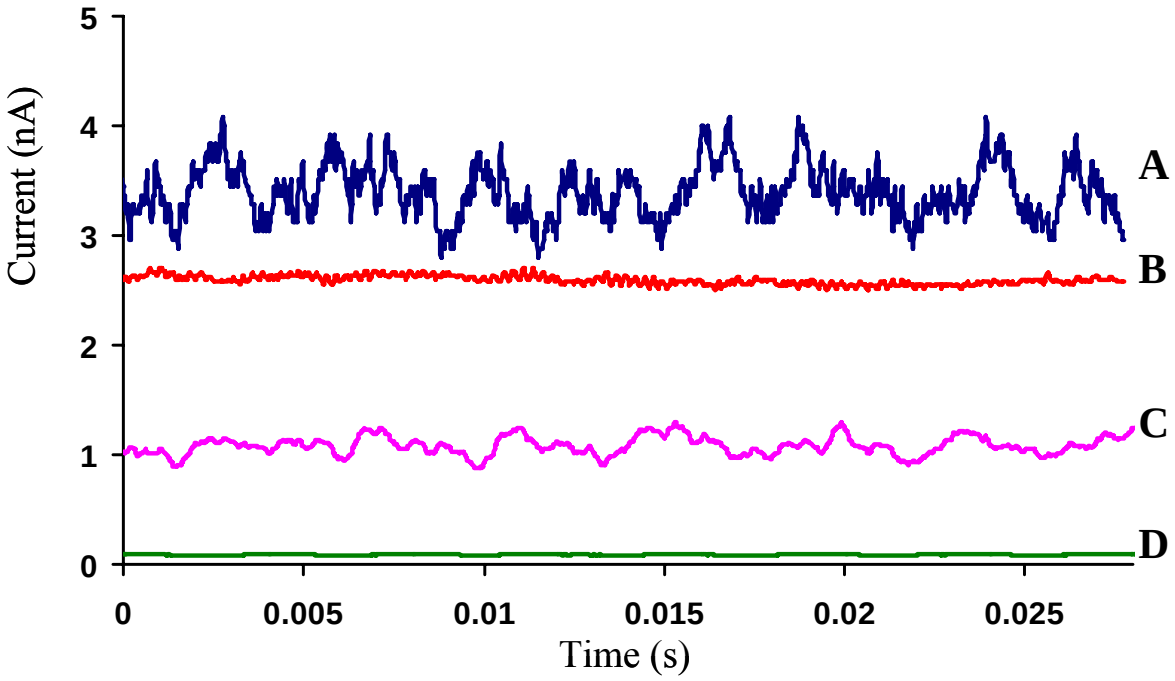

Figure 2. Current profile using different interface setups. (A) with flared inlet tube and no air amplifier; (B) with flared inlet tube and air amplifier (20 psi); (C) with standard inlet tube and no air amplifier; (D) with flared inlet tube and air amplifier (0 psi).

A

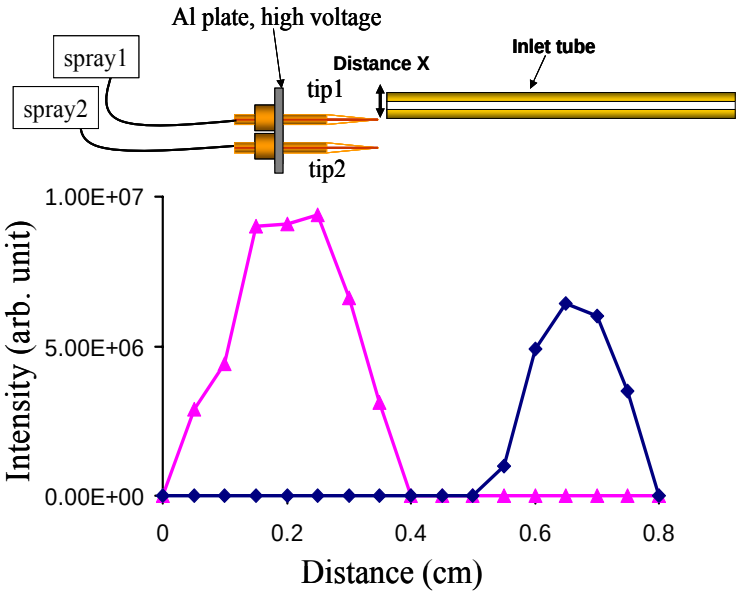

B

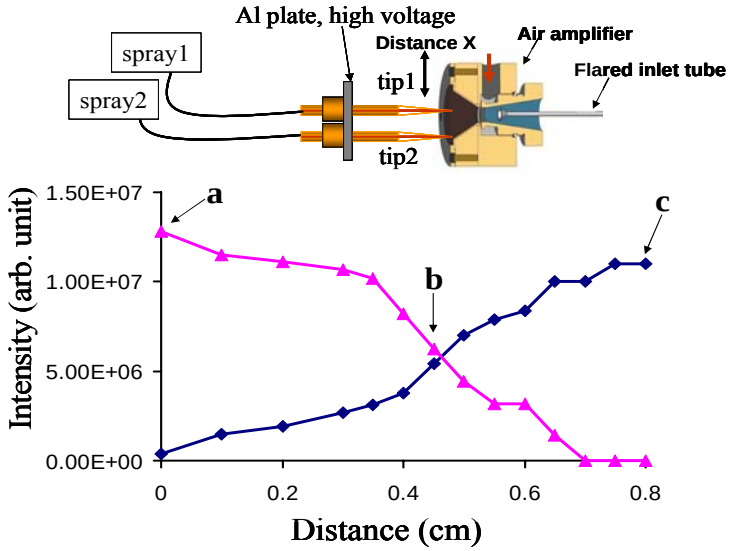

Figure 3. Ion intensity profile using a dual nanoelectrospray ionization device. (A) with the standard inlet tube interface; (B) with the hybrid air amplifier-flared inlet tube interface. Line with triangles indicates the ion intensity profile of angiotensin II, and line with squares indicates the ion intensity profile of substance P.

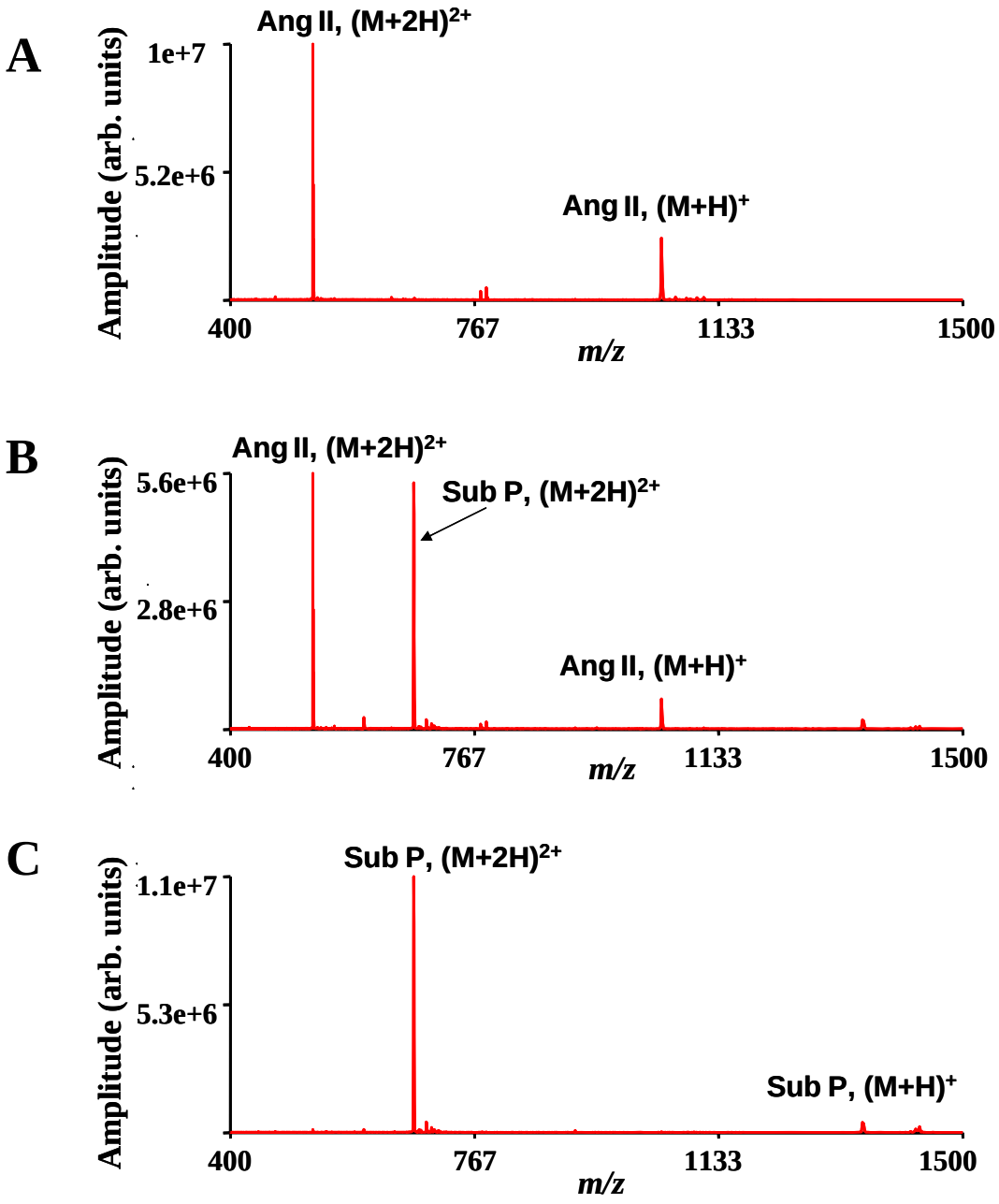

Figure 4. Corresponding mass spectra from the point a, b, c in Figure 3, which indicates that the adjustment of relative positions of spray tips allows the adjustment of the observed signal intensities of the two analytes.

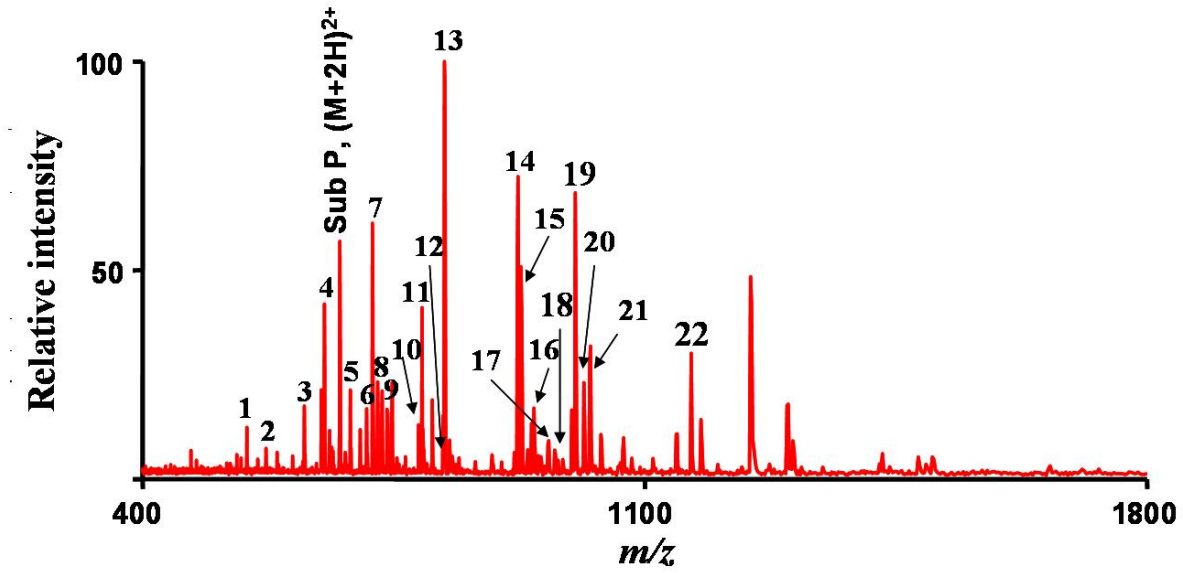

Figure 5. Mass spectrum obtained using the dual nanoelectrospray device: substance P (10 μM) in one spray tip and BSA digest (10 μM) in another spray tip. The distance X in Figure 3 was tuned until the intensity of substance P was close to the average intensity of the BSA digested peptides peaks. Peak marked with * indicates the noise peak. Some of identified BSA digested peptide peaks are marked with Δ, and the whole peak list is shown in Table 1.

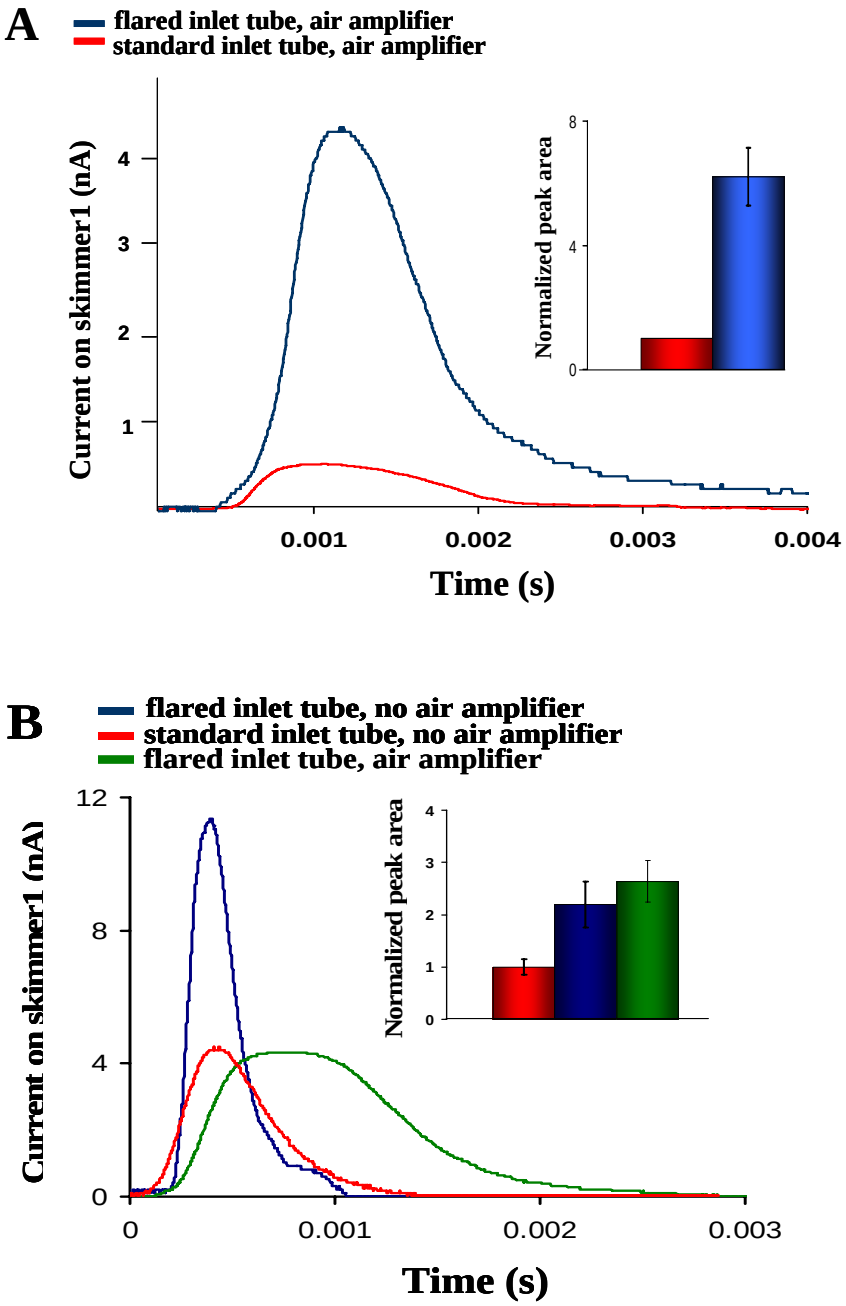

Figure 6. Average ion current (AP-MALDI) on skimmer1 with the air amplifier and the calculated average peak areas. (A) Coupling the air amplifier with different types of inlet tubes; (B) Comparing the interface with and without the air amplifier.

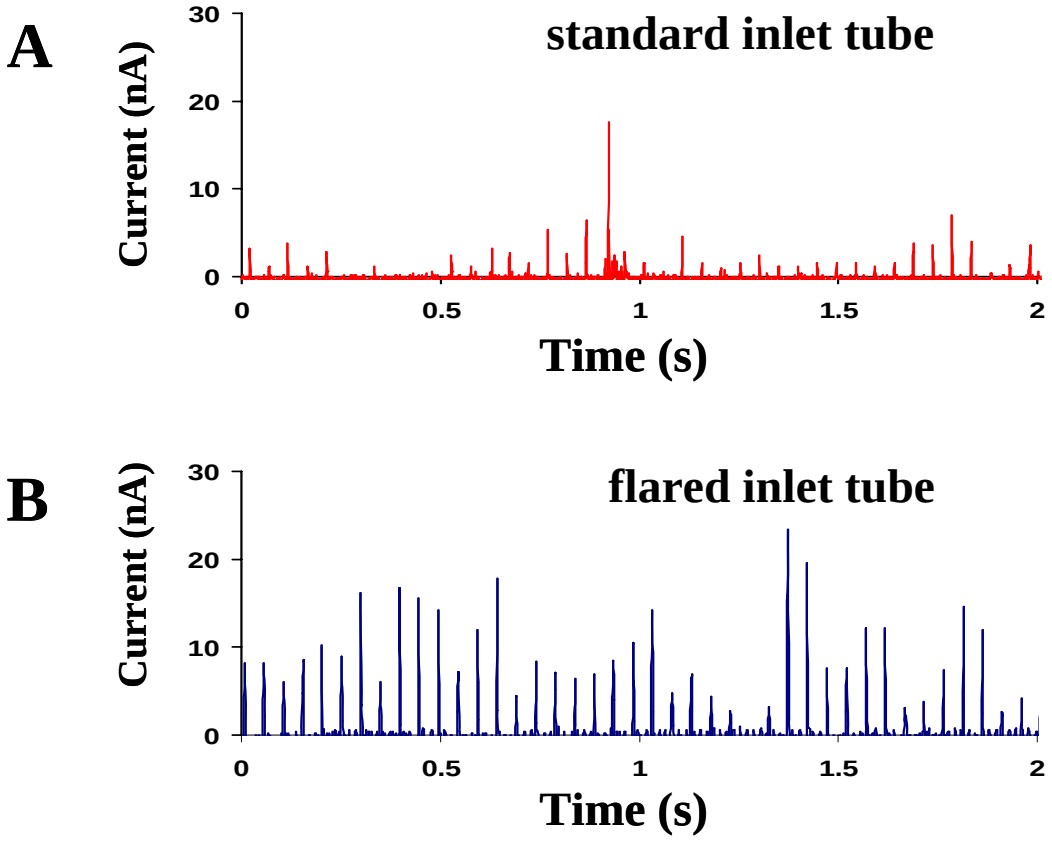

Figure 7. Two second ion current scan on skimmer1 using AP-MALDI ion source. A laser repetition frequency of 20 Hz was used. (A) with standard inlet tube; (B) with flared inlet tube.

CHAPTER SIX

Coupling On-Target Digestion with an Electrospray-Assisted Laser Desorption Ionization FTICR Mass Spectrometer

Si Wu[1], Kai Zhang[1], Gunnar Skulason[1], Nathan K. Kaiser[1], David C. Prior[2], Gordon A. Anderson[2], and James E. Bruce[1*]

[1] Department of Chemistry, Washington State University, Pullman, WA 99164

[2] Environmental Molecular Sciences Laboratory, Pacific Northwest National Laboratory, Richland, WA 99352

*Corresponding author: James E. Bruce
Washington State University
Department of Chemistry
P.O. Box 644630
Pullman, WA, 99164-4630
Phone: (509) 335-2116
Fax: (509) 335-8867
Email: james_bruce@wsu.edu

ABSTRACT

Electrospray-assisted laser desorption/ionization (ELDI) has been applied to rapid analysis of solid materials under ambient conditions. Analytes were desorbed from metal surfaces and biological samples using a pulsed nitrogen laser. Post-ionization produced high-quality mass spectra characteristic of electrospray, including protein multiple charging. In this work, we coupled the EDLI source with our 7T FTICR-MS, and modified the atmospheric pressure interface of the mass spectrometer using the flared inlet tube, as we have recently reported. We evaluated the ion transmission efficiency with the flared inlet tube compared with the standard inlet tube. Using ELDI-FTICR-MS, we observed about two to three fold improvement in the detected ion signal with the flared inlet tube compared with the standard inlet tube. The application of ELDI on different sample surfaces has also been demonstrated, such as the detection of peptides on a nitrocellulose membrane. Moreover, we reported the study of coupling on-target enzymatic digestion with ELDI-FTICR-MS. High mass measurement accuracy can improve the confidence of protein identification. This approach can potentially be incorporated with HPLC off-line systems or CE off-line systems for high throughput proteome profiling.

INTRODUCTION

Recently, there has been increased in mass spectrometry (MS) techniques which allow rapid and sensitive analysis of samples under ambient conditions [1-3]. A new family of techniques has been developed that allows ions to be created under ambient conditions and then collected and analyzed by MS. Of these techniques, the most well-known is the desorption electrospray ionization (DESI) method [1, 3-6]. In this method, the electrospray plume of the solvent hits the surface of interest, from which the solvent picks up the analyte molecules and then ionizes them. The ionized analyte species are then transferred into the mass spectrometer through several conductance limits and pumping regions. In the direct analysis in real time (DART) method, an electrical potential is applied to a gas with a high ionization potential (typically nitrogen or helium) to form a plasma of excited-state atoms and ions, which desorbs low–molecular weight molecules from the surface of a sample [7]. Desorption atmospheric pressure chemical ionization (DAPCI) uses gas-phase ions generated by atmospheric pressure corona discharge in the vapor of toluene or another compound, producing ions by charge-transfer between the gaseous ions and the adsorbed analyte [3]. In atmospheric solids analysis probe (ASAP), a heated gas jet is sprayed directly onto the sample surface, and desorbed species are ionized by corona discharge in the gas phase [8].

AP-MALDI, as the first developed atmospheric pressure desorption ionization method, has been implemented with a number of mass analyzers [9-12]. It has been widely reported that the ions generated by AP-MALDI are less energetic and have less metastable decay than those produced by vacuum MALDI [12, 13]. Therefore, AP-MALDI has been applied to different kinds of thermally labile analytes, such as oligosaccharides [12, 13]. However, it has been pointed out that

the number of neutrals desorbed by the laser beam is much larger than the number of analyte ions [14]. Therefore, the post-ionization of neutrals has become of growing interest due to the consideration of the increased sensitivity. The Shiea group has developed a novel ionization method, electrospray-assisted laser desorption ionization (ELDI), for the rapid and sensitive detection of proteins and other compounds [15, 16]. They also proposed the ionization mechanism: gaseous neutral analyte molecules are first desorbed from the sample surface by laser desorption, and are then post-ionized by their fusion with the charged solvent droplets. Since the post-ionization procedure of ELDI is similar to DESI, the ESI-like ion species are then generated and transferred into the mass detector. Since the ionization of analytes is by the interaction with the charged solvent droplets generated from an electrospray, a matrix is no longer necessary for ELDI. Therefore, ELDI can be easily applied to detection of the proteins and other compounds in biological samples such as tissues and bacterial cultures.

Similar to other atmospheric pressure ion sources, the gas-phase ions generated in ELDI are transferred through various stages of the mass spectrometer before they can be detected. It has been reported that the limiting factor in sensitivity is the transfer of ions through the mass spectrometer [17-19]. Since ions must enter the MS through a small aperture or capillary with limited cross section, the ion cloud expansion and dispersion as it enters the lower pressure region can significantly decrease the ion transmission, thus decreasing the sensitivity of the analysis. The majority of ion loss is believed to occur between the atmospheric pressure region and the first vacuum region. Therefore, different approaches have been developed to improve ion transmission efficiency between the ion source and the mass spectrometer [19-22].

One of the approaches we have reported is the utilization of the flared inlet tube [23, 24]. We incorporated the flared inlet tube in a 7T FTICR-MS instrument using different kinds of

atmospheric pressure ionization methods such as ESI, AP-MALDI, and DESI. We found that the flared inlet tube can efficiently focus ions at atmospheric pressure from a variety of ion sources. These improvements are likely related the convergence of the gas flow and larger angle of acceptance of the flared tubes, as compared with the conventional ion inlet tubes. With the flared inlet tube, the much larger entrance area and acceptance angle can help to transfer a much larger portion of the ions in the plume. Also, studies on the tip position relative to the inlet tube showed that ion intensities were less dependent on the central axis position of the spray tip.

Recently, there has been increasing interest in direct MS identification of proteins on the membrane after western blotting and other interactions such as lectin blotting [25]. This approach has some advantages such as easy handling of desalting and the potential for storage of used membranes. Furthermore, this approach can be applied to profile phosphor-proteins and glycol-proteins. The on-membrane tryptic digestion was applied to achieve the information for peptide mass fingerprinting [25, 26]. The detection method was mostly MALDI-TOF. Since the membrane was taped onto the sample target, it can be problematic under vacuum conditions. Here we demonstrate that ELDI can be applied to detect the solid peptide on the nitrocellulose membrane. This makes it feasible to use ELDI to detect the peptides from on-membrane digestion.

Enzymatic digestion on-plate MALDI is a promising method to significantly reduce the time required for tryptic digestion to obtain high-throughput analysis [27-30]. The on-plate digestions reported so far, however, were mostly performed on standard protein mixtures or cells from very simple organisms. Microscale HPLC provides rapid separation of proteins; in particular, the monolithic capillary column has drawn much attention in proteomic studies due to its high separation speed, high efficiency, and high recovery. Moreover, its low flow rate, typically in the range of a few microliters per minute, is ideally suited to be combined with off-

line peak collections for high-throughput analysis. However, the on-target digestion after off-line collection always produces limited number of digested peptides due to the incompleteness of the digest on the target. FTICR-MS, which can provide very high mass accuracy, will help to improve the protein identification confidence while using less number of peptides for peptide mass fingerprinting.

In this work, we incorporated the ELDI ion source with our 7T FTICR mass spectrometer. Instead of the standard inlet tube, we applied the flared inlet tube to the system. The ELDI-FTICR-MS was applied in the analysis of the complex peptide mixture such as protein digest. Different sample surfaces were used, such as a nitrocellulose membrane for western blotting. We compared the ion transmission and sensitivity with and without the flared inlet tube using different samples. We observed about a two to three fold improvement in the detected ion signal with the flared inlet tube while compared to the standard inlet tube. Moreover, we demonstrated the results of coupling on-target enzymatic digestion with ELDI-FTICR-MS. This approach can potentially be incorporated with HPLC off-line systems or CE off-line systems for high-throughput protein complex detection.

EXPERIMENTAL

Chemicals

Substance P and angiotensin II were purchased from Sigma (St. Louis, MO) and used without further purification. 10 mM solutions of each standard peptide were prepared in purified water (18 MΩ/cm) using a Nanopure ultra-purified water system (Barnstead International, Boston, MA). Analytical standards were prepared by dilution using 50/50 (v/v) methanol/water with 0.1% acetic acid.

ELDI setup and sample preparation

The aqueous solution of different samples was first mixed with an equal volume of saturated DHB in 50% acetonitrile/0.1% TFA, and then was spread uniformly by pipetting onto a defined surface area of an aluminum sample plate. For on-membrane ELDI study, the nitrocellulose membrane (Whatman Inc., Sanford, ME) was adhered to the sample target using a piece of double-sided tape. After pre-wetting the membrane with 50% methanol, the aqueous solution of sample was dispensed to the membrane, and then the saturated solution of DHB was applied to the membrane.

The setup of the ELDI instrument was similar to that described by Shiea, et al. The sample plate was first positioned on a 3D linear stage from Newport (Irvine, CA) in front of the sampling inlet tube. A pulsed nitrogen laser at a wavelength of 337.1 nm (model VSL337, Spectra-Physics) was focused onto the target plate with a repetition frequency of 20 Hz. The analytes due to laser ablation were then post-ionized in the electrospray solvent plume (50% methanol with 2% acetic acid). The flow rate of the charged solvent was 500 nl/min. The

position of the spray tip was parallel to the sample target and the distance between them was about 2 mm. The optimum location of the focused laser beam was close to the spray tip. Sample target was held at ground, while the high voltage applied to the electrospray tip was about 3 kV. For all the experiments, the incident laser angle was held constant.

In-solution and on-target tryptic digestion

100 μM BSA solution (in 100 mM ammonium bicarbonate buffer, pH=8.0) was first reduced at 50 ^{o}C for 45 minutes using 10 μl 50 mM DTT. 10 μl of 10 mM iodoacetamide was then added into the BSA solution for 30 minutes at room temperature. After alkylation, suitable trypsin was added into the BSA solution (about 1:100 ratio) and incubated at 37 ^{o}C overnight. After digestion, sample was kept at 4 ^{o}C, and further diluted to the desired concentration prior to MS analysis.

The on-target tryptic digestion of BSA was performed on a clean aluminum target. Four μl of BSA was spotted onto the sample target and was allowed to air-dry. One μl of 20 μg/ml trypsin (dissolved in 50 mM NH_4HCO_3) was then deposited onto the same sample spot by pipetting several times, which helps the mixture of trypsin and the protein on the target. The enzyme-to-substrate ratio was estimated to be approximately 1:100 (w/w). During digestion, the sample target was kept at 37 ^{o}C for 45 minutes. Buffer (50 mM NH_4HCO_3) was continuously added during the digestion process to keep the sample spot moist. After digestion, the spots were air dried, and then 2 μl saturated DHB in 50% acetonitrile/0.1% TFA was added to each spot by pipetting several times.

Instrumentation

The mass spectral data were collected using a Bruker Daltonics Apex-Q 7T FTICR mass spectrometer. The ions entered the instrument through the flared inlet tube, then passed through a hexapole followed by a mass selective quadrupole and a second hexapole. After accumulation in the second set of hexapole rods for the duration of several seconds, the ions were sent toward the ICR cell using an electrostatic ion guide. The ions were trapped in the ICR cell using a low energy sidekick potential to keep the ions close to the central *z* axis of the cell. All data sets acquired were 128k sample points/s. The mass spectral data were acquired using Xmass 7.0.6 as the data acquisition software program. The external calibration was done using a mixture solution of standard peptides. All the FTICR-MS data were analyzed using ICR-2LS software package.

RESULTS AND DISCUSSION

Sensitivity and detection limits

The detection of the solid peptide substance P on the surface of aluminum was demonstrated using ELDI-FTICR-MS (Figure 1). After mixing substance P with the saturated DHB solution at a 1:1 ratio, we deposited 2 μl of the mixture onto the sample target to the final surface concentration of 1 pmol/mm^2. A scan was acquired with 2s ion accumulation time in the second hexapole, and a spectrum was collected by the sum of 20 scans. Without laser ablation, we found that no analyte ions could be observed (Figure 1A). In contrast, the ESI-like spectra were obtained when we switched on the laser pulse (Figure 1B, C). This corresponds with the observation made by the Shiea group, which further proved that no DESI happened in this process. The entire observed ion signal was from ELDI. We also compared the ion intensity obtained using the flared inlet tube to the intensity using the standard inlet tube. The flared inlet tube used for this research was 0.02" i.d. and 1/16" o.d. at the unflared end, and was flared with a 10 degree angle from the center line to ~ 3 mm o.d. at the larger end. Standard non-flared tubes with the same i.d. and length were used for control studies to demonstrate the improvements using the flared tube. As shown in Figure 1B and Figure 1C, we found that the highest ion intensity among all the scans collected for a single spot using the flared tube is about 2-3 times that of the highest ion intensity using the standard inlet tube.

The detection limit of ELDI with different types of inlet tubes was estimated, using different sample spots with different solution concentrations of substance P. Each spot contained 1 μl of the analyte mixed with the same volume of saturated DHB solution at different concentrations. Five different surface concentrations of substance P were used: 5 pmol/mm^2,

2.5 pmol/mm^2, 1 pmol/mm^2, 0.5 pmol/mm^2, and 0.1 pmol/mm^2. For each spot, a series of scans with 3s ion accumulation time was acquired. The average of three highest ion intensities from the scans of one spot was plotted as a function of sample surface concentration, as shown in Figure 2. The error bars illustrated the standard deviation of 3 different spots at one sample surface concentration. To demonstrate the improvements using the flared inlet tube, we calculated the average intensity ratio of the flared inlet tube to the non-flared control inlet tube at each concentration. When compared with the standard inlet tube, we found an overall two-fold increase in the average ion intensity when using the flared tube with DESI. We chose the smallest sample surface concentration that gave the detected ion with a signal-to-noise ratio of 3 as the limits of detection (LODs). Therefore, the LOD for substance P is 0.1 pmol/mm^2 with the use of the non-flared inlet tube. The LOD for substance P with the use of the flared inlet tube decreased to 0.05 pmol/mm^2. These results show the improvement of a factor of two in both average ion intensity and limit of detection (LOD) with the use of the flared inlet tube with ELDI.

New surfaces of ELDI

To demonstrate that ELDI can be applied to different types of surfaces, we used the nitrocellulose membrane. We first attached a piece of the nitrocellulose membrane onto the aluminum sample target. After pre-wetting the membrane, 1μl of angiotensin II was mixed with the same volume of saturated DHB solution, and was then pipetted onto the membrane to the final concentration of 5 pmol/mm^2. A saturated solution of DHB was then deposited onto the same region of the membrane. After air-drying, the sample target was placed for ELDI experiments. Figure 3 is the ELDI spectrum of bradykinin on the nitrocellulose membrane. We found that an ESI-like spectrum was obtained for bradykinin. Also, lower ion intensity was

achieved for ELDI on the nitrocellulose membrane compared to ELDI on the metal surface (data not shown here). This may be related to the different laser ablation efficiency on different sampling surfaces. Overall, this result demonstrates the possibility of coupling ELDI with on-membrane digestion for protein identification and profiling.

ELDI of protein in-solution digestion

We applied a peptide mixture to the ELDI-FTICR-MS, as shown in Figure 4. After in-solution digestion, 1 μl of BSA digested peptides were mixed with the same volume of saturated DHB solution, and were then spotted onto the aluminum sample target. The final surface concentration of BSA digested peptides was 5 pmol/mm^2. ELDI-FTICR-MS was performed on the sample spot. Flared inlet tubes have been applied here to demonstrate the ability to improve the MS sensitivity compared to the standard inlet tubes. The flared inlet tube used here was the same as described above: 0.02" i.d. and 1/16" o.d. at the unflared end, and was flared with a 10 degree angle from the center line to ~ 3 mm o.d. at the larger end. Non-flared standard tubes with the same i.d. and length were used for control studies. The spectra in Figure 4 are the sum of 10 scans with 1s ion accumulation time per scan. For both types of the inlet tubes, BSA digested peptides were effectively detected. With the standard inlet tube, 20 of the detected peaks were identified as BSA digested peptide peaks, and the total ion intensity of all the peaks in the spectrum is 4.02E6. With the flared inlet tube, there are also 20 detected peaks identified as BSA digested peptide peaks, and the total ion intensity of all the peaks in the spectrum is 2.21E6. When comparing the total ion intensity with and without the flared tube, we found about a two-fold improvement using the flared inlet tube. This observation was similar to the

detection limit results described above. Therefore, improved sensitivity for peptide mixture using ELDI-FTICR-MS can be achieved with the implementation of flared inlet tubes.

ELDI of protein on-target digestion

We also coupled protein on-target digestion with ELDI-FTICR-MS. For this study, 4 μl of BSA was deposited on the sample target and was detected using ELDI-FTICR-MS. The final surface concentration was 10 pmol/mm^2. Since we have demonstrated that the flared inlet tube can also improve the sensitivity for peptide mixture such as BSA in solution digestion, we only applied the flared inlet tube for the study of on-target digestion. As shown in Figure 5A, nine BSA tryptic peptides were observed. Peptide mass mapping was performed by matching possible tryptic fragments (listed in Table 1) to the MSDB database using a Mascot search. The candidate peak list was generated by calculating the measured neutral mass of the peaks in the spectrum. The database search was performed based on following parameters: taxonomy (mammalia), enzyme (trypsin), missing cleavage (2), and mass tolerance (0.01 Da). As shown in Figure 5B, although not many peptides were obtained by the on-target digestion, the Mascot search still only gives a statistically significant score ($p<0.05$) for BSA, which is 101. This is due to the improved mass accuracy using FTICR-MS. When using much smaller mass tolerance for the Mascot search, fewer peptides were needed for the correct protein identification. After internal calibration, the average absolute mass measurement error for the identified peaks in Table 1 was 0.964 ppm. When we set the mass tolerance at 0.5 Da (which is normal for most of the peptide mass finger-printing using MALDI-TOF-MS), we found that no protein can be identified with a significant score, although BSA had the highest Mascot score at 74. Therefore, the ultra-high mass measurement accuracy achieved from FTICR-MS can benefit protein

identification using peptide mass fingerprinting. Fewer peptide peaks are needed at higher mass measurement accuracy. It can also be the advantage for the on-target digestion, since most of time this method produces less peptides than in-solution digestion. ELDI-FTICR-MS can potentially be a solution to coupling high throughput protein separation with on-target digestion for protein profiling.

CONCLUSIONS

A new atmospheric pressure ion source ELDI, which can couple some of the advantages of both MALDI and ESI, allows rapid analysis of solid samples under ambient conditions including biological samples such as tissues. Since the sampling step of ELDI is laser desorption that allows sampling over a small area, ELDI can potentially be applied to tissue imaging. The unique top-down ability and the high mass measurement accuracy of FTICR-MS can be extremely useful for the protein identification in the tissue imaging process. In this work, we reported our preliminary study of coupling the ELDI source with our Bruker Apex-Q 7T FTICR-MS. Instead of the standard inlet tube, we have applied the flared inlet tube as the atmospheric pressure interface to improve the ion transmission efficiency. We demonstrated the improvement in ion transmission efficiency and the detection limit by using the flared inlet tube. About a two-fold increase in the measured ion signal was achieved with the flared inlet tube. The limit of detection was also increased. We also applied ELDI-FTICR-MS to detect the peptides on the nitrocellulose membrane. The results demonstrate the possibility of coupling ELDI with on-membrane digestion for protein identification and profiling.

Recently, a different high-throughput protein profiling method has been proposed, which couples HPLC or CE separation of proteins offline with MALDI-TOF-MS. One of the important steps of this method is on-target digestion. However, relatively short digestion time and harsh digestion conditions result in fewer tryptic peptides from on-target digestion compared to in-solution digestion. This can be problematic for protein identification using peptide mass fingerprinting for MALDI-TOF-MS. In this study, we have coupled the on-target digestion of BSA with ELDI-FTICR-MS. By using ELDI-FTICR-MS, we have demonstrated that higher

protein identification confidence can be achieved with a relatively small number of peptides. This can be advantageous for the high throughput protein profiling using an offline digestion method.

ACKNOWLEDGEMENTS

This work was supported by grants from the M.J. Murdock Charitable Trust, the Directorate of Biological Sciences, National Science Foundation, Grant No. DBI-0352451, and the Office of Science (BER), U.S. Department of Energy, Grant No. DE-FG02-04ER63924. We are also grateful to PNNL for providing the software ICR-2LS used for data analysis.

REFERENCES

1. Cooks, R. G., Ouyang, Z., Takats, Z. & Wiseman, J. M. (2006). Detection Technologies. Ambient mass spectrometry. *Science* **311,** 1566-1570.

2. Cotte-Rodriguez, I., Takats, Z., Talaty, N., Chen, H. & Cooks, R. G. (2005). Desorption electrospray ionization of explosives on surfaces: sensitivity and selectivity enhancement by reactive desorption electrospray ionization. *Anal Chem* **77,** 6755-6764.

3. Takats, Z., Wiseman, J. M. & Cooks, R. G. (2005). Ambient mass spectrometry using desorption electrospray ionization (DESI): instrumentation, mechanisms and applications in forensics, chemistry, and biology. *J Mass Spectrom* **40,** 1261-1275.

4. Takats, Z., Wiseman, J. M., Gologan, B. & Cooks, R. G. (2004). Mass spectrometry sampling under ambient conditions with desorption electrospray ionization. *Science* **306,** 471-473.

5. Takats, Z., Cotte-Rodriguez, I., Talaty, N., Chen, H. & Cooks, R. G. (2005). Direct, trace level detection of explosives on ambient surfaces by desorption electrospray ionization mass spectrometry. *Chem Commun (Camb)* 1950-1952.

6. Van Berkel, G. J., Ford, M. J. & Deibel, M. A. (2005). Thin-layer chromatography and mass spectrometry coupled using desorption electrospray ionization. *Anal Chem* **77,** 1207-1215.

7. Cody, R. B., Laramee, J. A. & Durst, H. D. (2005). Versatile new ion source for the analysis of materials in open air under ambient Conditions. *Anal Chem* **77,** 2297-2302.

8. McEwen, C. N., McKay, R. G. & Larsen, B. S. (2005). Analysis of solids, liquids, and biological tissues using solids probe introduction at atmospheric pressure on commercial LC/MS instruments. *Anal Chem* **77,** 7826-7831.

9. Laiko, V. V., Moyer, S. C. & Cotter, R. J. (2000). Atmospheric pressure MALDI/ion trap mass spectrometry. *Anal Chem* **72,** 5239-5243.

10. Laiko, V. V., Baldwin, M. A. & Burlingame, A. L. (2000). Atmospheric pressure matrix-assisted laser desorption/ionization mass spectrometry. *Anal Chem* **72,** 652-657.

11. Kellersberger, K. A., Tan, P. V., Laiko, V. V., Doroshenko, V. M. & Fabris, D. (2004). Atmospheric pressure MALDI-fourier transform mass spectrometry. *Anal Chem* **76,** 3930-3934.

12. Tan, P. V., Taranenko, N. I., Laiko, V. V., Yakshin, M. A., Prasad, C. R. & Doroshenko, V. M. (2004). Mass spectrometry of N-linked oligosaccharides using atmospheric pressure infrared laser ionization from solution. *J Mass Spectrom* **39,** 913-921.

13. Kellersberger, K. A., Yu, E. T., Merenbloom, S. I. & Fabris, D. (2005). Atmospheric pressure MALDI-FTMS of normal and chemically modified RNA. *J Am Soc Mass Spectrom* **16,** 199-207.

14. Levis, R. J. (1994). Laser desorption and ejection of biomolecules from the condensed phase into the gas phase. *Annu Rev Phys Chem* **45,** 483-518.

15. Huang, M. Z., Hsu, H. J., Lee, J. Y., Jeng, J. & Shiea, J. (2006). Direct protein detection from biological media through electrospray-assisted laser desorption ionization/mass spectrometry. *J Proteome Res* **5,** 1107-1116.

16. Shiea, J., Huang, M. Z., Hsu, H. J., Lee, C. Y., Yuan, C. H., Beech, I., *et al.* (2005). Electrospray-assisted laser desorption/ionization mass spectrometry for direct ambient analysis of solids. *Rapid Commun Mass Spectrom* **19,** 3701-3704.

17. Fenn, J. B., Mann, M., Meng, C. K., Wong, S. F. & Whitehouse, C. M. (1989). Electrospray ionization for mass spectrometry of large biomolecules. *Science* **246,** 64-71.

18. Cech, N. B. & Enke, C. G. (2001). Practical implications of some recent studies in electrospray ionization fundamentals. *Mass Spectrom Rev* **20,** 362-387.

19. Shaffer, S. A., Prior, D. C., Anderson, G. A., Udseth, H. R. & Smith, R. D. (1998). An ion funnel interface for improved ion focusing and sensitivity using electrospray ionization mass spectrometry. *Anal Chem* **70,** 4111-4119.

20. Tan, P. V., Laiko, V. V. & Doroshenko, V. M. (2004). Atmospheric pressure MALDI with pulsed dynamic focusing for high-efficiency transmission of ions into a mass spectrometer. *Anal Chem* **76,** 2462-2469.

21. Henion, J. D., Covey, T. R. & Bruins, A. P. (1989). US patent 4,861,988.), US patent 4,861,988.

22. Covey, T. R. (1995).), U.S. Patent 5,412,208.

23. Wu, S., Zhang, K., Kaiser, N. K., Bruce, J. E., Prior, D. C. & Anderson, G. A. (2006). Incorporation of a flared inlet capillary tube on a fourier transform ion cyclotron resonance mass spectrometer. *J Am Soc Mass Spectrom* **17,** 772-779.

24. Prior, D. C., Price, J. & Bruce, J. E. (2002). Sample inlet tube for ion source of a mass spectrometer.), US patent 6,455,846.

25. Ohtsu, I., Nakanisi, T., Furuta, M., Ando, E. & Nishimura, O. (2005). Direct matrix-assisted laser desorption/ionization time-of-flight mass spectrometric identification of proteins on membrane detected by Western blotting and lectin blotting. *J Proteome Res* **4,** 1391-1396.

26. Sloane, A. J., Duff, J. L., Wilson, N. L., Gandhi, P. S., Hill, C. J., Hopwood, F. G., *et al.* (2002). High throughput peptide mass fingerprinting and protein macroarray analysis using chemical printing strategies. *Mol Cell Proteomics* **1,** 490-499.

27. Nedelkov, D., Tubbs, K. A., Niederkofler, E. E., Kiernan, U. A. & Nelson, R. W. (2004). High-throughput comprehensive analysis of human plasma proteins: a step toward population proteomics. *Anal Chem* **76,** 1733-1737.

28. Hunzinger, C., Schrattenholz, A., Poznanovic, S., Schwall, G. P. & Stegmann, W. (2006). Comparison of different separation technologies for proteome analyses: Isoform resolution as a prerequisite for the definition of protein biomarkers on the level of posttranslational modifications. *J Chromatogr A*.

29. Zheng, S., Yoo, C., Delmotte, N., Miller, F. R., Huber, C. G. & Lubman, D. M. (2006). Monolithic column HPLC separation of intact proteins analyzed by LC-MALDI using on-plate digestion: An approach to integrate protein separation and identification. *Anal Chem* **78,** 5198-5204.

30. Zuberovic, A., Ullsten, S., Hellman, U., Markides, K. E. & Bergquist, J. (2004). Capillary electrophoresis off-line matrix-assisted laser desorption/ionisation mass spectrometry of intact and digested proteins using cationic-coated capillaries. *Rapid Commun Mass Spectrom* **18,** 2946-2952.

Table 1. Summary of identified peptides originating from the on-target tryptic digestion of BSA

peak in fig. 5	charge state	measured ***m/z***	theoratical ***m/z***	mass error (ppm)	peptide sequence
1	1	733.4219	733.4203	0.965	VLTSSAR
2	1	789.4713	820.4725	-0.741	LVTDLTK
3	2	820.472	847.5036	0.288	KVPQVSTPTLVEVSR
4	1	922.4867	922.4880	0.180	QTALVELLK
5	1	1001.5869	1001.5891	0.853	AEFVEVTK
6	1	1014.6182	1014.6194	1.174	ALKAWSVAR
7	1	1163.6291	1163.6307	-2.575	LVNELTEFAK
8	1	1479.7919	1479.7954	1.323	LGEYGFQNALIVR
9	1	1640.9515	1639.9377	-0.584	KVPQVSTPTLVEVSR

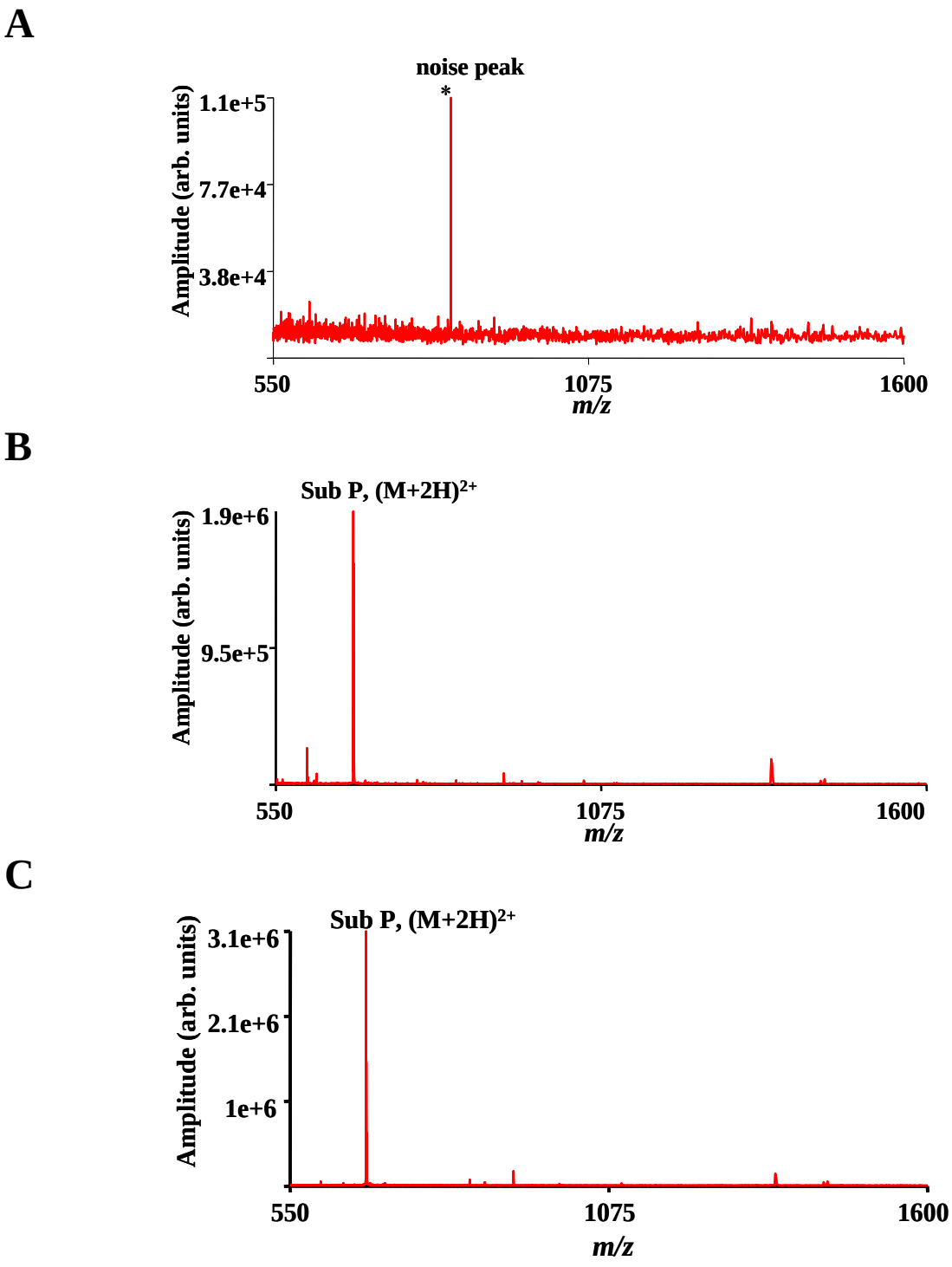

Figure 1. Mass spectra obtained from substance P deposited on the surface of aluminum using the ELDI set-up. The following operating conditions of ELDI are compared: (A) no laser pulse applied; (B) ELDI with the standard inlet tube; and (C) ELDI with the flared inlet tube.

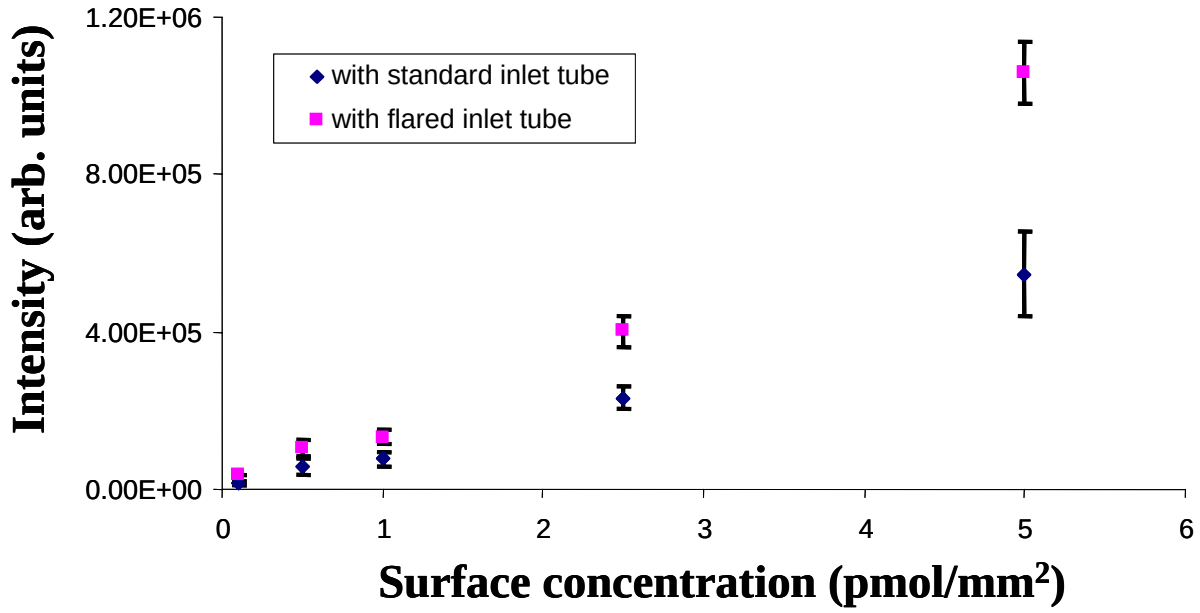

Figure 2. Plot of mass spectral total ion intensity using ELDI versus the amount of substance P spotted on the sample target.

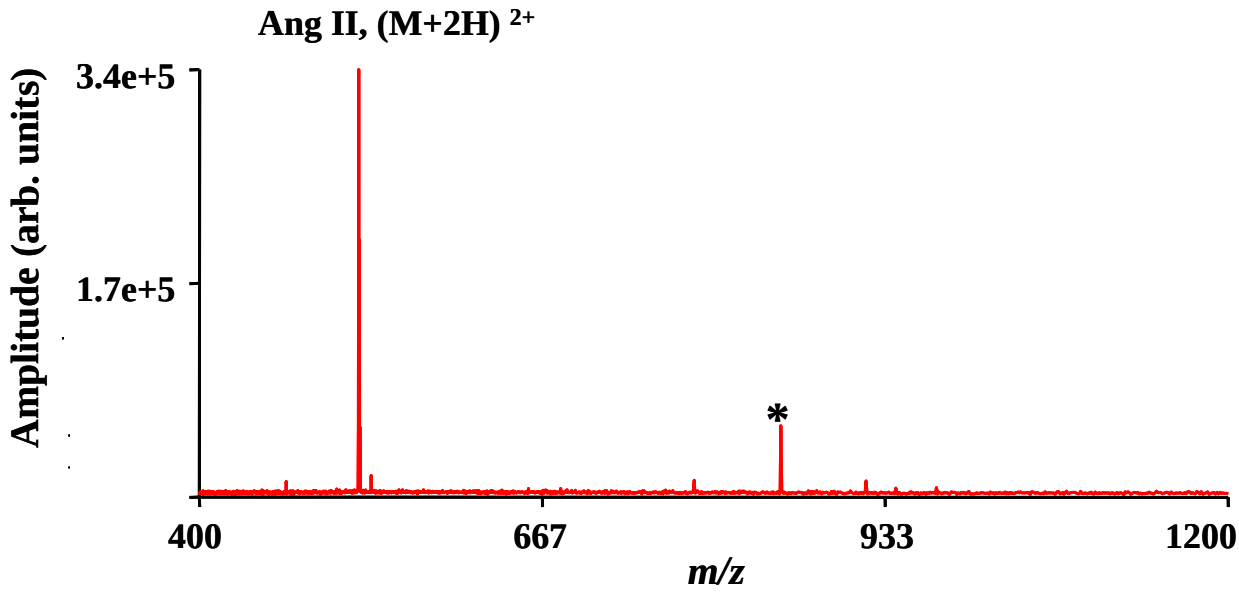

Figure 3. ELDI mass spectrum of angiotensin II deposited on the surface of nitrocellulose membrane. The peak marked with * is noise peak.

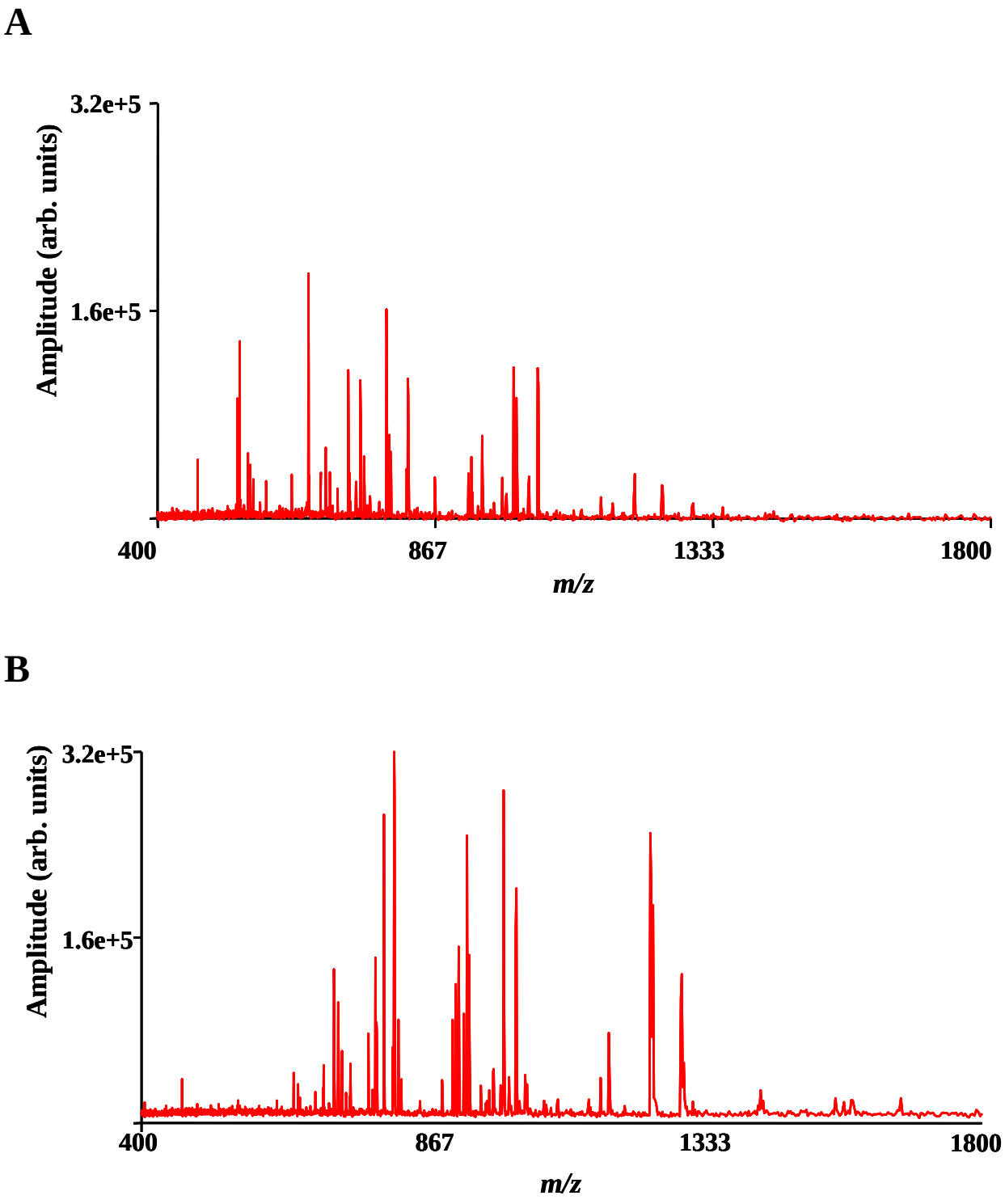

Figure 4. ELDI mass spectra of BSA in-solution digestion deposited on the surface of aluminum. (A) with the standard inlet tube; and (B) with the flared inlet tube.

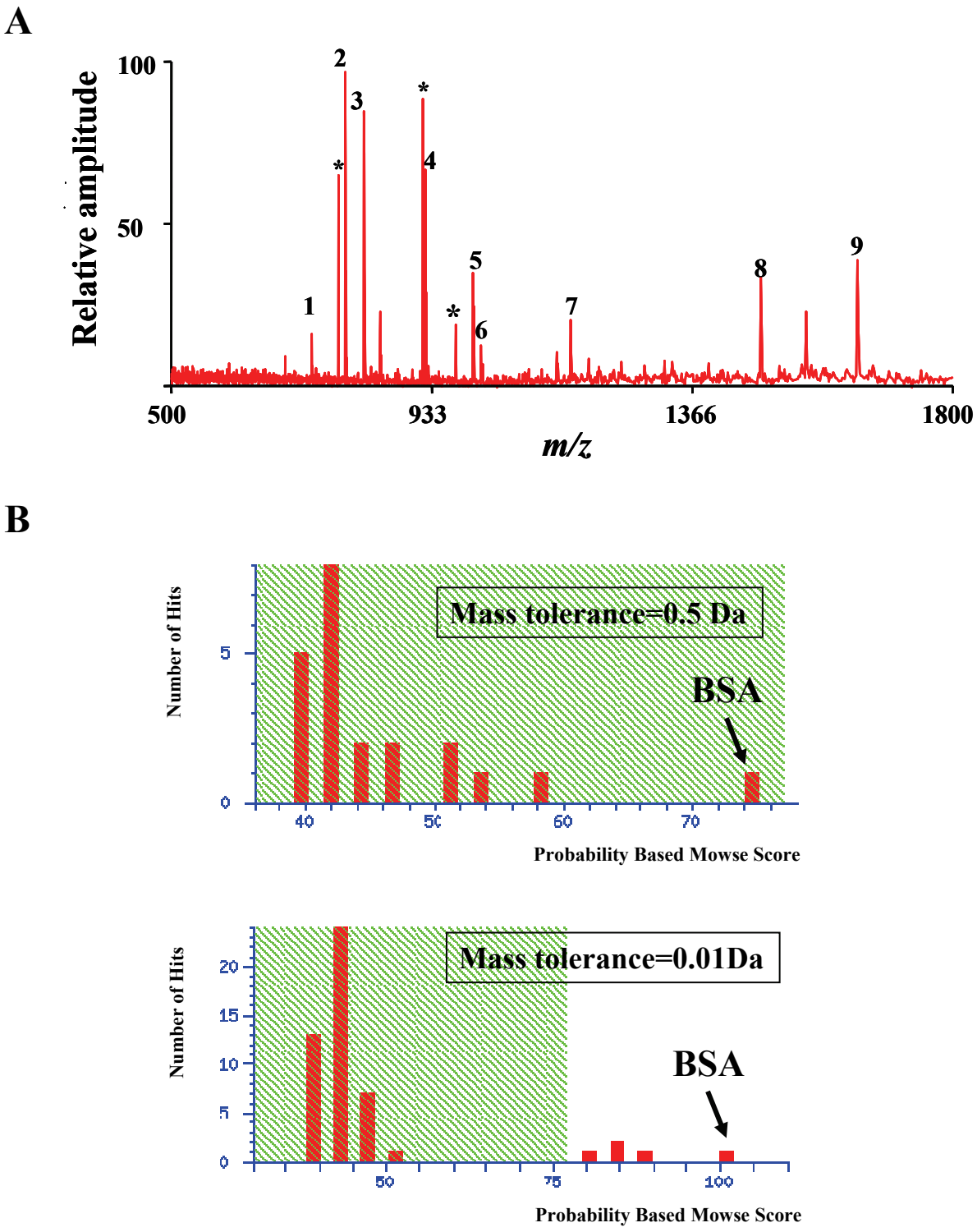

Figure 5. (A) ELDI mass spectrum of tryptic peptides produced by on-target digestion of BSA; (B) MASCOT search results using different mass tolerances. Peaks marked with * are noise peaks.

CHAPTER SEVEN

Conclusions

Chapter 2: Increased Protein Identification Capabilities through Novel Tandem MS Calibration Strategies. A novel calibration method, Calibration Optimization on Fragment Ions (COFI), has been developed to correct for space charge-induced frequency shifts in FTICR fragment spectra. Examples in the paper demonstrated that the calculated frequency shifts to correct the mass differences between two neighboring peptide fragment ions (such as y_1 and y_2) were close to each other, and these frequency shifts were also close to the space charge-induced frequency shifts in the spectrum. A Java executable program COFI has then been developed based on this idea. This program has successfully applied to LC-FTICR fragmentation data. For LC-FTICR-MS/MS experiment, Mascot MS/MS ion search data demonstrate that most of the fragments from BSA tryptic digested peptides can be identified using a much lower mass tolerance window after applying COFI to LC-FTICR-MS/MS of BSA tryptic digest. We also demonstrated the feasibility of COFI applied to multiplexed LC-CID-FTICR-MS which is an attractive technique because of its increased duty cycle and dynamic range. After the application of COFI to a multiplexed LC-CID-FTICR-MS of BSA tryptic digest, we achieved an average measured mass accuracy of 2.49 ppm for all the identified BSA fragments.

Chapter 3: A Hybrid HPLC-Gel-MS Method for Proteomics Research and Its application to Protease Functional Pathway Mapping. We described a two dimensional method for protein mixture separation using a combination of high performance liquid chromatography (HPLC) and 1D SDS-PAGE. In stead normally used continuous elution

gradient, we applied the step-wise gradient for fractionation from the strong anion exchange column. We demonstrated that this step-wise gradient provided excellent reproducibility, which can be advantage for comparative proteomics study. The BSA and ovalbumin spiking experiments showed that this newly developed method can be applied to the protein differential expression profiling since protein abundance level changes can be easily visualized with side-by-side vertical comparison in one gel. Separation of multi-samples in the same gel significantly reduces run-to-run variation. The detection limit of this method (~ 170 ng) was close to the detection limit of the gel staining method (30-100 ng). This chapter also presented the results of our developments and our initial application of this strategy for mapping protease function of beta amyloid cleaving enzyme (BACE) in biological systems.

Chapter 4: Incorporation of a Flared Inlet Capillary Tube on a Fourier Transform Ion Cyclotron Resonance Mass Spectrometer. We incorporated the flared inlet capillary tubes with our Bruker 7T Apex-Q FTICR mass spectrometer to help the ion transmission from the atmospheric pressure to the first vacuum region. Different types of atmospheric pressure ionization methods such as ESI, ESSI, DESI, and AP-MALDI were set up to investigate the ion transmission efficiency with the flared inlet tube compared to with the standard inlet tube. For most of the ionization methods, such as ESI and DESI, the improvement of ion intensity detected on a FTICR-MS was observed with the use of our enhanced ion inlet designs. However, for ESSI, no significant improvement was found. For AP-MALDI, the measured ion current transferred through the flared inlet tube was about 2-3 times larger than the ion current through the control non-flared inlet tube. Increased spray tip positional tolerance was also observed with

implementation of the flared inlet tube, which is advantage to achieve more reproducible ion signal.

Chapter 5: Integration of a New Atmospheric Pressure Interface with Atmospheric Pressure Ionization Methods. We reported our investigations a new hybrid atmospheric pressure interface which couples an air amplifier with a flared inlet tube. We also incorporated this new interface with our 7T Apex-Q FTICR mass spectrometer. While coupling the nano-electrospray ion source and the new hybrid interface, we found better desolvation using the new interface while comparing the ion current responses. The increased ion intensity from mass spectra was also observed with the high-velocity gas flow compared to without gas flow. Using AP-MALDI with the air amplifier, we observed more than a 5-fold increase in measured ion current with the flared inlet tube compared to the non-flared tube. About 3-fold increase in the measured ion current was found while using the new interface compared to the standard inlet tube interface. A two nano-electrosprayer device has been coupled with the hybrid air amplifier-flared inlet tube. Internal calibrant can be easily introduced by using this setup, while the ratio of the calibrant and the analytes can be tunable by changing the relative position of the two-sprayer device to the acceptance region of the air amplifier. By using substance P as the internal standard, the absolute average mass error of the BSA tryptic digested peptide peaks from direct infusion decreased to 2.2 ppm.

Chapter 6: Coupling On-Target Digestion with an Electrospray-Assisted Laser Desorption Ionization FTICR Mass Spectrometer. Electrospray-assisted laser desorption/ionization (ELDI) source was set up and coupled with our 7T Apex-Q FTICR-MS.

We also modified the atmospheric pressure interface of the mass spectrometer using the flared inlet tube we described in chapter 4 and chapter 5. Using ELDI-FTICR-MS, we observed about two fold improvement in the detected ion signal with the flared inlet tube compared with the standard inlet tube. The application of ELDI on different sample surfaces was performed, such as the detection of peptides on a nitrocellulose membrane. We also coupled on-target enzymatic digestion with ELDI-FTICR-MS. High mass measurement accuracy from FTICR mass spectrum can improve the confidence of protein identification. This approach can potentially be incorporated with HPLC off-line systems or CE off-line systems for high throughput proteome profiling.